THE EVOLUTION OF GALAXIES IN GROUPS: HOW GALAXY PROPERTIES ARE AFFECTED BY THEIR GROUP PROPERTIES

by Melissa Gillone

A thesis submitted to the University of Birmingham

for the degree of

Doctor of Philosophy

Astrophysics and Space Research Group

School of Physics and Astronomy

University of Birmingham

September 2015

Abstract

It has been long known that galaxy properties are strongly connected to their environment; however, a complete picture is still missing. This work's aim is to better understand the role of environment in shaping the galaxy properties, using a sample of 25 redshift-selected galaxy groups at $0.060 < z < 0.063$, for which 30 multi-wavelength parameters are available. Given the wide variety of group dynamical states, it was fundamental to try and identify different classes of groups performing a statistical clustering analysis using all the available parameters independently of their physical meaning, which resulted in two classes distinct by their mass. To move beyond mass-driven correlations, a new clustering analysis was performed removing the mass dependent properties, this approach provided a categorisation in four classes with distinctive group properties. Based on this, the galaxy properties were investigated and the classes interpreted as follows: a class of field-like galaxies in the early stage of structure formation; a class of low-mass groups either still in formation phase, or evolved, but small because they are isolated; a class of massive groups with no, or very little, ongoing star formation, likely in a more evolved stage of structure formation; and a class of massive groups possibly experiencing merger events. The result obtained have shown that it is possible to distinguish between classes of groups and thus be able to study the property of galaxies in systems with homogeneous properties. The method developed applied to data sets with larger statistics and good data quality could be a powerful tool to study galaxy evolution in galaxy groups.

To Willy, I miss you every day...

Acknowledgements

This is the end of another era...

Thank you Andrea for being next to me no matter what and even from far away.

Four years are a long time, I met lots of wonderful people who helped me throughout, but I didn't think I could meet someone so special that sometimes it felt like she was in my brain. I really enjoyed all of our adventures # roadtrip, all the nights watching stupid TV series and all the drinks. Then suddenly someone else joined the duo and made it into a trio, and I had the best time of my life. The drinks increased, but I am still looking forward to our first # roadtrip in three, so Sarah and Sean start packing, I'll drive!

A special thanks to all the people that made the office a nice place to go every day: Miranda, Will, Richard, Maggie, Aurelia, Simon and Anna.

To my oldest friends in this country: Matt, Laura, Brigid and all the others. And to Dave the pub quiz master. To my old friends in Italy (and all the new babies that were born when I was away) for wanting to see me at all costs every time I went home. I missed you a lot.

Thanks to Jacqui and her family to make me feel at home for four years, and to Louis who likes sleeping in my bed and singing to me the song of his people: ppprrrrrrr.

Thanks to all the people in the department, in particular to Trevor Ponman who was a great supervisor and taught me so much during these years. A special thanks to my present supervisor Sean McGee who supported me, believed in me and made this

work so exciting.

Finally, a great thanks to my family. Mum and Cristiano who talked to me almost every night and were happy to have me back hanging in their living room. Marta because she is cool and laughs funny. Dad who calls me whenever he sees me online, at any time of the day or night and complained that the weather in Madagascar is terrible... Grandma for the amazing lunches at San Bartolomeo. Marco and Alice, they are too tall, but they are cool. Last but not least Padi, I won't blame him again, but I did all this because of him, so thanks for showing me the stars for the first time and for always being there for me.

Then I found myself in the middle of a Shakespearian play...

Button.

Contents

List of Figures

List of Tables

Statement of originality

I hereby declare that this project was entirely my own work and that any additional sources of information have been duly cited.

As part of the XI collaboration some of the data utilised for this work were obtained and reduced by collaborators, all the previous published works have been cited.

I hereby declare that any internet sources, published or unpublished works from which I have quoted or drawn reference have been referenced fully in the text and in the contents list.

Chapters 1 and 2 are review chapters where literature results have been summarised and referenced at all times.

Chapter 3 describes the data samples as obtained and published in [Bai et al., 2010; Rasmussen et al., 2006b, 2012]. The Lick indices analysis and model comparison described in Section 3.5 and Appendix 2 were performed by me. The algorithm described in section 3.6 was developed in collaboration with Will Farr.

Chapter 4 describes the correlation and multi-variate clustering analysis performed by me. For the clustering analysis the public algorithm X-means described in Dan Pelleg [2000] was utilised.

Chapter 5 presents the galaxy properties in view of the results of the previous chapter with input in the interpretation from Sean McGee.

Chapter 6 summarises the conclusion and outlines improvements to the analysis and future works.

Chapter 1

Introduction

According to the ΛCDM cosmology, all the structures in the Universe form via accretion/merger of smaller structure, with a merger rate declining as the Universe ages [Berrier et al., 2006; McGee et al., 2009]. The first to collapse are the dark matter particles that form the so-called dark matter haloes. These structures gravitationally attract baryonic matter which then will collapse and form stars. Stars will aggregate to form isolated (or field) galaxies, these will interact and form bound groups of galaxies which will keep to accrete more galaxies and will become the largest structure in the Universe: the galaxy clusters. In these structures galaxies will continue to evolve interacting with each other and eventually merging. A schematic of how hierarchical structure formation works is shown in Figure 1.1.

Galaxy groups and clusters are physically bound systems that evolve toward virial equilibrium. Galaxies come together under the pull of their relative gravitational force and become gravitationally bound. The higher the number of bound objects the deeper the gravitational potential well formed, thus more galaxies from the surroundings will be 'captured' and will join the larger structure. Because of the way galaxies are accreted, a group or cluster can be virialised only in the core, since in the outskirts there is continuous infall of new objects. When a new galaxy enters a larger structure it moves

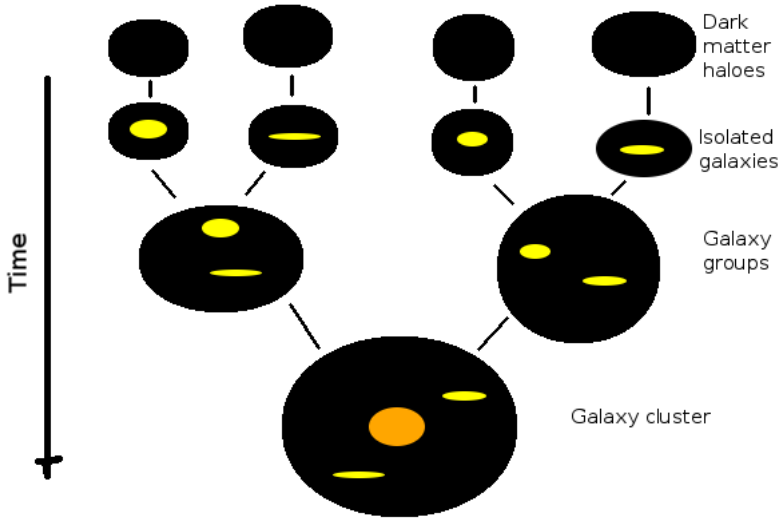

Figure 1.1: Cartoon illustrating the hierarchical growth of structures, time increases from top to bottom. First the dark matter collapses and forms dark matter haloes. The gravitational potential of the haloes attracts baryonic matter which collapses to form stars and isolated galaxies (in yellow). Dark matter haloes attracted by each other merge and the galaxies they contained become part of a larger halo (galaxy groups). The intermediate size haloes merge to form larger structures (galaxy clusters) inside which galaxies interact as well eventually merging to form more massive galaxies (in orange).

toward the centre, and crosses it several times before settling in the central regions: typically the crossing time of a Virgo-like cluster is $\sim$ 1.7 Gyr [Boselli and Gavazzi, 2006].

The virial equilibrium is described by the virial theorem:

$$2E_k = U \tag{1.1}$$

where E_k is the kinetic energy and U is the gravitational potential energy. If the structure is in virial equilibrium it is possible to infer its dynamical mass (halo mass) from its velocity dispersion as:

$$M = \frac{2\sigma^2 R}{G} \tag{1.2}$$

where M is the total mass, σ is the velocity dispersion, G is Newton's gravitational constant, and R is the characteristic radius of the group/cluster [for more details see Section 5.4.4 Mo et al., 2010].

Galaxy clusters are massive objects made of few hundreds of galaxies, virialised in their core where a massive elliptical galaxy usually resides. These massive objects ($\sim$ 10^{14}-10^{15} $M_\odot$) are easy to observe: they are bright at optical wavelengths due to the presence of massive galaxies and the Inter-Galactic Medium (IGM) ($\sim$ 75 % of the total cluster mass, Ettori et al. [2009]), heated in the gravitational potential well at a temperature typically between 2 and 10 keV [Sarazin, 1986], emits at X-ray wavelengths. Despite being easy to detect in multiple wavelengths, they are relatively rare and they only show the final stage of structure growth.

Galaxy groups are instead an intermediate environment between the field and the big clusters of galaxies. Despite the fact that not all groups necessarily end up in clusters, observations show that most clusters are made up of groups [McGee et al., 2009]. Furthermore, they host most of the galaxies in the local Universe, thus they are

ideal to understand galaxy evolution.

The following section will describe in more detail the properties of galaxy groups since they will be the object of study of this work.

1.1 Group Properties

As mentioned above, groups are the most common environment for galaxies, compared to clusters or field, and they contain most of the stellar mass in the local Universe [Eke et al., 2004a, 2005; Tully, 1987]. The definition of galaxy group is not unique: it can vary according to the purpose of the study and the selection method. Generally a group is described as a system made of $\sim$ 50 galaxies, or less, above a defined luminosity , usually L^*, with typical halo mass between $10^{12.5}$ and 10^{14} $M_\odot$, and size $\sim$ 1 Mpc [Eke et al., 2004a; Huchra and Geller, 1982].

Groups exist in a wide variety of dynamical and evolutionary states. They can be virialised systems or still in a collapsing phase, as reflected by the wide variety of morphologies, sizes and shapes, (e.g. poor, rich, loose, compact, see Figure 1.2). This is because they are an intermediate environment between the field and the big clusters, also suggested by the fact that a significant fraction of cluster galaxies are accreted through groups [McGee et al., 2009].

Compared to clusters, groups contain fewer galaxies, are less massive, and have smaller velocity dispersions, however they can also have similarities, such as an early-type galaxy in their centre or diffuse X-ray emission if massive enough.
Virialised groups, similarly to clusters, have a nearly spherical shape and a Gaussian velocity distribution [Faltenbacher and Diemand, 2006; Hansen and Sommer-Larsen, 2006; Hoeft et al., 2004], while non-virialised systems can show elongated shapes [Plionis et al., 2004], non-Gaussian velocities, and the presence of sub-structures. Hou et al. [2012] studied a sample of intermediate redshift groups (z $\sim$ 0.4) from the GEEC

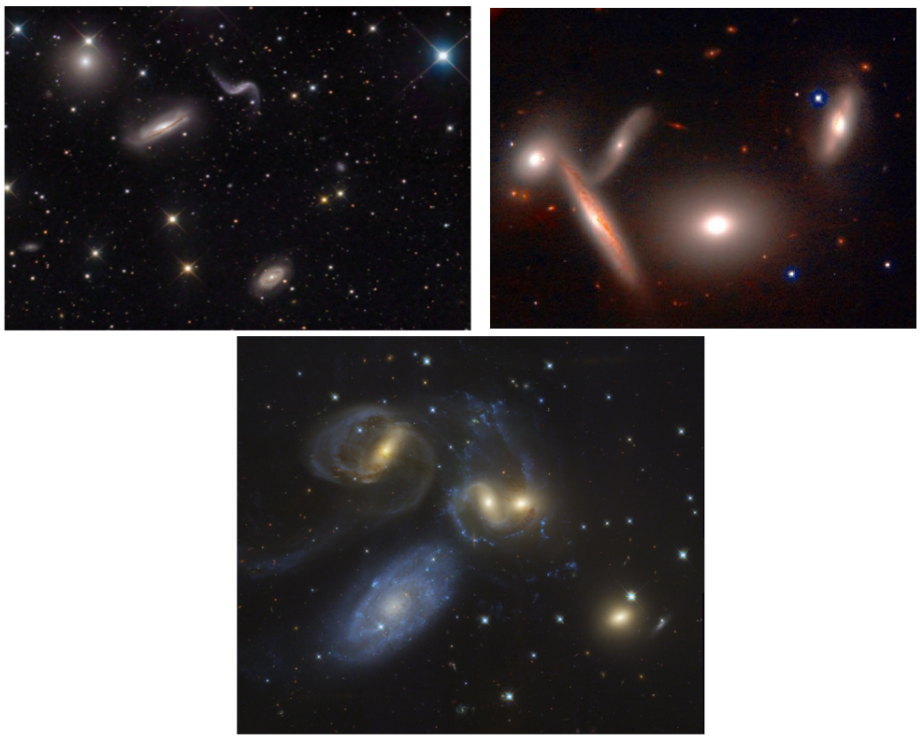

Figure 1.2: Pictures displaying the variety of group morphology. Top left Hickson 44 [MASIL] is mainly populated by late-type galaxies. Top right Hickson 40 [CISCO] is a compact group with an early-type galaxy in its centre. Bottom Stephan's Quintet [HLA, a] famous compact group populated by interacting late-type galaxies.

catalogue, and found that most of the groups with substructures have non-Gaussian velocity. Furthermore the colour of galaxies within the sub-structures is comparable to the colour of galaxies in the field, suggesting that they are not quenched by environmental effect. By contrast, red and passive galaxies were observed in groups with no substructures [Masters et al., 2010; Wolf et al., 2009]. Observing substructures in groups and clusters also supports the hierarchical structure formation scenario.

Other differences between virialised and non-virialised groups emerged from the work by Ribeiro et al. [2013] who observed the presence of faint galaxies near the centre of Gaussian clusters, compared to non-Gaussian, suggesting that these could be used as dynamical indicators of cluster dynamics. In addition, in non-Gaussian clusters the passive galaxies position segregation is not observed, in agreement with previous studies.

The magnitude gap between the first and second brightest galaxies can also be used as indicator of the dynamical state of a group. For instance, a system with large magnitude gap is likely to have formed earlier respect to one with a small gap, as supposedly all the bright galaxies have merged into a central elliptical and the group is now accreting small and faint galaxies. This parameter was used to define fossil groups as galaxy groups with R-band magnitude difference between the first and the second brightest galaxy within $0.5R_{200}$ of the group centre > 2 [Jones et al., 2003]. Dariush et al. [2010] concluded that the fossil group state is a temporary phase in a group's life, which ends as soon as an infalling galaxy of magnitude similar to the BGG enters the inner region of the group.

To identify a group and its member galaxies, two methods have historically been used, similarly to clusters: X-ray detection and optical selection.

The observed X-ray emission comes from the Intra-Group Medium (IGM) heated to temperatures $\gtrsim 10^7$ K (≈ 1 keV) mainly by thermal bremsstrahlung, reaching a typical luminosity in the range of 10^{41} - 10^{43} erg s^{-1}. This selection method is biased toward

those systems that are more evolved and relaxed or experiencing a merger events [Briel et al., 1991; Sun et al., 2002], hence not representative of the main group population since it does not detect groups in all possible evolutionary states.

The optical selection is done using spectroscopic redshift surveys [Eke et al., 2004a], which allow to perform a three-dimensional search for overdensities. This method allows to find groups in all possible dynamical states, and the availability of many redshift surveys and ground facilities to collect data makes it popular and effective. It is common to use a friends-of-friends (FOF) algorithm, as per this study, developed in the early '80s by Geller and Huchra [1983], to determine its members. The algorithm works generally as follows:

- chooses a galaxy not assigned to a group or a cluster;
- defines a characteristic length called 'linking length', conventionally b=0.2 for Ω=1 cosmologies [Davis et al., 1985; Lacey and Cole, 1994];
- searches for 'friends' (i.e. galaxies) within the linking length;
- adds the 'friends' as members of the group;

the search is repeated using every new member as centre until no new 'friends' are found. If no galaxies are found after the first run, the galaxy is defined as isolated. The main disadvantage of this method is the limited depth of spectroscopic surveys (the 2-degree-Field Galaxy Redshift Survey (2dFGRS) used in this work goes down to a magnitude $b_J = 19.45$, Colless et al. [2001]), because of which many galaxies are left out from the search being too faint to observe. However, the optical selection was used for this work since the main aim was to select a sample of groups in a wide range of evolutionary states.

The study of groups and clusters relies on the study of their member galaxies. The next section will describe some of the galaxy properties known from literature.

1.2 Galaxy Properties

Historically, the study of galaxies started from observing their morphology. A study by Oemler [1974] and then formalised by Dressler [1980] discovered the well known morphology-density relation in clusters [and then by Blanton and Moustakas, 2009; Boselli and Gavazzi, 2006; Goto et al., 2003; Whitmore et al., 1993]: early-type morphologies (i.e. ellipticals, lenticulars) are more likely to be found in denser environments, while spirals inhabit low density regions. This relation, originally found in clusters, is also observed at lower densities and within groups [Hashimoto and Oemler, 1999; Postman and Geller, 1984; Tran et al., 2001; Zabludoff and Mulchaey, 1998].

However, accurately inferring galaxy morphology requires a time consuming visual inspection, high-quality imaging which often isn't available and does not necessarily correlate with other galaxy properties. As an alternative, galaxy-type studies are more often performed using colours, which are sensitive to a combination of stellar population age, metallicity and dust. As expected, the results from these studies are consistent with those based on visual morphology with the fraction of red galaxies higher in dense environments, $\sim$ 70 %, than in lower density regions, $\sim$ 10 - 30 % [Baldry et al., 2004; Balogh et al., 2004; Hogg et al., 2004; Strateva et al., 2001].

Many works have observed and confirmed that the star formation properties of galaxies in different environment (i.e. clusters, field) are considerably different [e.g. Balogh et al., 1997; Dressler et al., 1985; Koopmann and Kenney, 1998].
The star formation rate (SFR) distribution is traced by colour and thus shows a dependence with environment [Balogh, 1999; Balogh et al., 1997, 1998; Poggianti et al., 1999], galaxies found in a low density environment have a higher star formation rate than those in areas with a higher local galaxy density [Gómez et al., 2003; Lewis et al., 2002; Mahajan and Raychaudhury, 2009]. However, the trend is observed only in the fraction of star-forming galaxies, not in the rate at which star formation occurs [McGee

et al., 2011; Peng et al., 2010; Wetzel et al., 2012].
Furthermore, from recent observations the decline in star formation appears to be slow (few Gyrs), suggesting that only the hot gas is removed, while the reserve of cold gas is consumed [Balogh, 1999; Balogh et al., 2000; Gallazzi et al., 2009; McGee et al., 2008, 2009; Moran et al., 2006].

It was also observed that the evolution of the star formation depends on the halo mass to light ratio (M_{200}/L_B), which increases with the group mass [Eke et al., 2004b; Girardi et al., 2002]. In a large halo the star formation rate depends on the amount of gas cooling, in smaller haloes feedback processes are more efficient at disrupting the star formation.

Although these three indicators (morphology, colour and SFR) roughly correspond to each other, it is not the case for all galaxies. In fact, red passive spiral galaxies have been observed in the infall region of clusters. The existence of this population suggests that there may be separate processes which transform morphology and SFRs [Masters et al., 2010; Wolf et al., 2009].

Some works discern between the brightest group galaxy (BGG) and satellite galaxies (i.e. all the other members), finding that the properties of satellite galaxies in groups are strongly correlated with the properties of the BGG. In particular, Weinmann et al. [2006] demonstrated that quenched BGGs are surrounded by a larger fraction of quenched satellites even at fixed halo mass, which has been subsequently confirmed and explored in several papers [Hartley et al., 2014; Hearin and Watson, 2013; Hearin et al., 2014; Kauffmann et al., 2010, 2013; Knobel et al., 2015; Phillips et al., 2014; Prescott et al., 2011; Wang and White, 2012]. This correlation is known as 'galactic conformity'.

Other properties studied such as the presence of Active Galactic Nuclei (AGNs), the position of galaxies and their properties in the Large Scale Structure (LSS) of the Universe.

For instance, the distribution of AGN in dense environment compared to the field showed an excess of AGNs in the central regions of clusters, which seems to increase at higher redshift [Galametz et al., 2009; Martini et al., 2007, 2009].
On the LSS side, redshift surveys of the nearby Universe showed that, if compared to the distribution of all the galaxies in the sample, the distribution of group centres traces the large-scale structure [e.g Ramella et al., 1989]. While, Lietzen et al. [2012] concluded that galaxies in groups of similar richness (i.e. number of members) are more likely to be passive if the group is in a super-clusters.

Since the galaxy properties hence their evolution, appear to depend on the environment in which the galaxy resides, many studies tried to uncover what mechanism were responsible for galaxy evolution.
Galaxies evolve driven by internal processes and by the physical interaction with their surroundings. Figure 1.3 shows a cartoon listing the mechanisms responsible for galaxy evolution and their relative timescale.
Different processes are invoked to explain how the environment can affect galaxy evolution. The most efficient in groups appears to be the direct galaxy-galaxy interactions, mergers and tidal effects, due to the low velocity dispersion of the systems [Barnes, 1989; Governato et al., 1991]. Other mechanisms, such as ram-pressure stripping and harassment, are known to be more efficient in the more massive cluster environment [Abadi et al., 1999; Brüggen and De Lucia, 2008; Gunn and Gott, 1972].
In the following sections the mechanisms that may be responsible for the evolution of galaxies are briefly described.

1.2.1 Internal Evolution

Internal (or passive) evolution only depends on a galaxy's internal processes:

- gas cooling,

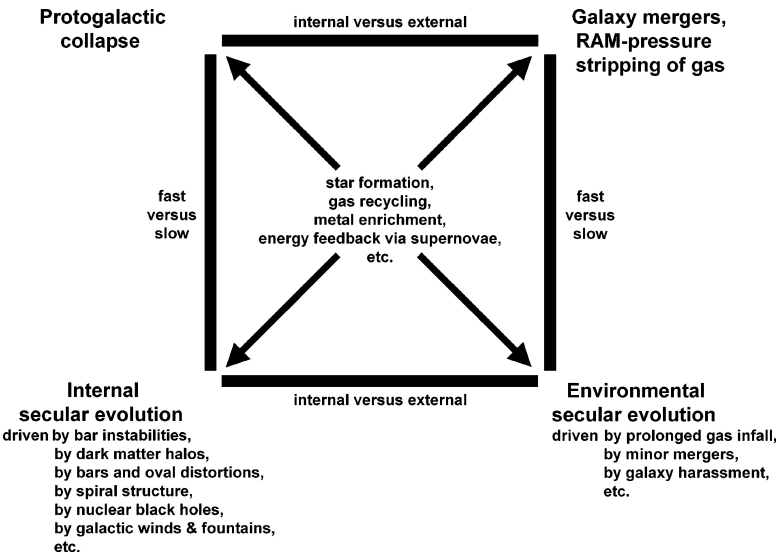

Figure 1.3: Cartoon showing the processes of galactic evolution and their qualitative timescales [Kormendy, 1982]. Processes are divided into fast (top) and slow (bottom). Fast evolution happens on a 'dynamical' timescale, $\sim (G\rho^{-1/2})$, where ρ is the density of the object and G the gravitational constant. Slow means many galaxy rotation periods. Processes are further divided into internal (left) and driven by the environment (right) [Kormendy and Kennicut, 2004].

- supernovae (SN) feedback,
- AGN feedback and
- presence of a bar.

Galaxies form stars as long as there is a gas reservoir, sometimes supplied with gas cooling from the outer hot gas halo, then the stars will age, turn redder [Gadotti, 2011], and the gas will be metal enriched [De Propris et al., 2005]. When the gas reserve is depleted, the star formation will cease, leaving the stars to passively age. This is usually the way isolated elliptical galaxies evolve [Combes, 2005].

SN and AGN feedbacks can prevent the gas from cooling or push the internal gas out in the IGM, stopping the star formation [Cattaneo et al., 2009; Dekel and Silk, 1986; Efstathiou, 2000], while barred spiral galaxies usually evolve into bulgy galaxies via the bar-instability process [Bower et al., 2006].

This kind of evolution continues undisturbed until galaxies interact with each other or with the surrounding environment.

1.2.2 Environment-related Processes

When galaxies live in dense environments, they interact with the surrounding medium (i.e. hot gas residing in the gravitational potential well of a cluster) and with each other. Different processes are invoked to explain galaxy evolution in dense environments:

- ram-pressure stripping,
- strangulation,
- starvation
- mergers,
- harassment,
- tidal fields.

Ram-Pressure stripping

Ram-pressure stripping is due to the pressure exerted by the ICM/IGM (Intra-Cluster Medium/Intra-Group Medium) on the infalling galaxy. It affects the intra-galactic medium, cold gas, which is stripped away [Gunn and Gott, 1972; Larson et al., 1980]. It has an induced pressure force $\sim \rho\sigma^2$, where ρ is the density of the IGM and v the velocity of the galaxy [Gunn and Gott, 1972]. This process appears to be efficient in galaxy clusters, while as the velocity dispersion of galaxy groups are typically $\lesssim 500$ km s^{-1} galaxies infalling are slower, thus the pressure exerted on the gas is smaller. However, Fabello et al. [2012] found evidence for rapid ram-pressure stripping even in small haloes ($\sim 10^{13}$ M$_\odot$) [see also Bösch et al., 2013; Catinella et al., 2013], this could be due to the density distribution of the Intra-Group Medium.

The timescale for stripping, from the time the galaxy enters the cluster to the time all the gas is stripped, is estimated to be of the order of $\sim$ 100-200 Myr [Boselli and Gavazzi, 2006; Crowl and Kenney, 2008; Roediger and Brüggen, 2007; Vollmer et al., 2004, 2008, 2009, 2012], although in massive galaxies only a fraction of the total gas is removed, while the star formation is completely stopped in dwarf galaxies [Boselli et al., 2008].

Despite the fact that ram-pressure stripping is considered a quenching mechanism, Sun et al. [2007] suggested that initially it might trigger star formation, both within the galaxy (as the gas gets compressed by the pressure) and in the stripped material where the gas is compressed by turbulent motion. It is widely believed that spiral galaxies stripped of their gas transform into lenticular galaxies [Boselli et al., 2006, 2009; Gunn and Gott, 1972; Kormendy and Bender, 2012; Laurikainen et al., 2010; Moran et al., 2007].

Simulation of ram-pressure stripping showed that it takes $\geq$ 1 Gyr [Tonnesen et al., 2007] to completely remove the gas from the galaxy. It also appears that this mechanism can be efficient out to the cluster virial radius [Fossati et al., 2012; Gavazzi et al., 2001; Scott et al., 2012; Yagi et al., 2010]. Abadi et al. [1999] simulated winds typical of those experienced by group and cluster galaxies, and concluded that ram-pressure was only efficient in the cores of massive clusters, but not in less dense environments (i.e. galaxy groups) [see also Brüggen and De Lucia, 2008; Gunn and Gott, 1972]. However simulations depend hugely on the assumptions on the gas distribution and do not include proper feedback, so the results obtained remain uncertain.

Strangulation/Starvation

Strangulation occurs when the hot gas of a galaxy halo is stripped by the group or cluster halo, preventing it from cooling to supply cold gas for star formation, hence once the cold gas reserve is depleted the galaxy cannot form new stars [Balogh et al.,

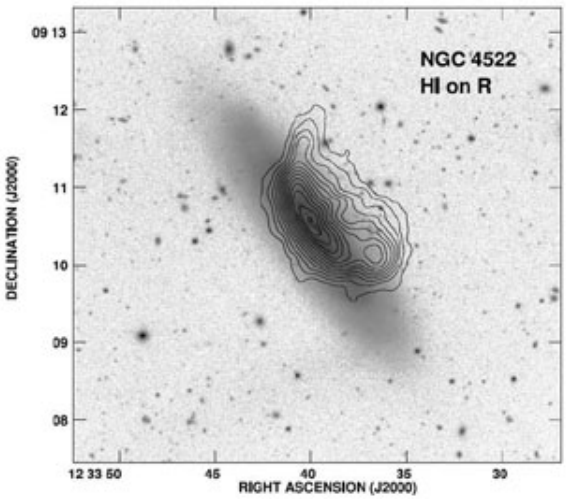

Figure 1.4: Galaxy NGC 4522 in the Virgo Cluster affected by ram-pressure stripping. The image is in the R-band while the contours represent the HI emission (1.4 GHz). This processes has no effects on the stellar distribution, but it acts on the gas which is bent in the direction opposite to that of infall [Kenney et al., 2004].

2000; Bekki et al., 2002; Larson et al., 1980]. Figure 1.5 illustrates how the process works.

Rasmussen et al. [2006a] suggested that strangulation could be important in groups since in this environment stripping is not sufficient to deprive the galaxy of its cold gas as well. However it could deplete the hot gas reserve leading to a strangulation process. In addition, simulations confirmed that strangulation is still effective in low mass groups [Kawata and Mulchaey, 2008; McCarthy et al., 2008].

Peng et al. [2015] estimated the typical timescale for local galaxies of mass $M^* < 10^{11}$ $M_\odot$ to be 4 Gyr before all the gas is consumed.

Similarly to ram-pressure stripping, strangulation is believed to produce lenticular galaxies from spirals [Larson et al., 1980].

Merger

Mergers are low-speed encounters between galaxies, very efficient in groups because of their low velocity dispersion (a few hundred km s^{-1}) and the close proximity of the

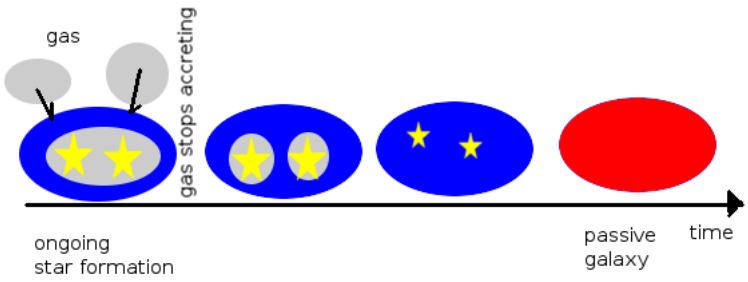

Figure 1.5: Cartoon illustrating the strangulation process, time moves from left to right. Initially gas is accreted onto the galaxies and fuels the star formation. When gas stops being accreted the star formation continues until the gas reserve is depleted. When no more gas is available the stars simply age and no new one are formed.

members, with a merger timescale given by $\tau_{merge} \sim \sigma^3$.

This process is responsible for the change in galaxy morphology, bringing to the disruption of the spiral arms in spirals and leading to the formation of massive ellipticals, effectively decreasing the number of galaxies [Toomre, 1977].

When gas-rich galaxies interact and merge, their interstellar gas can be compressed and driven to the inner regions through shocks and gravitational torques, triggering intense starbursts [Sanders et al., 1988]. Simulations confirm this scenario and show that mergers induce an intense and brief (of the order of a hundred Myr) burst of star formation before the final coalescence [Hopkins et al., 2006].

Harassment

Galaxy harassment is the result of high speed galaxy encounters within clusters or groups [Moore et al., 1998]. It occurs when a low mass galaxy passes within 50 kpc of a massive galaxy, however the velocity is too high to slow down the galaxy and lead to a minor merger. It can produce a disturbed galaxy morphology (i.e. formation of a bar, prolate morphology) and starbursts, it can also cause the loss of peripheral stars

Figure 1.6: Figure shows the final stage of a galaxy-galaxy merger. In this object known as NGC 2623 the disrupted spiral arms are well visible as long tails, also noticeable are star-forming regions originated where shock waves compress the gas [HLA, b].

which will become intra-cluster stars [Willman et al., 2004].

Due to the high relative velocity of the galaxies, this process is more likely to happen in clusters compared to groups.

As a consequence of harassment it is thought that spirals evolve into dwarf ellipticals [Moore et al., 1998].

Tidal Interaction

Tidal effects where described for the first time by Zwicky [1956, 1959].

Given the low velocity dispersion of galaxies in groups (a few hundred km s^{-1}), comparable to those of individual galaxies, tidal interactions play a prominent role in galaxy evolution. Both galaxies feel each other gravitational force causing the outermost stars and gas to get pulled away, forming long tails.

Tidal fields, due to a close encounter between galaxies, can be responsible for the suppression of star formation, since they remove the galaxy interstellar gas, necessary to

Figure 1.7: Close encounter between two late-type galaxies known as Arp 237. The image shows the spiral arms distorted due to the tidal interaction between the two galaxies [HHT].

form stars, or they can ignite a starburst because the disturbed gas is compressed. Eventually, the two galaxies will merge. Tidal forces due to the group or cluster potential can have a similar effect [e.g. Willman et al., 2004].

All of these processes are ongoing, but their strength and time scales are still very much debated.

Recent observations suggest that galaxies are influenced by the local environment even at mass scales much smaller than those of big galaxy clusters [Balogh and McGee, 2010]. However, galaxies are not necessarily transformed as soon as they are accreted by a larger structure, as supported by the observation of star-forming galaxies in groups and clusters. To do this the color-magnitude plot is observed. It shows three distinct regions: the red sequence, the blue cloud and the green valley (see Figure 1.8). The red sequence is mainly populated by passive early-type galaxies, the blue cloud by star-forming late-type galaxies, while the green valley is the scarcely populated area between the two. This diagram suggests that when quenching occurs it acts rapidly, thus explaining the absence of a shift in the blue cloud population, as well as an increased population of green valley galaxies in a colour magnitude diagram [Wetzel et al., 2012]. Wetzel et al. [2013] suggested that these clues support a 'delayed-then-rapid' quenching scenario in which satellites continue forming star for several Gyrs after their first infall, then quenching occurs rapidly.

The results from the GIMIC simulation [Bahé et al., 2013] suggest an 'interrupted strangulation' scenario where the galaxy evolution is initially dominated by internal processes that consume the available gas. Once part of the gas has been used, stripping then removes the remaining ISM.

Many recent observation are in disagreement with this descriptions suggesting that the decline of star formation occurs slowly in both groups and clusters [e.g. Balogh, 1999;

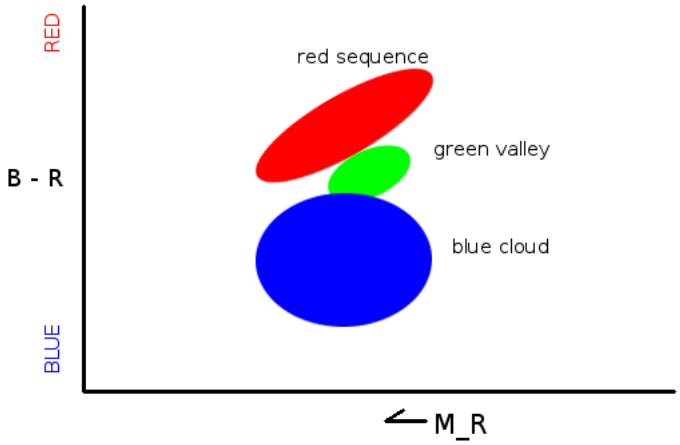

Figure 1.8: Cartoon illustrating the colour-magnitude diagram, R-band absolute magnitude is on the x-axis, B-R colour on the y-axis. The red sequence is populated by red and dead massive galaxies while the blue cloud by star-forming galaxies. The green valley is an intermediate region scarcely populated where galaxies such as red spirals can be found.

Balogh et al., 2000; De Lucia et al., 2012; Gallazzi et al., 2009; McGee et al., 2008, 2009; Moran et al., 2006; Rasmussen et al., 2012; Taranu et al., 2014; von der Linden et al., 2010; Vulcani et al., 2010]. This is supported by observations of galaxies with truncated or distorted $H\alpha$ disks, suggesting that star formation is truncated in the outskirts of a galaxy first rather than all at once [e.g. Bamford et al., 2007; Koopmann and Kenney, 2004].

The current picture of galaxy evolution suggests that galaxies are affected in different ways by their surrounding environment, and this depends on the galaxy stellar mass and on the host halo mass . On top of this all the processes invoked have different efficiencies at different epochs. Furthermore, it not clear whether the galaxies are uniformly affected or the outer and inner regions go through different transformations.

Many works done on this topic have shown the importance of the environment in influencing the evolution of galaxies, the first observational evidence for this was the

morphology-density relation discovered in the early 80s. Other similar studies on morphology, colour, and star formation properties, confirmed that the environment is responsible for the quenching of the star formation in a galaxy, which leads to old stellar populations with typical red colour, and to morphological evolution towards massive red, passive elliptical galaxies.

The study of groups is a powerful tool to understand the history of galaxies evolution, given their variety of dynamical states, densities, etc. Furthermore, the cluster physics alone is not able to explain the galaxy properties in rich structures, for that reason Zabludoff and Mulchaey [1998] suggested the necessity to invoke a pre-processing mechanism which would be effective in groups.

Despite the fact that many studies were carried and the field is progressing, a complete picture based on multi-wavelength observations is still missing. This work will try to present a broad view on the group properties described in this chapter, and how galaxy properties are affected, by studying a set of groups with available multiple wavelength data. The final aim of the work is to look for hidden correlation in the data and to classify the groups according to their evolutionary state, in order to study how the galaxies are affected by them. This might give new insights on the evolution and growth of structure, as well as on the way the environment influences the galaxy evolution.

This thesis is structured as follows: Chapter 2 is a general introduction of optical spectroscopy, Chapter 3 describes the data sample used and the data analysis performed to pre-process the data, Chapter 4 describes the analysis correlation and clustering analysis performed on the group properties, Chapter 5 illustrates the study of the galaxies properties based on the group properties, finally the Conclusions are presented.

Throughout the analysis we use the AB magnitude system and a flat, ΛCDM cosmology of h=0.7, $\Omega_m = 0.3$, and $\Omega_\Lambda = 0.7$.

Chapter 2

Optical Spectroscopy

This chapter will present an overview on spectroscopy and its importance in deriving the properties of a galaxy stellar population, the informations it contains will be used in the Lick indices analysis described in Section 3.5.

Spectroscopy is the study of the energy distribution, in wavelength or frequency, of the light emitted by an astronomical source.

All objects and physical electro-magnetic processes emit light at one or more wavelengths. If this light is dispersed using a prism (or a grating), one can see the spectrum; this word refers to the plot of light intensity as a function of frequency or wavelength, and it is characterised by a continuous shape plus numerous features, the emission and absorption lines. The ability to identify such features depends on the spectral resolution of the instrument R:

$$R = \frac{\lambda}{\delta\lambda} = \frac{\nu}{\delta\nu}, \tag{2.1}$$

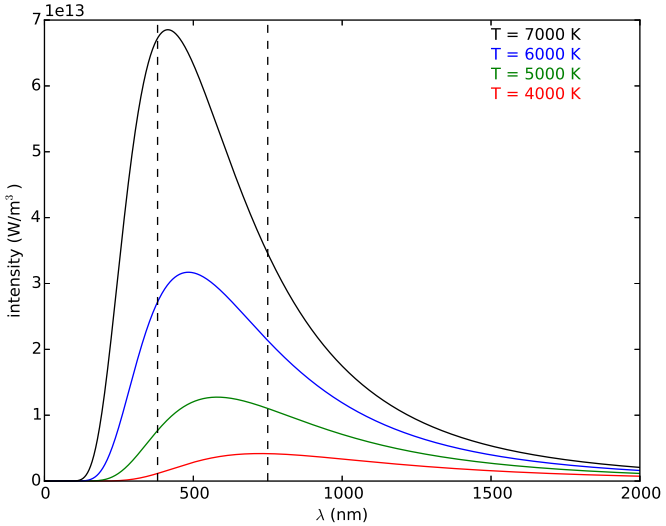

Figure 2.1: Blackbody spectra shown for four different temperatures (7000, 6000, 5000 and 4000 K), the vertical dashed lines show the wavelength range of the optical window. On the x-axis it is shown the wavelength in nm, on the y-axis the intensity in W/m^3.

defined as the smallest difference in wavelength $\delta\lambda$ (or frequency $\delta\nu$) that can be distinguished at a given wavelength λ (or frequency ν) [Tennyson, 2005].

A spectrum is made of three essential elements:

- the continuum emission,
- the absorption lines,
- the emission lines.

The continuum spectrum of a body in thermal equilibrium, such as a star, is a blackbody spectrum (Figure 2.1): the height and position of the peak depend on the temperature of the source. As the temperature of the emitting body increases, the position of the emission peak (λ_{peak}) moves to shorter wavelength as described by Wien's displacement law

$$\lambda_{peak} T = 2.898 \times 10^{-3} mK, \tag{2.2}$$

and the height of the curve increases as described by Stefan-Boltzmann's law [for more details see Section 1.5 Rybicki and Lightman, 1979]

$$I = \sigma T^4, \tag{2.3}$$

where I is the energy emitted per unit surface area, T the temperature, and $\sigma = 5.67 \times 10^{-8}$ W m^{-2} K^{-4} the Stefan-Boltzmann constant.

Emission and absorption lines derives from atomic or molecular transition of the elements or compounds present in the observed source, each one typical of a certain element or compound. The wavelength at which the line is observed corresponds to the difference between the energy levels involved in the transition according to Planck's Equation [for more details see Section 2.1 and 2.2 Tennyson, 2005]:

$$E = h\nu = \frac{hc}{\lambda}, \tag{2.4}$$

where $h = 4.135667662 \times 10^{-15}$ is the Planck constant, c the speed of light, and λ and ν the wavelength and frequency respectively. All energy levels of an atomic or molecular species define a line series, unique for each atom or molecule, however single lines can be overlapping for different species. A line is in emission when an electron jumps from a higher to a lower level (i.e. the electron loses energy), and in absorption when the jump occurs from a lower to a higher level (i.e. the electron gains energy); each transition is characterised by a wavelength, as previously stated, and a probability of occurrence. A distinct class of lines, called 'forbidden', originate from transitions that require a long time to happen and have a very low probability of occurrence (10^{-9}-10^{-10}). These can only take place in very rarefied gas where the probability of the atom to interact is low, for this reason they are observed in astronomical spectra, but not in laboratory spectra [Section 5.3 Tennyson, 2005].

To measure absorption and emission line strengths a quantity called equivalent

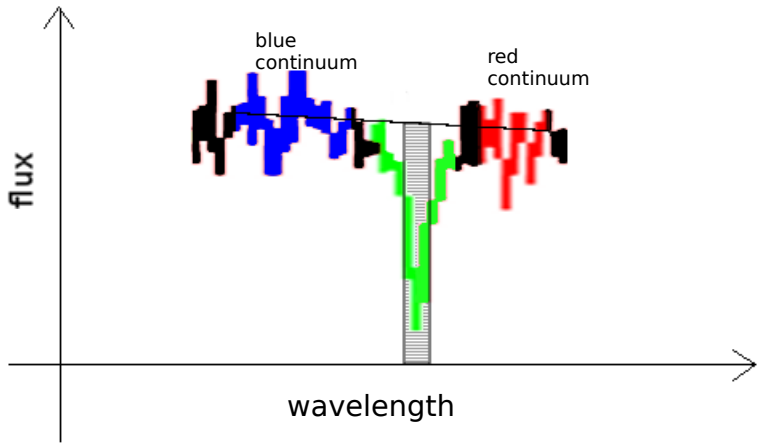

Figure 2.2: Cartoon showing the equivalent width corresponding to the absorption line, in green. The shaded rectangle is defined to contain the same area as the green line. The original spectrum is in black while in blue and red the continuum at shorter (blue passband) and longer (red passband) wavelengths respectively. The spectrum is fitted on both sides of the line in order to define the continuum level from which to measure the line strength.

width is defined. It is described as a rectangle with height equal to that of the line peak-to-continuum emission, and width such that the area of the rectangle is equal to the area described by the spectral line. The continuum emission from which to measure the line is derived interpolating the flux on each side of the line, hence a blue (lower wavelength) and a red (higher wavelength) passbands need to be defined. Figure 2.2 illustrates the definition of equivalent width, the equation used to calculate it is [for details see Section 9.1 Draine, 2011]:

$$W_\lambda = \int \left(1 - \frac{F_\lambda}{F_0}\right) d\lambda, \tag{2.5}$$

where F_λ is the line flux and F_0 is the continuum flux.

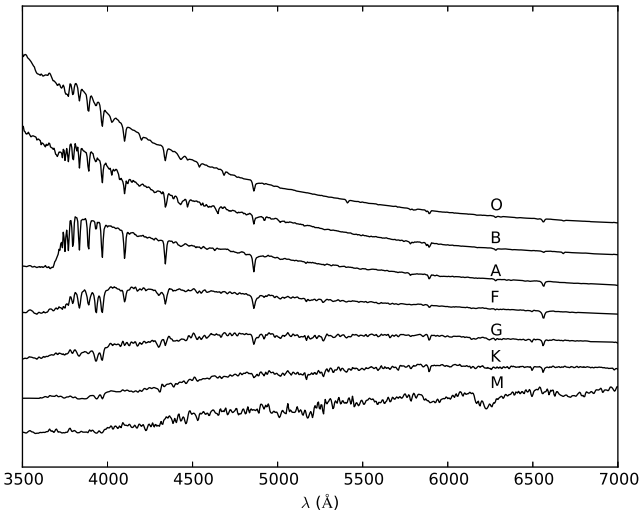

Figure 2.3: Spectra of different stellar types (O, B, A, F, G, K, M) in the visible wavelength.

The Sun was the first star observed with a spectrograph, and since then many of the stars in the Milky Way have been observed, all showing somewhat similar spectra but with very distinctive features. This led to the classification of stars into seven main types (O, B, A, F, G, K, M), based on the shape of their spectrum and hence their physical properties. For instance, the temperature of the star can be inferred from the shape of the continuum and its chemical composition from the study of the absorption lines. The type is also tied to the star mass and evolutionary state. Figure 2.3 shows the spectra of different stellar types in the visible wavelength. In massive young and hot stars (Type O and B) the peak of the continuum spectrum is in the ultra-violet (UV), then it moves toward longer wavelengths as mass decreases and age increases; the absorption lines, being signatures of specific elements, do not move in wavelength [for more details see Section 2.2.1 Gray et al., 2009].

Galaxy spectra are a combination of stellar spectra, hence being able to study them can reveal insights on the stellar population properties. The next section will describe galactic spectra and how to interpret them in view of the spectral analysis performed in this work.

2.1 Galaxy Spectra

A galaxy spectrum is the superposition of the spectra of all the stars in the galaxy and the gas that fills the space among them, the IGM (Inter Galactic Medium). Hence, using the spectrum we can infer galaxy properties (i.e. redshift, type), stellar properties (i.e. kinematics and star formation history), and gas properties (i.e. density, metallicity). Different components characterise a galaxy spectrum:

- the continuum,
- the absorption lines,
- the emission lines,
- the 4000 Å breaks and
- the Balmer breaks.

The continuum and the absorption lines derive from the sum of the stellar spectra continuum and absorption lines respectively. Lines in absorption originate on the surface of cold and metal rich stars, or are due to the presence of cold gas or dust in the interstellar medium (ISM). Some lines are more evident than others and easily recognisable in the continuum shape, the main one originating in cold stars are the Calcium K and H lines (λ3933.66 and λ3968.47) [NIST], Mg_b(λ5142.63), NaD(λ5860.63) 3.2, and various

$\Delta n = (n_2 - n_1)$	transition	name	λ_0 Å
1	3 - 2	Hα	6563
2	4 - 2	Hβ	4861
3	5 - 2	Hγ	4340
4	6 - 2	Hδ	4102

Table 2.1: Table showing the wavelength at which the Balmer lines are observed. The first column shows the transition number, the second the orbitals between which the transition occurs, the third the line name, and the fourth the wavelength in Å [Seeds and Backman, 2016].

iron lines scattered at different wavelengths. Absorption lines are a powerful tool to infer the metal content and the age of the stars populating a galaxy.

Emission lines originate when the ISM gas is ionised either by hot stars or by active galactic nuclei (AGNs). In the first case the gas is excited by the UV radiation emitted from young and massive stars (i.e. OB stars with a temperature of 30000 K or higher), while in the second case the same thing happens by means of the high energy photons or particles emitted by an AGN. The main lines observed in emission are $[OII](\lambda 3727.32)$, $[OIII](\lambda 5006.84)$, $[NII](\lambda 6583.45)$, and $[SII](\lambda\lambda 6716.44, 6730.82)$ [NIST].

Hydrogen, the most abundant element in the Universe, populates the optical spectrum with a series of four lines arising from the transition between the second orbital (i.e. principal quantum number = 2) and the higher levels, called the Balmer series [see Section 3.7 Tennyson, 2005]. The position of the lines is given by:

$$\frac{1}{\lambda_0} = R_H \left(\frac{1}{n_1^2} - \frac{1}{n_2^2} \right), \tag{2.6}$$

where λ_0 is the wavelength, n_1 and n_2 are the orbitals between which the transition occurs, and $R_H = 1.0968 \times 10^7$ m^{-1} is the Rydberg constant for Hydrogen. Table 2.1 describes the visible transitions and the wavelength at which they can occur, both in absorption and in emission.

The Balmer lines in absorption strongly depend on the age of the star, since their depth and width (i.e. their strength) are observed to increase with time after a starburst. The maximum strength observed when the dominating stars are type A stars of age 0.3-1.0 Gyrs.

The Balmer break corresponds to the limit of the Balmer series, it is due to the presence of the high order Balmer lines, which produce a discontinuity in the spectrum at wavelengths smaller than 3650 Å. It overlaps with the 4000 Å break, but has a different origin due of the presence of an intermediate age stellar population.

The 4000 Å break is due to the absorption of high energy photons by the metals in the stellar atmosphere and the high opacity of the gas, indicating the presence of mainly old, cold and metal rich stars with low surface temperature.

2.1.1 How to interpret a spectrum.

Many informations can be inferred by analysing a galaxy spectrum, most of which is deduced studying the lines, both in emission and absorption.

The position of the lines is sometimes observed to be shifted compared to the wavelength seen in laboratory, this effect, known as Doppler shift, is due to the radial motion of a galaxy with respect to the Milky Way. The shift can be observed towards longer and shorter wavelengths for nearby galaxies, where the peculiar motion prevails. It is observed toward longer (more red) wavelengths for galaxies outside the Local Group where the expansion of the Universe is the main component of the motion and it defines the astronomical distance known as redshift [Sections 1.2 Tennyson, 2005]:

$$z = \frac{v}{c} = \frac{\Delta\lambda}{\lambda}, \tag{2.7}$$

where v is the velocity of the source, c is the speed of light, λ the rest-frame wavelength of the transition, and $\Delta\lambda$ the observed change in wavelength.

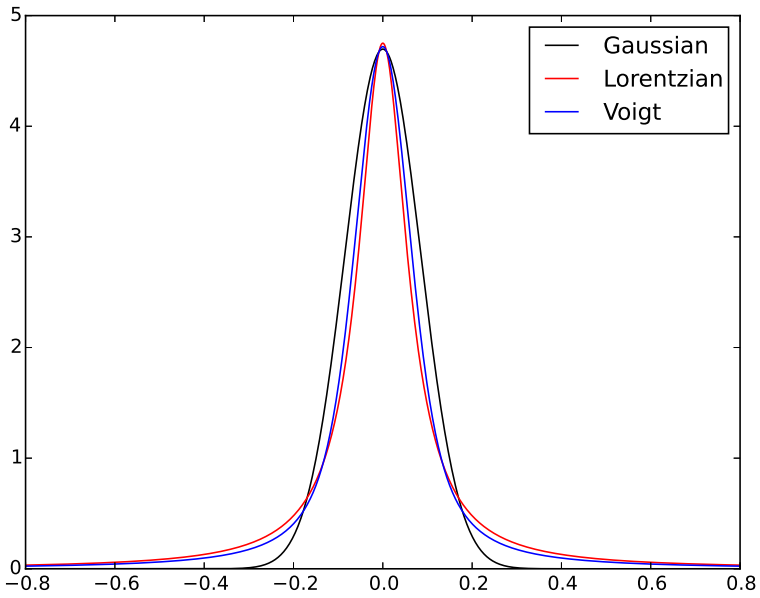

Figure 2.4: Voigt profile shown in blue, resulting from the sum of a Gaussian, in black, and a Lorentzian profile, in red.

The 'strength' or intensity of the spectral lines, whether in emission or in absorption, depends on the number of atoms in which a transition occurs, hence it depends on the density of the gas, and also on its temperature, which determines how many atoms are excited.

Since the lines in a spectrum arise because of the occurrence of electron transitions from two different energy levels, we would expect them to be very narrow, different from a δ-function only because of the natural broadening due to the uncertainty principle. Instead we observe them to have a bell-shape known as Voigt profile, which results from the convolution of a Gaussian and a Lorentzian profile (Figure 2.4).

The two main mechanisms responsible for Gaussian line broadening are: the Doppler broadening due to the thermal motion of the gas within the stars, and the 'turbulent' broadening, which derives from the proper motion of the stars in the galaxy.

The Lorentzian profile is produced by collisional broadening, which occurs if the main

atom experiences a collision while an electron is changing orbital, making this mechanism efficient in high gas density environments. The combination of these effects leads to the final line shape observed: the Voigt profile [see Section 10.6 Rybicki and Lightman, 1979]. These broadening effects need to be taken into account when analysing absorption and emission lines to study the stellar or gas properties within a galaxy.

Absorption lines can be used to infer the properties of the stars in a galaxy, since they originate on the stellar surface. The main properties to be inferred about a stellar population are its age and metallicity. The latter, historically considered as a unique parameter, thanks to a better understanding of stellar evolution, is now described by two components: the α-elements (N, C, Mg, O) abundance and the Fe-peak elements (V, Cr, Mn, Fe, Co, Ni) abundance. These are produced at different stages of the stellar nucleosynthesis, hence on different time-scales. The lighter α-elements originate in Type II supernovae, which occur in massive stars of age 100 Myr or less [Tinsley, 1979], while the Fe-peak elements are formed in Type Ia supernovae which occur in binary systems of age 1 Gyr or more, since one of the two components has to be a white dwarf star.

The major issue in determining age and metallicity of a stellar population from a spectral analysis is the existence of an age-metallicity degeneracy [Worthey et al., 1994]. For instance, for ages > 5 Gyr, if we observe the spectrum of known age and metallicity, we cannot distinguish it from the spectrum of another population three times older and half the metal content (see an example in Figure 2.5).

2.1.2 Stellar population models

All the analysis aimed at studying stellar population properties are based on the availability of synthetic galaxy spectra or stellar population models.

The main ingredient necessary to build a model spectrum is a single stellar population (SSP), which in turn needs four pieces:

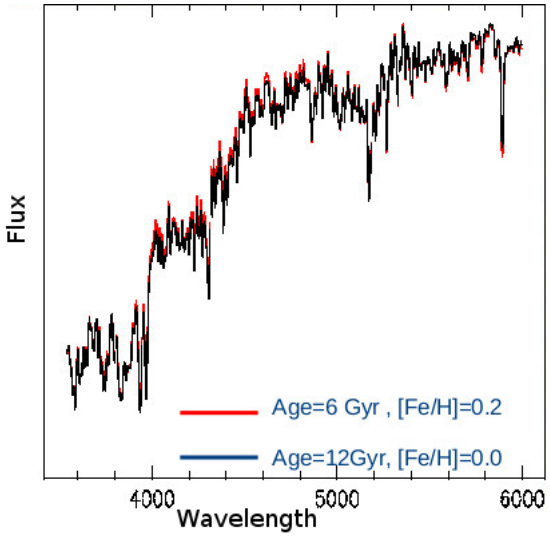

Figure 2.5: Plot showing two degenerate galaxy spectra models: in red the modelled spectrum of a 6 Gyr old galaxy with metallicity 0.2, in black a 12 Gyr old galaxy with solar metallicity. On the x-axis is plotted the wavelength, on the y-axis the flux [Proctor et al., 2005]

.

- isochrones, lines on a temperature luminosity diagram (Hertzsprung-Russell) populated by stars of the same age, but different masses; they determine the relation between mass, surface gravity (log g) and effective temperature (T_{eff}) of a star at a given time and metallicity,
- stellar spectral libraries, catalogues of observed or synthetic stellar spectra; the spectral resolution and wavelength range of these spectra determine the spectral resolution and wavelength range of the models,
- initial mass function (IMF), the number of stars per mass interval at the moment the stars were born,
- dust attenuation law, to take into account the effects of dust on the observed spectrum.

The last two points will be briefly described in the following paragraphs.

The first attempt to describe the IMF was made by Salpeter [1955], and was in the form of a power law:

$$dN = cM^{-\alpha}dM, \tag{2.8}$$

where dN is the number of stars with mass between M and M+dM, and c is the normalisation constant. Salpeter [1955] constrained the value of α to 2.3 for $0.4 <$ m $< 10\ M_{\odot}$, observing stars in the solar neighbourhood. However, given the proximity of the observations, the model is mostly based on low mass stars. The IMF in this form tends to infinity at low masses, thus a different α or shape is expected for M < 0.5 $M_{\odot}$, where the curve flattens as suggested by observations. A later study by Kroupa [2001] lead to an IMF in the form of a broken power-law:

α_0=0.3 for $0.01 \leq m/M_{\odot} < 0.08$,

α_1=1.8 for $0.08 \leq m/M_{\odot} < 0.50$,

α_2=2.7 for $0.50 \leq m/M_{\odot} < 1.00$,

α_3=2.3 for $1.00 \leq m/M_{\odot}$.

Alternatively, Chabrier [2003] introduced a log-normal distribution at low stellar masses ($\sim 1\ M_{\odot}$):

$$M\phi(M) = A_1 exp[-(LogM - LogM_c)^2/2\sigma^2] \quad for \quad m \leq 1M_{\odot}, \tag{2.9}$$

$$= A_2 M^{-x} \quad for \quad m > 1M_{\odot}, \tag{2.10}$$

where A_1 and A_2 are normalisations, M_c is the mean mass and σ is the variance in $logM$.

The most popular IMF used is the one defined by Chabrier, although the consensus is low and all of them are still used in literature.

Dust is a big contributor to the spectral flux shape, thus a stellar population model needs to take this into account. Dust absorbs, scatters and re-emits light in the NUV, optical and IR, with a spectral shape dependent on the grain size, shape and distribution.

The dust mass is estimated to be $\sim$ 1 % of the total HI gas mass, it mainly consists of silicates (Mg/Fe rich) or graphites (C) and its temperature range in emission spans from $\sim$ 10 - 100° K. Light coming from young stars, usually embedded in their formation clouds, is the most affected by dust which absorbs the UV radiation emitted and produces thermal IR radiation, usually observed in highly star-forming galaxies.

Attenuation due to dust is defined as:

$$A_V = m_\lambda - m_{\lambda,0}, \tag{2.11}$$

with m_λ the observed apparent magnitude at a certain wavelength and $m_{\lambda,0}$ the apparent magnitude of a non-attenuated source at the same wavelength. The observable linked to the attenuation is the reddening defined as the difference between the observed and expected B-V colour:

$$E(B-V) = (B-V) - (B-V)_0. \tag{2.12}$$

Attenuation and reddening are linked by:

$$A_V = RE(B-V), \tag{2.13}$$

where R $\sim$ 3.1 for the Milky Way [for details see Section 21.1.1 Draine, 2011].

One of the main problems in modelling dust attenuation is the existence of a dust-age degeneracy: the optical spectrum of a young and dusty galaxy will look similar to that of an old dust-free one.

The most popular dust correction law was empirically estimated by Calzetti et al.

[1994]:

$$Q_e(x) = -2.156 + 1.509x - 0.198x^2 + 0.011x^3. \tag{2.14}$$

Once all the necessary ingredients are available, the synthetic spectrum is obtained integrating the spectrum of all the stars along the line of sight belonging to an SSP. The combination of more than one stellar population defines a composite stellar population, supposedly better descriptive of a real system. The most popular stellar population models available are Bruzual and Charlot [2003]; González Delgado et al. [2005]; Le Borgne et al. [2004]; Leitherer et al. [2010]; Maraston [2005]; Schiavon [2007]; Vazdekis et al. [2010]; Worthey et al. [1994].
The major uncertainties that still remains in the modelling process are:

- the poor understanding of specific stellar evolution phases (i.e. super-giant and asymptotic giant branch (AGB) phases);
- the existence of the age-metallicity degeneracy;
- the non-universality of the chemical abundance ratio.

Stellar population models will be used to fit galaxy spectra in order to infer some of their properties in a later stage of the analysis.

Chapter 3

Data Sample and Analysis

The XI (XMM-IMACS) Groups Project [Rasmussen et al., 2006b] is a multi-wavelength study of 25 groups selected from the group catalogue of Merchán and Zandivarez [2002], derived from a friends-of-friends analysis on the first data release of the 2dF Galaxy Redshift Survey (2dFGRS) [Colless et al., 2001].

The groups were selected between $0.06 < z < 0.063$, the narrow range was chosen to avoid redshift dependence of the group properties, thus no k-correction was necessary. In fact to make sources at different redshifts comparable they need to be corrected by

$$K = 2.5log(1+z) + 2.5log\left\{\frac{\int_0^\infty F(\lambda_0)S_i(\lambda)d\lambda}{\int_0^\infty F[\frac{\lambda_0}{1+z}]S_i(\lambda)d\lambda}\right\}. \tag{3.1}$$

A further selection was applied so that the characteristic radius $R_{200} \sim 1$ Mpc, which corresponds to $13'$ in the sky, matched the field of view of both IMACS (Inamori Magellan Areal Camera and Spectrograph, on the Magellan telescope at Las Campanas Observatory in Chile) used for spectroscopic observation, and XMM-Newton used for X-ray observation. Other selection criteria were: velocity dispersion of the group $\sigma <$ 500 km/s, to include only the poorer and more common systems in the local Universe, and number of confirmed members ≥ 5, to reduce the risk of including groups which

are not real physical associations. Although for this low richness groups the velocity dispersion calculation is not reliable [Old et al., 2014]

3.1 Optical Data

The photometric images were taken using the 100-in Du Pont telescope at Las Campanas Observatory (Chile), using the 2048 × 2048 Wide Field Camera (WFCCD) and the Bessel filters B and R. Each group was observed entirely in one pointing given the telescope field of view of 25 arcmin. Twelve dithered exposures were taken for each group and filter, with exposure times of 24 min in R and 60 min in B. The images were processed and median-combined using IRAF, the sources were identified using SExtractor [Bertin and Arnouts, 1996] and considered only if the stellarity index was > 0.9 and Full Width at Half Maximum FWHM > PSF (Point Spread Function). A fixed aperture slightly larger than the seeing was used to extract the magnitudes, which have been corrected for galactic extinction using the dust map by Schlegel et al. [1998] [Bai et al., 2010; Rasmussen et al., 2006b, 2012].

The spectroscopic observations were obtained with the IMACS spectrograph on the 6.5 m Baade/Magellan telescope at Las Campanas Observatory (Chile) [Bigelow and Dressler, 2003] with a grism made of 300 lines mm^{-1} covering a wavelength range between $3900 \leq \lambda \leq 10000$ Å and with a dispersion of 1.34 Å $pixel^{-1}$. The exposures were 2 hours long per each multi-slit mask, the objects to follow up were selected in the photometric R-band images with priority to the brightest objects in the field of view. Further photometric images of all the 25 groups were also acquired in the R-band covering a field of view of $\sim 15'$ radius corresponding to 1 Mpc, extending at least out to R_{200} for all the groups [Bai et al., 2010; Rasmussen et al., 2006b, 2012].

The photometric data outside the IMACS Field of View (FoV) were obtained from the SuperCOSMO Sky Surveys (SSSs, Hambly et al. [2001]). The spectroscopic data

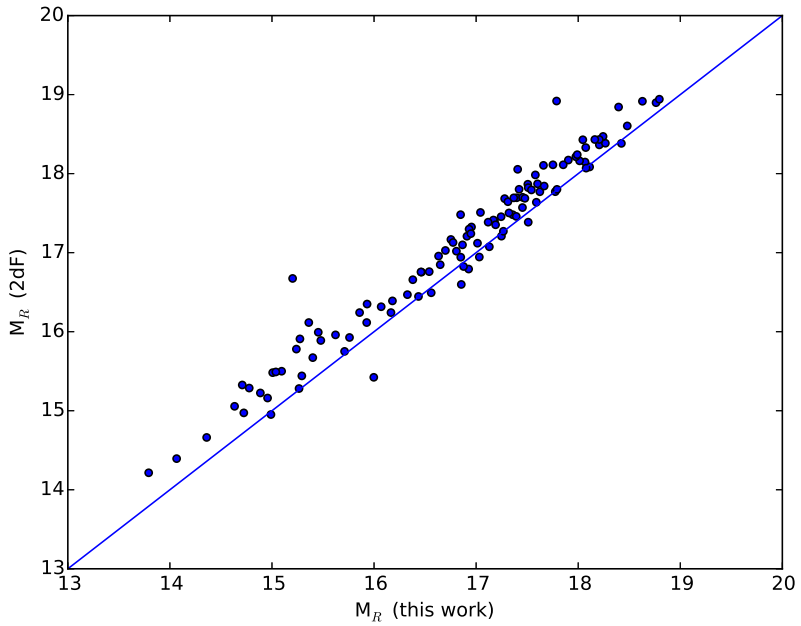

Figure 3.1: This plot shows the comparison between the R-band photometry measured in this work (x-axis) and the one extracted from 2dF (y-axis). The solid line is the identity line.

were extracted from the 2dFGRS (down to $b_J \leq 19.45$) and 6dFGRS (6-degree-Field Galaxy Redshift Survey) [Jones et al., 2009] (down to $b_J \leq 16.75$) [Bai et al., 2010; Rasmussen et al., 2006b, 2012]. However no spectroscopic analysis was performed on these data because of the poor quality and non-uniformity with the IMACS data Furthermore most of these galaxies were at higher radii hence not relevant to the analysis.

To make sure the data are uniform Figure 3.2 shows the comparison between the z obtained in this work with that given by the 2dF survey for the overlapping galaxies. The standard deviation of the distribution $\sigma_{cz} = 107.65$ km/s, hence the two measurement are consistent given the error on cz of 2dF ~ 85 km/s [Colless et al., 2001] and of this work ~ 50 km/s.

A comparison with the original group velocity dispersion was not performed given the

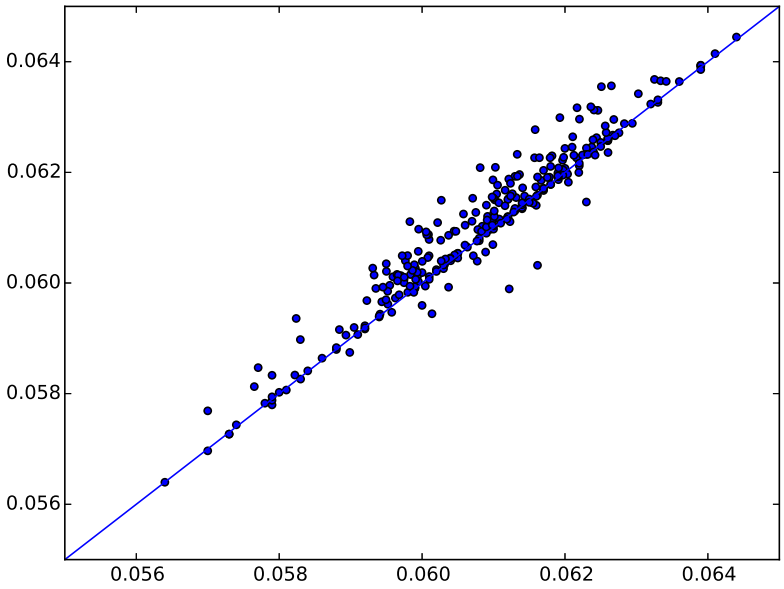

Figure 3.2: This plot shows the comparison between the redshift measured in this work (x-axis) and the one extracted from 2dF (y-axis). The solid line is the identity line.

consistency between the two cz measurement and the fewer number of members of the original 2dF groups.

The final spectroscopic catalogue was 100% complete down to M_R = -20 within 15′ radius, > 80% complete down to $M_R \simeq$ -19 in the internal region (< 10′ ∼ 0.7 Mpc) and > 50% complete out to 25′ (∼ 1.7 Mpc).

The galaxy velocities (cz) were obtained cross-correlating the spectra with SDSS templates, as described in Zabludoff and Mulchaey [1998], with errors of $\delta v \approx 50$ km/s. The velocity dispersion (σ) and membership of the groups were defined using a bi-weight estimator of σ [Beers et al., 1990] which iteratively discards 3σ outliers in redshift from a list of objects within 2000 km/s from the group main velocity, until the number of group members converged. 1σ error on σ was estimated using the bootstrap technique from Beers et al. [1990].

From the velocity dispersion and the redshift of the group the characteristic quantities R_{200} and M_{200} were calculated as Finn et al. [2004] [Bai et al., 2010; Rasmussen et al., 2006b, 2012]:

$$M_{200} = 1.2 \times 10^{15} (\frac{\sigma}{1000})^3 [\Omega_\Lambda + \Omega_m (1+z)^3]^{-\frac{1}{2}} h_{100}^{-1} M_\odot. \tag{3.2}$$

and

$$R_{200} = 1.73 \frac{\sigma}{1000} [\Omega_\Lambda + \Omega_m (1+z)^3]^{-\frac{1}{2}} h_{100}^{-1} Mpc. \tag{3.3}$$

They refer to mass and radius calculated where the density is 200 times the critical matter density of the Universe at that redshift ($\Omega_\Lambda = 0.7$, $\Omega_m = 0.3$). Completeness issues would not bias the total mass estimated with this method, however a biassing factor could be the non-virialised state of the groups which would lead to an overestimate of the velocity dispersion hence of the mass. The complete list of XI groups with some of their optical properties is shown in Table 3.1.

The group centres, or centroids, were defined as the brightest galaxy within 0.5 Mpc

Group Name	z	σ (km/s)	RA (deg) (J2000)	Dec (deg) (J2000)	M_{200} $M_\odot$	R_{200} (Mpc)
MZ770	0.0606	215	334.013364	-27.948993	1.68×10^{13}	0.52
MZ1766	0.0610	227	9.615492	-27.188079	1.96×10^{13}	0.55
MZ3067	0.0602	168	334.181945	-25.754789	8.01×10^{12}	0.41
MZ3182	0.0612	244	334.785208	-27.061269	2.42×10^{13}	0.59
MZ3541	0.0627	121	150.970816	-4.145322	2.99×10^{12}	0.29
MZ3698	0.0609	215	149.971906	-5.753289	1.67×10^{13}	0.52
MZ3849	0.0606	284	157.028493	-3.321549	3.85×10^{13}	0.68
MZ4001	0.0593	324	154.063201	-3.238172	5.70×10^{13}	0.78
MZ4548	0.0625	156	163.514718	-5.951039	6.41×10^{12}	0.38
MZ4577	0.0621	231	173.155471	-4.010130	2.07×10^{13}	0.56
MZ4592	0.0616	205	172.625530	-3.736310	1.45×10^{13}	0.49
MZ4881	0.0613	509	175.050688	-3.532303	2.21×10^{14}	1.22
MZ4940	0.0620	64	173.963707	-3.761676	4.44×10^{11}	0.15
MZ5293	0.0620	103	184.183716	-3.430441	1.87×10^{12}	0.25
MZ5383	0.0595	189	188.788030	-3.597105	1.14×10^{13}	0.46
MZ5388	0.0598	143	188.634702	-3.428302	4.95×10^{12}	0.35
MZ8816	0.0608	290	1.776022	-27.761532	4.08×10^{13}	0.70
MZ9014	0.0608	288	9.413943	-27.466271	4.01×10^{13}	0.69
MZ9069	0.0615	361	7.136590	-27.506352	7.85×10^{13}	0.87
MZ9137	0.0601	328	4.669429	-27.898349	5.92×10^{13}	0.79
MZ9307	0.0598	334	10.139198	-27.504457	6.23×10^{13}	0.80
MZ9994	0.0621	224	30.535098	-29.227547	1.88×10^{13}	0.54
MZ10167	0.0606	200	27.792321	-27.721146	1.34×10^{13}	0.48
MZ10300	0.0618	271	36.105660	-28.365762	3.33×10^{13}	0.65
MZ10451	0.0610	454	37.439008	-29.631234	1.57×10^{14}	1.09

Table 3.1: Group sample: the first column contains the name of the groups, second and third columns are redshift and velocity dispersion (not corrected for the velocity uncertainty) respectively, RA and Dec are the group centroid coordinates, and the last two columns are M_{200} and R_{200}.

of the old group centre and with velocity within 2σ of the group mean velocity.

To calculate the galaxy stellar mass the galaxies which overlap with SDSS had to be used to derive a calibration for the R-band mass-to-light ratio and the B-R colour using the *kcorrect* package by Blanton and Roweis [2007]. The derived relation was used to estimate the stellar mass for all the other galaxies, included those with no B-band observation. The uncertainty on the stellar mass calculation is ~ 45 % for each galaxy [Bai et al., 2010; Bell et al., 2003].

The Sersic indices were obtained using GALFIT v3.0 [Peng et al., 2010] to fit a 2-D Sersic profile to the surface brightness distribution of 471 spectroscopically confirmed members, fit region was chosen manually (Rasmussen in preparation). Galaxies with Sersic index > 8 and $\chi^2 > 10$ were visually inspected and re-fitted with masking of nearby objects.

3.2 Infra-Red Data

The 24 μm infra-red (IR) observations were performed with the Spitzer satellite in 2007-2008, using MIPS (Multiband Imaging Photometer for Spitzer) [Rieke et al., 2004], with field of view $20' \times 45'$ ($\sim 1.4 \times 3.1$ Mpc^2) and spatial resolution ~ 5", centred on the group centroid. The data were processed with the MIPS Data Analysis Tool (DAT ver. 3.02, Gordon et al. [2005]) and the final exposure time was ~ 80 s pixel^{-1}. The sources were extracted with SExtractor [Bertin and Arnouts, 1996] using a variable aperture with a 3σ point source detection limit ≤ 0.35 mJy and cross-correlated with the galaxy optical images within the spatial resolution.

The star formation rate (SFR) was extracted from the 24 μm flux for 6×10^8 L$_\odot \leq$ L(24) $\leq 1.3 \times 10^{10}$ L$_\odot$ and for L(24) $> 1.3 \times 10^{10}$ L$_\odot$ respectively as[Rieke et al., 2009]

$$SFR(M_{\odot}\mathrm{yr}^{-1}) = 7.8 \times 10^{-10} L(24\mu m, L_{\odot}) \tag{3.4}$$

$$SFR(M_{\odot}\mathrm{yr}^{-1}) = 7.8 \times 10^{-10} L(24\mu m, L_{\odot}) \times (7.76 \times 10^{-11} L(24\mu m, L_{\odot}))^{0.048}. \tag{3.5}$$

These equations are valid for initial mass function (IMF) as derived in Rieke et al. [1993]; for further details see Bai et al. [2010].

The IR data are complete down to the SFR limit of the observation of 0.1 $M_{\odot}$ yr^{-1} [Bai et al., 2010; Rasmussen et al., 2006b, 2012].

3.3 Ultra-Violet Data

The ultra-violet (UV) data, available for 22 out of 25 groups, were obtained with the GALEX satellite in two bands out to $2R_{200}$: near UV band (NUV) ($1770 \leq \lambda \leq 2830$ Å) and far UV band (FUV) ($1340 \leq \lambda \leq 1790$ Å). The exposure time of 1600 s in both bands was chosen to measure the flux down to $m_{AB} \approx 21.75$ in the NUV band, roughly corresponding to a SFR of 0.1 $M_{\odot}$ yr^{-1}. The sources were extracted with SExtractor [Bertin and Arnouts, 1996] and, similarly to the IR analysis, cross-correlated with the galaxy optical images within 5" and corrected for galactic extinction [Schlegel et al., 1998].

Before inferring the UV SFR it was necessary to apply a dust correction to the flux obtained from the 24 μm data, following Buat et al. [2005] method the FUV attenuation was defined as:

$$A_{FUV} = (-0.0333)y^3 + 0.3522u^2 + 1.1960y + 0.4967, \tag{3.6}$$

where y = $\log[L_{TIR}/(\nu\ L_{\nu})]$ (L_{TIR} is the total IR luminosity), $\nu = 1.96 \times 10^{1}5$ Hz is the effective frequency of GALEX FUV band, and L_{ν} is the FUV luminosity in erg s^{-1}

Hz^{-1}.

The dust-corrected SFR is calculated as in Salim et al. [2007]:

$$SFR_{FUV}(M_{\odot}\mathrm{yr}^{-1}) = 1.08 \times 10^{-28} L_{FUV} \tag{3.7}$$

where L_{FUV} is the dust-corrected specific FUV luminosity. Equation 3.7 is valid for mean stellar metallicity of 0.8 $Z_{\odot}$ and a Salpeter IMF; for further details see Rasmussen et al. [2012].

The NUV data are complete down to $m_{AB} = 22.0$. Furthermore, the data are UV complete for objects with NUV-R < 4.5 down to M_R = -18.

UV data are not available for three groups: MZ 770, MZ 3849 and MZ 9994. However NUV informations for the BGGs were retrieved from the GALEX online catalogue to be able to include these groups in the multi-variate analysis.

The above data, given by the collaboration, are not corrected for completeness. However, the analysis performed in previous works confirmed that including or excluding the dimmer members to the analysis did not change the overall result [see Rasmussen et al., 2012, for details].

3.4 X-ray Data

This project was originally designed to compare the group optical and X-ray properties. The X-ray observations were performed with the XMM satellite, but unfortunately due to a lack of allocated time as a consequence of a low rate of X-ray detection of the observed groups this project was never completed. The results obtained with the data available are published [Rasmussen et al., 2006b, 2010; Shen et al., 2007] and will be summarised below.

Of the 25 XI groups only 9 were allocated time on XMM, they were observed for ~ 20 ks with the aim to detect luminosities $\lesssim 10^{41}$ erg s^{-1}.

The first four groups studied in Rasmussen et al. [2006b] were MZ4577, MZ5383, MZ9024 and MZ9307 with the following outcome:

- MZ5383 and MZ9307 showed no diffuse emission;
- MZ4577 showed evidence of diffuse emission, but with a significance lower than 3σ;
- MZ9014 showed diffuse emission at a 3σ level of significance.

Although detected, MZ9014 had a very low luminosity and the X-ray mass was not calculated. Comparing these X-ray luminosities and upper limits with the values obtained in Osmond and Ponman [2004] for X-ray bright groups, showed that these systems are under-luminous given their velocity dispersion. Another peculiarity is that none of the groups hosts an elliptical galaxy in their centre.

On top of these, five more groups were studied in Shen et al. [2007] with the purpose to characterise X-ray AGNs, one of these was further analysed in Rasmussen et al. [2010]: MZ3849, MZ4592, MZ4940, MZ5293 and MZ10451.

Among these only MZ10451 showed X-ray diffuse emission with $L_x \gtrsim 10^{42}$ erg s^{-1}.

This result led to the conclusion that these groups are still in a collapsing phase hence the velocity dispersion is not a good indicator for the gravitational potential depth. This explanation allows for the presence of intra-group gas although not yet shock-heated to emit in the X-ray.

Among these, the only group in a more evolved dynamical state appears to be MZ10451 which shows X-ray emission.

The high number of groups still in a collapsing phase confirms the outcome of cosmological simulations and is in agreement with previous optical group studies.

The data described above (except for the X-ray data) will be used in a multi-parameter analysis. However some of them need to be analysed further in order to extract physical quantities. It is the case for the spectral data and some of the optical spatial parameters. The next two sections will describe the Lick indices analysis performed on the spectral data, and a dynamical analysis performed on the spatial parameters.

3.5 Lick Indices Analysis

The spectral data needed to be analysed in order to obtain quantifiable parameters, specifically age and metallicity of the stellar population. For this purpose a Lick indices analysis was performed.

The Lick indices are absorption features defined to study galaxy stellar populations properties. Originally, eleven indices were defined by Faber et al. [1985]: CN, G-band (CH molecule absorption line), Hβ, Mg b, Mg_1 (MgH), Mg_2 (MgH + Mg b), two Fe lines, NaD, and two TiO bands.

With the improvement of stellar population models, which allowed to reproduce the real spectra in more detail, it was possible to include weaker absorption features, together with the higher order Balmer lines (i.e. Hδ and Hγ) [Worthey and Ottaviani, 1997]. This brought the number of measurable indices to twenty five [see Vazdekis, 1999; Vazdekis et al., 1996]. All the indices are single absorption lines except for the pairs $H\delta_A$ and $H\delta_F$, and $H\gamma_A$ and $H\gamma_F$ which are two definitions for the line, involving a narrow and a wide central bandpass. All the Lick indices were fitted to determine the light-weighted stellar population parameters excluding Na_D, TiO_1 and TiO_2 because in their region the data were too much affected by noise.

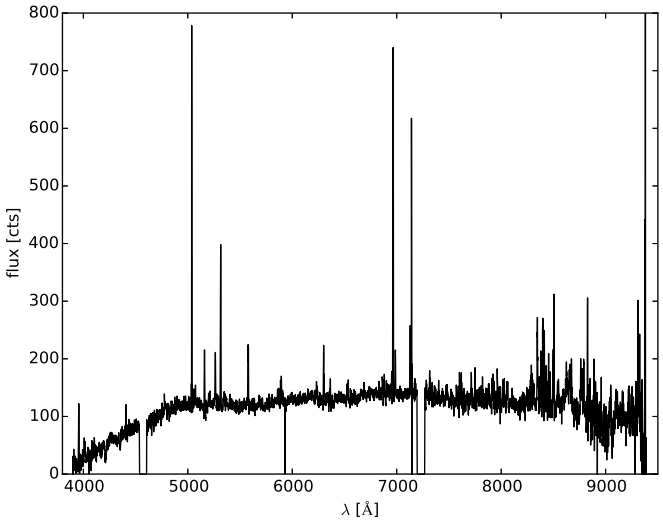

Figure 3.3: Plot showing the raw spectrum for one of the galaxy studied (MZ 9307-5). The wavelength in Å is shown on the x-axis and the flux in counts on the y-axis. Two chip gaps are visible at $\sim$ 4500 Å and $\sim$ 7200 Å respectively, there is a negative spike at $\sim$ 7100 Å and some positive ones in all the wavelength range due to reduction errors. The noise at red wavelengths ($\gtrsim$ 8000 Å) does not allow to study this region of the spectrum.

The indices allow to determine the light-weighted age and metallicity ([Fe/H] and [α/Fe]) of the galaxy stellar populations (i.e. the light deriving from the sum of all the different stellar population in the galaxy), bearing in mind that young stars are $\sim$ 20 times more luminous than old stars. Thus, when we observe a galaxy containing young stars, these are not necessarily the largest fraction of stars despite contributing more to the galaxy luminosity. The theoretical values of the indices have been calibrated on synthetic spectra with known stellar population compositions [Lee et al., 2005; Trager et al., 1998].

This method was chosen for the analysis due to the low galaxy spectra quality, not only beacuse of low signal-to-noise ratio (S/N) for the dimmest galaxies, but also because of the presence of chip gaps and reduction defects clearly visible in Figure 3.3.

The advantages of the Lick indices analysis, compared to methods that fit the contin-

uum together with absorption and emission features to determine age and metallicity of composite stellar populations, are:

- minimisation of effects due to calibration errors (e.g. sky subtraction, flux calibration, presence of cosmic rays), since by definition the indices do not need an absolute calibration of the spectrum;
- minimisation of effects due to modelling errors, since the continuum, where the models are weaker, is not fitted;
- ability to break the age-metallicity degeneracy (see 2.1.1) for light-weighted stellar populations [Tripicco and Bell, 1995; Worthey et al., 1994].

The last point is explained by the fact that some features are more affected by a change in metallicity and some are more age-dependent (hence their depth changes as these two parameters change). Tripicco and Bell [1995] performed a detailed study on how each index is influenced by these two parameters, the main results are described below.

- G4300: very sensitive to the abundances of C and O;
- Fe4383: Fe is the dominant species, but its strength is also affected by Mg and C. This is the most sensitive of all the Fe indices to the change in abundance of Fe, respect to a change in the overall metal abundance;
- Ca4455: it is almost insensitive to the variation of Ca, but it is mainly affected by a variation in Fe and Cr;
- Fe4531: dominated by abundance of Ti;
- Fe4668: sensitive to the abundance of Ca;
- Hβ: very little metallicity sensitivity, but can be contaminated by many emission features;

- Mg_1, Mg_2, Mg_b: very sensitive to Mg, but also to C, Fe, and other species;
- Fe5270, Fe5335, Fe5406: strongly dependent on Fe abundance;
- Fe5782: nearly independent of Fe abundance, it is mainly affected by Cr;
- Na_D the dominant element is Na, but this index is often contaminated by interstellar absorption.

The higher order Balmer lines (Hγ and Hδ), are not as good indicators of the age of the stellar population as Hβ, so they cannot be used as substitutes. This result, although not directly applied to this work, is the reason why it is important to use as many indices as possible in the analysis, and justified the decision of cleaning the spectra from the emission line as described in Section 3.5.2 below. The Balmer lines, especially Hβ, required cleaning given their strong dependence on the stellar population age.

The procedure followed to perform a Lick indices analysis is made of several steps, and the final result will consist of a measure for the light-weighted age, [Fe/H], [α/Fe], [Z/H], the total number of indices used in the fit, and a value for the goodness of the fit (χ^2). The analysis was performed on all the galaxies with spectrum available and $m_R < 17.6$ corresponding to $M_R \sim$ -19.5. However the spectra were visually inspected and excluded in case of major calibration errors or included if the major indices were recognisable. Figure 3.4 shows examples of galaxies with different noise level.

The first step of the study was to measure the velocity dispersion of the galaxy (i.e. the velocity of the stars in the galaxy). The value obtained was used to correct the line for broadening, so that the shape of the line was depending entirely on the stellar population properties. To calculate the velocity dispersion the pPXF (Penalised Pixel-Fitting) routine developed by Michele Cappellari [Cappellari and Emsellem, 2004] was used as described below.

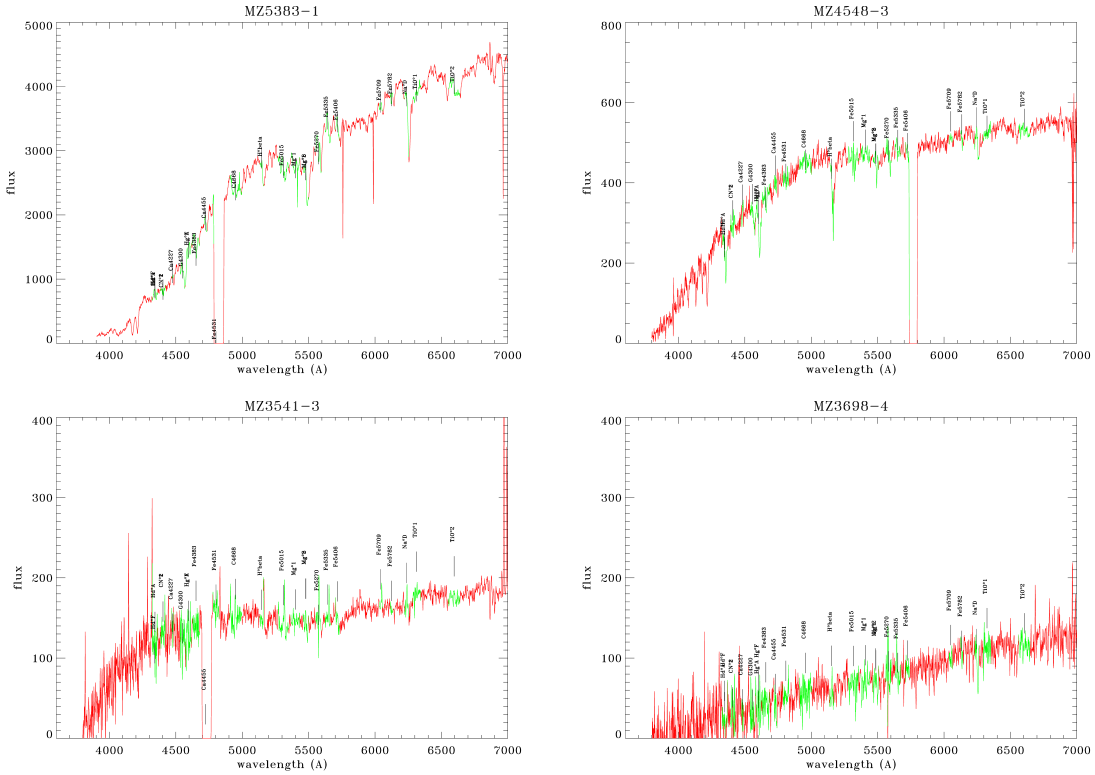

Figure 3.4: This figure shows four galaxy spectra, the wavelength in Å is on the x-axis, the flux in counts on the y-axis. The spectrum is shown in red, while the Lick indices central bands are highlighted in green. Each band is labelled with the name of the corresponding index. The top panels show a galaxy with a very low level of noise on the left, and a galaxy with higher noise but where the absorption features are still well visible on the right. Both these galaxies are suitable for the Lick indices analysis. The bottom left panel shows a galaxy where the blue part of the spectra is too noisy for the Lick indices analysis, but the red end of the spectrum can be analysed. The result in this case would have a higher uncertainty given the lower number of indices used. The bottom right panel shows a galaxy where the absorption features are not discernible from the noise thus making the Lick analysis not possible.

3.5.1 pPXF

The pPXF algorithm was designed to study the stellar dynamics of nearby galaxies, more precisely to study the line of sight velocity dispersion (LOSVD) of the projected galaxy in the sky at all galaxy radii. In this work, the algorithm was used to infer the velocity dispersion of each galaxy by fitting the spectrum and measuring the line broadening due to the stars in the galaxy.

The algorithm works in pixel space and uses a Gauss-Hermite parametrisation for the LOSVD as shown by the following equation [Gerhard, 1993; van der Marel and Franx, 1993]:

$$\mathcal{L}(v) = \frac{e^{(-1/2)y^2}}{\sigma\sqrt{2\pi}}[1 + \sum_{m=3}^{M} h_m H_m(v)] \tag{3.8}$$

where $y = (v - V)/\sigma$, v is the LOSVD, V the mean radial velocity, σ the velocity dispersion, h_m free parameters, and the H_m are the Hermite polynomials.

A spectrum model, to fit the observed spectrum, is created convolving the templates with the parametrised LOSVD, then the best fit parameters are determined minimising the χ^2.

The strongest assumption made was considering the galaxies as pure stellar systems, hence their spectrum is simply the sum of all stellar spectra, each one redshifted according to the line-of-sight velocity of the stars.

pPXF was chosen for the optimisation because it is able to recover the details of the LOSVD profile in case of high S/N, and tends to a Gaussian shape (expected for LOSVD) in case of low S/N. All the free parameters (h_m) are fitted simultaneously (V, σ, h3, ..., hM) and a penalty term ($\mathcal{P}$) is added to the χ^2 in order to bias the solution toward a Gaussian when the S/N is low (i.e. when the higher moments are not constrained by the data).

The final χ^2 is

$$\chi^2_P = \chi^2 + \alpha\mathcal{P} \tag{3.9}$$

where

$$\alpha(y) = \frac{1}{\sqrt{2\pi}} e^{-\frac{1}{2}y^2}. \tag{3.10}$$

The algorithm works as follows:

1. the user gives an initial guess for V and σ, while the higher order parameters are set h3,...,hM = 0;
2. the galaxy spectra templates are weighted and combined, and the optimal spectrum is chosen;
3. the algorithm computes the residuals from the fit;
4. the residuals are perturbed;
5. the least squares optimisation starts and iterates from the second step to fit the parameters (V, σ, h3,..., hM).

In this work pPXF was applied to galaxies with velocity dispersion > 100 km s^{-1} or $m_B \lesssim 15$, in the wavelength range $\lambda\lambda$ 3800,7000 Å where the spectra were less affected by noise. The MILES models were used to fit the spectra [Vazdekis et al., 2010], their wavelength range is $3540.5 < \lambda < 7409.6$ and the resolution 2.54 Å. Figure 3.5 shows a fit example.

For the remaining galaxies the velocity dispersion was extrapolated using the Faber-Jackson relation:

$$\sigma_0 = 10^{A-BM} \tag{3.11}$$

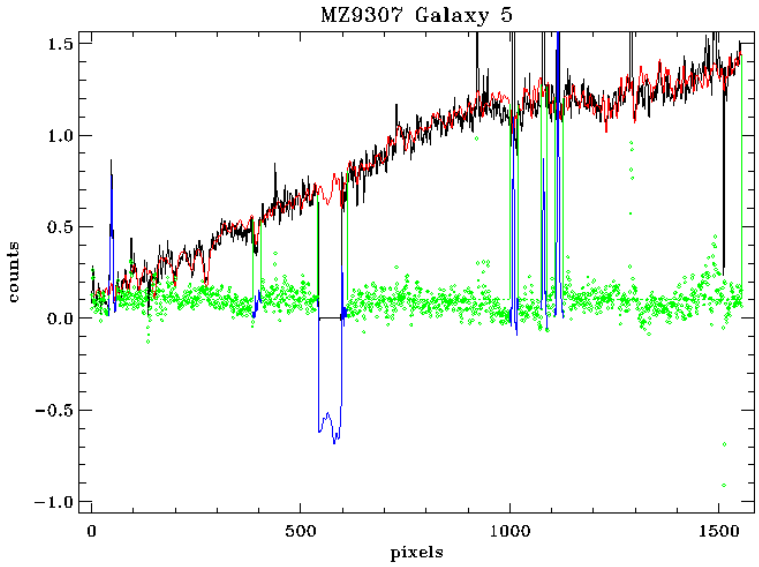

Figure 3.5: Plot output by pPXF. The original spectrum is in black and the fit in red. The blue colour shows the masked regions (i.e. the chip gap and the emission lines), in green are shown the residuals. The algorithm works in pixel space so pixel instead of wavelength is shown on the x-axis and flux in counts is on the y-axis.

where A = -2.889 ± 0.028, B = 0.239 ± 0.013, from Nigoche-Netro et al. [2010], and M is the B-band absolute magnitude. The absolute magnitude was calculated from

$$M = m - 5(log_{10}D_L - 1) \tag{3.12}$$

where m is the apparent magnitude in the B-band and D_L is the luminosity distance

$$D_L(z) = (1 + z)D_M(z) \tag{3.13}$$

where z is the redshift and D_M is the comoving distance.

The Faber-Jackson relation is valid for elliptical galaxies, thus the values of σ obtained with this method are an approximation, since we use it for all the group members independent of their morphology. However the error does not interfere with the results since it is below the resolution of the spectra.

Given that most of the sample galaxies showed the presence of emission lines, and that some of these occur at the same wavelength as some of our key indices (i.e. Hβ), a further step had to be added to the analysis. The emission lines removal was performed using the algorithm GANDALF[1] (Gas AND Absorption Line Fitting algorithm), together with pPXF. It consisted in measuring the emission lines flux then remove them from the spectrum effectively cleaning it, and giving back as a result a measure for the emission lines strength.

3.5.2 GANDALF

GANDALF is an algorithm designed to measure the gas fluxes and kinematics in galaxy spectra, separating the stellar continuum from the nebular emission. It is an extension of pPXF which alone masks the emission lines while fitting the spectral continuum. GANDALF instead allows simultaneously fitting of the emission lines as additional Gaussian profiles. The flux value for each line is obtained from the best-fit of line width and peak flux density.

GANDALF outputs the measured equivalent width of the emission lines and the 'cleaned' spectra with emission lines subtracted to be used in the Lick indices analysis. Unfortunately, because of the quality of most of the spectra it was necessary to run GANDALF separately for the red and blue part of the optical spectrum (as shown in Figure 3.6), then collate the result. The derived ASCII spectra had to be converted into FITS files using the task 'rspectext' in IRAF.

In this work GANDALF was applied to all galaxies, in fact it is sometimes possible to detect emission lines even when the continuum is impossible to discern from the noise. In this case, though, it is not possible to use the absolute value of the line strength, it is however possible to use the ratios to study diagnostic diagrams (see Sections 4.1.2 and 5.1) in order to distinguish between AGNs and star forming galaxies. The number of

[1]GANDALF was developed by the SAURON team and is available from the SAURON website (www.strw.leidenuniv.nl/sauron). See also [Sarzi et al., 2006] for details.

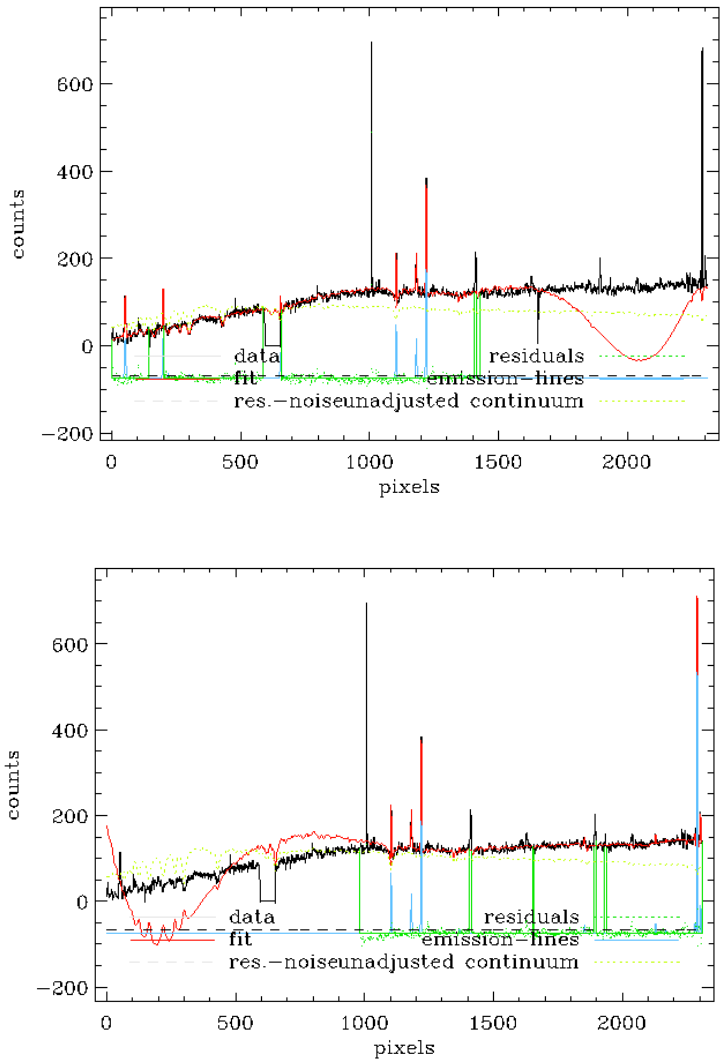

Figure 3.6: Plot showing the fit performed with GANDALF for the blue end of the spectrum (top) and for the red end (bottom). The original spectrum is in black and the fit in red. The green colour shows the residuals, while the light blue shows the fitted emission lines minus the continuum. Similarly to pPXF GANDALF woks in pixel space, so pixels are shown on the x-axis and flux in counts on the y-axis.

galaxies for which the emission line measurement was possible are shown in Appendix 1 for each group.

3.5.3 Spectral Fitting

After the preparatory work, the 'cleaned' spectra were ready for the Lick indices measurement.

The analysis consisted on measuring the spectral line strength using the equivalent width described in Chapter 2. Hence it was necessary to define three passbands (i.e. wavelength bands): a central one where the line is, with the typical width of the line itself, and two side ones, on the blue (shorter wavelength) and on the red (longer wavelength) side of the line. The flux value in the two side bands is averaged, then interpolated to determine the continuum flux from which to consider the line height. The central and side passbands are defined for every index as listed in Table 3.2.

The indices were measured using a routine written by Rob Proctor [see Proctor and Sansom, 2002] and modified to use the Gaussian broadening developed by Mike Beasley [Beasley et al., 2004; Worthey and Ottaviani, 1997].

Subsequently, they were fitted with the Korn, Maraston & Thomas models (KMT) [Korn et al., 2005] using a Fortran routine written by Alexandre Vazdekis [Vazdekis, 1999] and adapted by Robert Proctor [see Proctor and Sansom, 2002; Proctor et al., 2004a,b]. These models were chosen after having compared them with the Bruzual & Charlot models (BC03) [Bruzual and Charlot, 2003], for details see Appendix 2. The KMT models estimate [Z/H] and α-enhancement in their original formulation for [E/H] = +0.0, +0.3, +0.5 dex (see Table 1 for the complete model parameter ranges), then [Fe/H] was extrapolated as

$$[Fe/H] = [Z/H] - 0.942[E/Fe], \tag{3.14}$$

where the value 0.942 is given in Proctor and Sansom [2002].
The values obtained from the fit were the light-weighted age, [Fe/H], α-enhancement, and [Z/H] of each galaxy, together with the number of indices used (limited by the S/N of the spectrum, the presence of chip gaps or hot pixels), and the value of the χ^2.
The number of galaxies for which the analysis was possible are shown in Appendix 1 for each group.

3.6 Galaxy Cluster Fitting with Background

This section describes the analysis performed on the optical spatial data to obtain dynamical parameters. The tool used was an algorithm based on Bayesian technique that models the 3-D distribution of the group galaxies (this algorithm was developed in collaboration with Dr Will Farr).

The data required for the analysis were the centroid coordinates (i.e. RA and dec), redshift z and velocity dispersion σ of the groups, together with coordinates, redshift and its uncertainty for all the galaxies in a cylinder of diameter $\sim 1.5^\circ$ up to z $\sim$ 0.1 centred on the group centroid. The algorithm fitted two 3-dimensional Gaussian profiles, one to model the group galaxies distribution and the other (expected to be almost flat) to model the background/foreground galaxies distribution.
If the galaxies belong to the group then their redshifts are Poisson distributed according to:

$$\frac{dN_{group}}{dz}(z) = \Lambda_{group} N[\mu_z, \sigma_z](z), \tag{3.15}$$

where $N[\mu, \sigma]$ is a Gaussian distribution with mean μ and standard deviation σ, Λ_{group} is the number of group galaxies, μ_z and σ_z the mean group redshift and velocity dispersion respectively.
Similarly, if the galaxies belong to the background they are Poisson distributed accord-

ing to:

$$\frac{dN_{bg}}{dz}(z) = 2\Lambda_{bg}\left(\frac{A}{z_{max}^2}(z_{max}-z) + \frac{(1-A)}{z_{max}^2}z\right), \tag{3.16}$$

where A is related to the redshift density profile, Λ_{bg} is the number of background galaxies, and z_{max} is the highest redshift available in the galaxy sample (z $\sim$ 0.1 in this case). If A=1 all background galaxies are concentrated at $z = 0$, if A=0 all background galaxies are at $z = z_{max}$.

The parameters derived with this technique are (see Figure 3.7):

- size of the distribution in ra, dec and z (σ_{ra}, σ_{dec}, σ_z): the average width, in degree for ra and dec and in km/s for redshift, of the projected galaxy distribution assumed spherical;
- richness (N_{group}): the number of galaxy group members;
- projected ellipticity of the group;
- R_+ and R_-, correlation coefficient between the major and minor axis of the projected group distribution on the sky and the redshift: the higher this number is the more the major (or minor) axis of the projected distribution of galaxies correlates with the redshift distribution;
- the number density of group members per squared degrees on the sky;
- the probability of each galaxy being a group member;
- the projected density of group members.

The algorithm finds a probability distribution, for the purpose of the analysis the peak value of the distributions is considered.

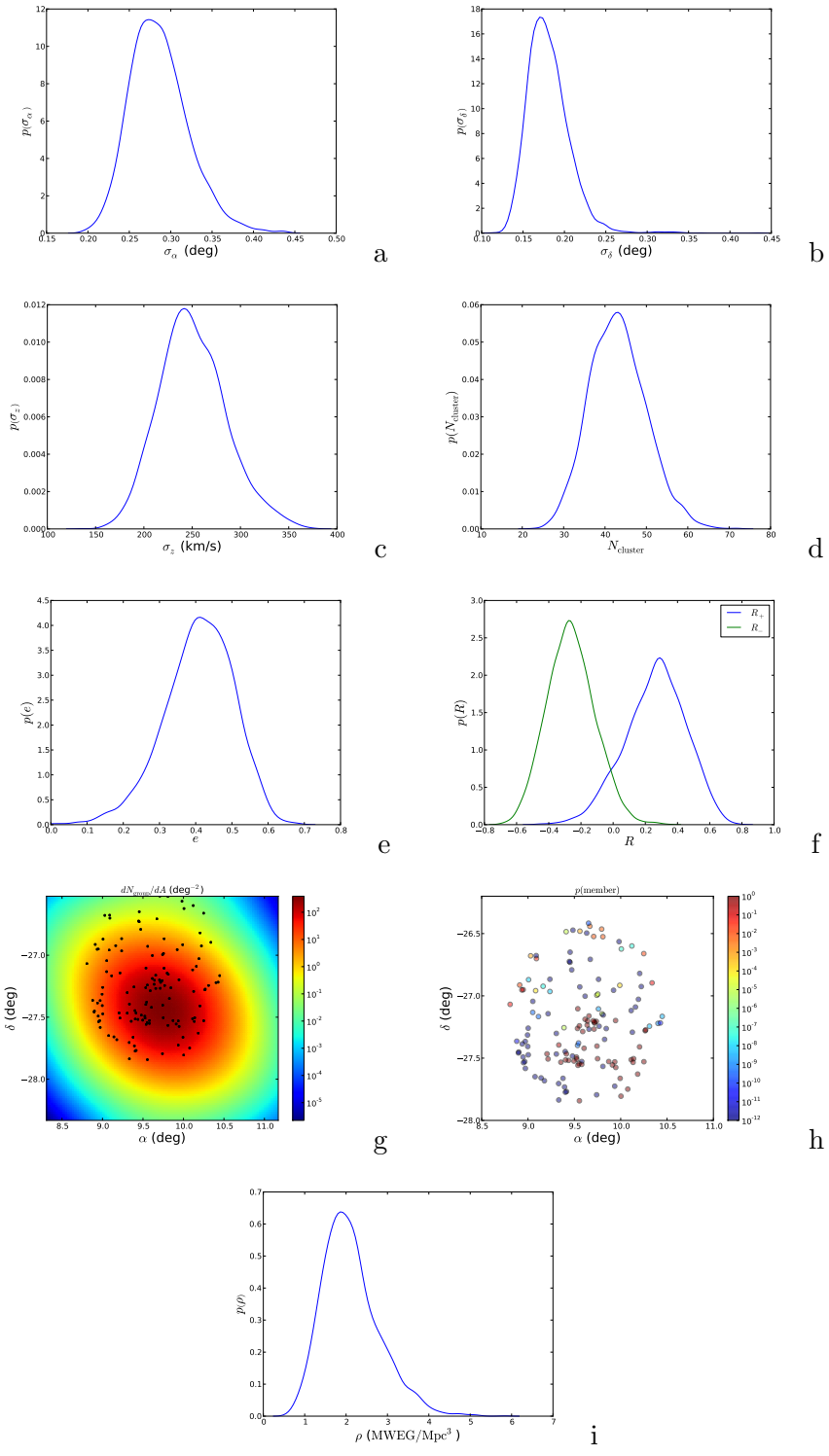

Figure 3.7: Parameters obtained with the group fitting routine for group MZ1766. On the y-axis of panels a),b),c),d),e),f) and i) there is the probability distribution of each quantity. The x-axis in panels a) and b) shows the RA and Dec in degrees respectively, in panel c) cz in km/s, and in panel d) the richness. In panel e) the x-axis shows the ellipticity, while in panel f) it is the value for both R_+ and R_-. Panel g) and h) have the RA and Dec in degrees on the x and y-axis respectively, they show all the galaxies in a cylinder of diameter $\sim$1.5° up to z *sim* 0.1. The background colour-coding in g) represent the projected density, while in h) it shows the probability for each galaxy of being a member. The x-axis in panel i) is the projected density of group members.

The above analysis was aimed at producing physical quantities to be used in the multi-parameter analysis described in the following chapter.

The properties of each group (plots, number of galaxies used in each step of the analysis, etc.) are schematically summarised in Appendix 1.

Index	Blue continuum (Å)	Band (Å)	Red continuum (Å)
$H\delta_A$	4041.600 – 4079.750	4083.500 – 4122.250	4128.500 – 4161.000
$H\delta_F$	4057.250 – 4088.500	4091.000 – 4112.250	4114.750 – 4137.250
CN_1	4080.125 – 4117.625	4142.125 – 4177.125	4244.125 – 4284.125
CN_2	4083.875 – 4096.375	4142.125 – 4177.125	4244.125 – 4284.125
Ca_{4227}	4211.000 – 4219.750	4222.250 – 4234.750	4241.000 – 4251.000
G_{4300}	4266.375 – 4282.625	4281.375 – 4316.375	4318.875 – 4335.125
$H\gamma_A$	4283.500 – 4319.750	4319.750 – 4363.500	4367.250 – 4419.750
$H\gamma_F$	4283.500 – 4319.750	4331.250 – 4352.250	4354.750 – 4384.750
Fe_{4383}	4359.125 – 4370.375	4369.125 – 4420.375	4442.875 – 4455.375
Ca_{4455}	4445.875 – 4454.625	4452.125 – 4474.625	4477.125 – 4492.125
Fe_{4531}	4504.250 – 4514.250	4514.250 – 4559.250	4560.500 – 4579.250
C_{4668}	4611.500 – 4630.250	4634.000 – 4720.250	4742.750 – 4756.500
$H\beta$	4827.875 – 4847.875	4847.875 – 4876.625	4876.625 – 4891.625
Fe_{5015}	4946.500 – 4977.750	4977.750 – 5054.000	5054.000 – 5065.250
Mg_1	4895.125 – 4957.625	5069.125 – 5134.125	5301.125 – 5366.125
Mg_2	4895.125 – 4957.625	5154.125 – 5196.625	5301.125 – 5366.125
Mg_b	5142.625 – 5161.375	5160.125 – 5192.625	5191.375 – 5206.375
Fe_{5270}	5233.150 – 5248.150	5245.650 – 5285.650	5285.650 – 5318.150
Fe_{5335}	5304.625 – 5315.875	5312.125 – 5352.125	5353.375 – 5363.375
Fe_{5406}	5376.250 – 5387.500	5387.500 – 5415.000	5415.000 – 5425.000
Fe_{5709}	5672.875 – 5696.625	5696.625 – 5720.375	5722.875 – 5736.625
Fe_{5782}	5765.375 – 5775.375	5776.625 – 5796.625	5797.875 – 5811.625
Na_D	5860.625 – 5875.625	5876.875 – 5909.375	5922.125 – 5948.125
TiO_1	5816.625 – 5849.125	5936.625 – 5994.125	6038.625 – 6103.625
TiO_2	6066.625 – 6141.625	6189.625 – 6272.125	6372.625 – 6415.125

Table 3.2: Definition of the Lick indices. The first column shows the index names, the second defines the passband range at lower wavelength (blue passband), the third defines the line itself (central passband), and the fourth the passband at higher wavelength (red passband) [Vazdekis, 2001; Worthey and Ottaviani, 1997; Worthey et al., 1994].

Models	Log age (yr)	[Z/H] (dex)	[Fe/H] (dex)	[E/H] (dex)
KMT	-1.0 – 1.175	-2.25 – +0.8	–	-0.3 – +0.8

Table 3.3: KMT parameter ranges, this model gives the total metallicity and the α-enhancement [Korn et al., 2005].

Chapter 4

Multi-variate analysis to reveal the existence and properties of classes of low redshift galaxy groups

The data described in the previous chapter will be used in the multi-variate analysis, however some of them need to be further manipulated before being used.
In the next section the data manipulation and the tools used will be described, then the correlation and multi-variate analysis will be presented and the results discussed.

4.1 Data sample

For the purpose of this analysis the multi-wavelength parameters were divided into five categories: scaling properties, specific properties, dynamical properties, BGG properties, and environmental properties. The following sections will describe how the parameters in each category were calculated for each group.

4.1.1 Scaling properties

The scaling properties are in some way related to the mass of the group, either because they describe a global property (e.g., mass or radius), or because they are integrated quantities (e.g., integrated luminosities or SFRs). They were calculated using all the data available within R_{200}, issues of completeness have been discussed in Chapter 3.

σ, M_{200}, and R_{200} were the main indicator of group mass and size, however σ was the only one considered since it was used to derive the other two.

The integrated quantities calculated for each group were R-band and far ultra-violet (FUV) luminosities, infra-red (IR) and ultra-violet (UV) SFR, and stellar masses. These were simply obtained adding the values for each galaxy within R_{200}. For a description of how the original quantities were calculated see Chapter 3.

The richness (N) was defined as the number of galaxies within 1 Mpc from the group centroid with $M_R < -16.5$.

4.1.2 Specific properties

The specific properties are, by definition, normalised either by the mass of the system or by the number of galaxies within R_{200}. IR- and UV- specific star formation rates (sSFRs) were obtained by dividing the integrated SFR by the integrated stellar mass. The stellar mass fraction is simply the integrated stellar mass ($intSM$) divided by M_{200}.

The early-type fraction was calculated by dividing the number of early-type galaxies by the total number of galaxies within R_{200}. To determine the galaxy morphologies the results from the Sersic indices extraction described in Chapter 3 were used. Early-type galaxies were identified as having a Sersic index value > 2.5 [Patel et al., 2012], all the others were considered late-type.

The AGN fraction was also calculated. AGNs were identified using a BPT-type diagram (Baldwin et al. [1981]), based on line ratios using either the [OI] or [NII] lines.

Both methods were used to have as much information as possible, and because they depend on different features, but give similar information. For the [OI]-based ratios, the following equations defined an AGN (see Figure 4.1):

$$log\left(\frac{[OIII]}{H\beta}\right) \geq \frac{0.73}{log\left(\frac{[OI]}{H\alpha}\right) + 0.59} + 1.33 \tag{4.1}$$

and

$$log\left(\frac{[OI]}{H\alpha}\right) > -0.7, \tag{4.2}$$

while for [NII]-based ratios, the following equations were used (see Figure 4.2):

$$log\left(\frac{[OIII]}{H\beta}\right) \geq \frac{0.61}{log\left(\frac{[NII]}{H\alpha}\right) - 0.47} + 1.19 \tag{4.3}$$

and

$$log\left(\frac{[NII]}{H\alpha}\right) > 0.215. \tag{4.4}$$

Similarly, composite galaxies (both AGN and SF) are found in the region where:

$$\frac{0.61}{[log\left(\frac{[NII]}{H\alpha}\right) - 0.05]} + 1.3 < log\left(\frac{[OIII]}{H\beta}\right) \tag{4.5}$$

and

$$\frac{0.61}{[log\left(\frac{[NII]}{H\alpha}\right) - 0.47]} + 1.19 > log\left(\frac{[OIII]}{H\beta}\right) \tag{4.6}$$

(Kewley et al. [2001], Kauffmann et al. [2003], Kewley et al. [2006]). The values indicated as [OIII], [NII], [OI], $H\beta$, and $H\alpha$ represent the equivalent width of the lines in emission of OIII, NII, OI and two of the hydrogen Balmer lines. They were obtained using GANDALF as described in Section 3.5.2, no errors were available for this measurement. After distinguishing between [OI] AGNs, [NII] AGNs and [NII] composite galaxies, their fraction for each group was calculated by dividing the total number of

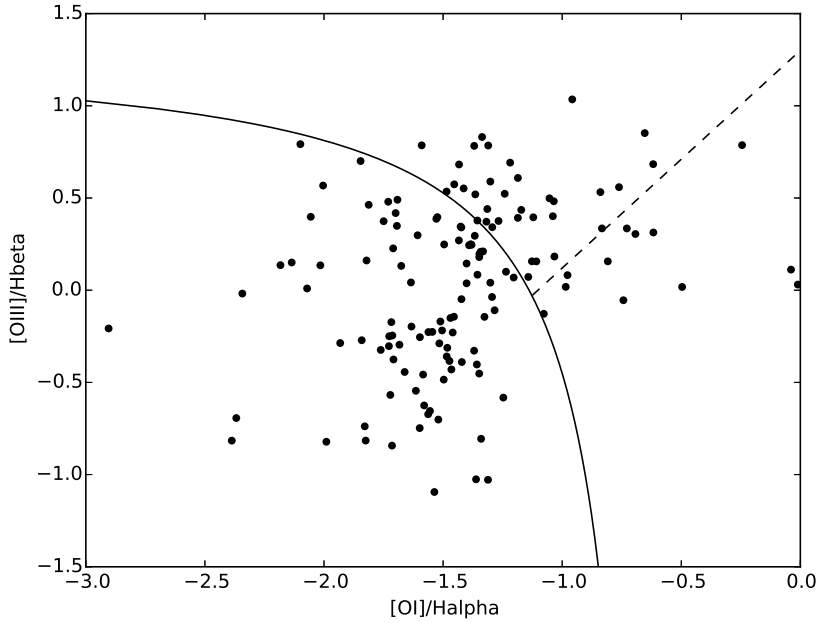

Figure 4.1: BPT diagnostic diagram [Baldwin et al., 1981; Kewley et al., 2006] containing all the galaxies within R_{200} in each group for which the line ratio were measured. On the x-axis it is shown the ratio [OI]/Hα, on the y-axis the ratio [OIII]/Hβ. The solid line divides the star-forming galaxies (below) from the AGNs (above), the dashed line divide Seyfert galaxies (above) and LINERs (below).

each type by the number of galaxies within R_{200}.

4.1.3 Dynamical properties

The dynamical properties give an indication of the evolutionary state of the group. They are a powerful tool, but can be difficult to interpret, mainly due to projection effects.

To study these properties, a Bayesian technique was applied to model the 3-D distribution of the group galaxies as described in Section 3.6. For the purpose of this analysis three of the derived parameters were used (i.e. the peak values of the probability distribution): the projected ellipticity of the group, the correlation coefficient between the major axis of the projected group distribution on the sky and the redshift (R+), and

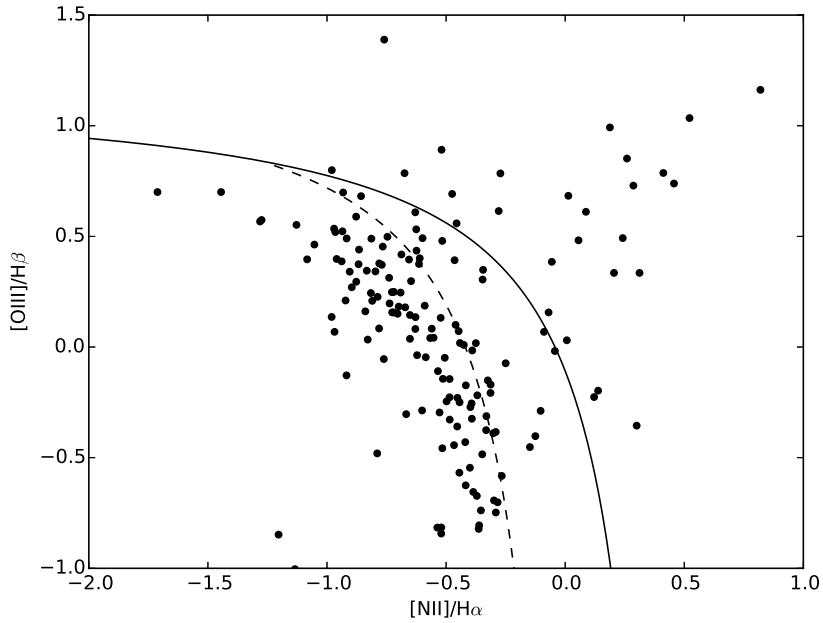

Figure 4.2: BPT diagnostic diagram [Baldwin et al., 1981; Kewley et al., 2006] containing all the galaxies within R_{200} in each group for which the line ratio were measured. On the x-axis it is shown the ratio [NII]/Hα, on the y-axis the ratio [OIII]/Hβ. The solid line divides the star-forming galaxies (below) from the AGNs (above), the region between the solid and the dashed line contains the composite galaxies (star-forming galaxies showing signs of AGN activity).

the virial ratio defined as σ/R, where σ is the velocity dispersion and R is the effective radius of the group, both independently obtained from the fit.

A further property which gives indication on the dynamical state of a group is the Brightest Group Galaxy (BGG) distance, namely the distance of the brightest galaxy (R-band) within R_{200} from the group centroid. A large distance is expected to be an indicator of a non-evolved group since the most massive clusters, assumed to be relaxed in the central region, host a bright elliptical galaxy in their very centre.

4.1.4 BGG properties

The BGG was defined as the brightest galaxy in the R-band within R_{500}. The BGG-specific properties utilised were:

- R-band luminosity,
- $B - R$ and $NUV - R$ colours,
- R-band magnitude gap between the first and the second brightest galaxies within $\frac{1}{2}R_{200}(\sim R_{vir})$,
- Sersic index,
- light-weighted age, iron abundance ([Fe/H]), α-enhancement ([E/Fe]) and total metallicity ([Z/H]) from the Lick indices analysis of the BGG spectra (see Section 3.5).

For three BGGs (MZ 4592, MZ 5388 and MZ 9014) it was not possible to perform the Lick indices analysis thus no stellar population parameters were available. However since these quantities were not used for the clustering analysis the groups were included. The magnitude gap could not be calculated for three groups because they only had one galaxy within $\frac{1}{2}R_{200}$: MZ 4940, MZ 5293, MZ 5388. These groups were excluded from the clustering analysis which thus only contains 22 groups.

4.1.5 Environmental properties

The environmental properties are an attempt to describe the global environment surrounding the group.

To study the large scale structure (LSS), the distribution of galaxies extracted from the 2dFGRS within 10 Mpc from the group centroid and ±1500 km/s from the group redshift was visually inspected. Four different LSS environments were defined (see Figure 4.3):

1) isolated group: lack of galaxy overdensities up to at least 5 Mpc;

2) group offset from a cluster: presence of a large structure between 5 and 10 Mpc, but no obvious link with the group visible;

3) group part of a sparse supercluster: presence of several structures within 10 Mpc of the group, but no obvious link with the group visible;

4) group part of a supercluster: presence of large structures near the group, visibly linked with each other and with the group itself.

As a further measure of the large scale environment the projected density of galaxies within ±1500 km/s were calculated from 1 to 3, 3 to 5 and 5 to 10 Mpc respectively.

Table 4.1 summarises all the parameters available for the correlation and multi-variate analysis described in the following two sections: the notation used, the name of the variable, its definition, the range of values (minimum and maximum), the number of groups for which the parameter is available and if the quantity has been logged.

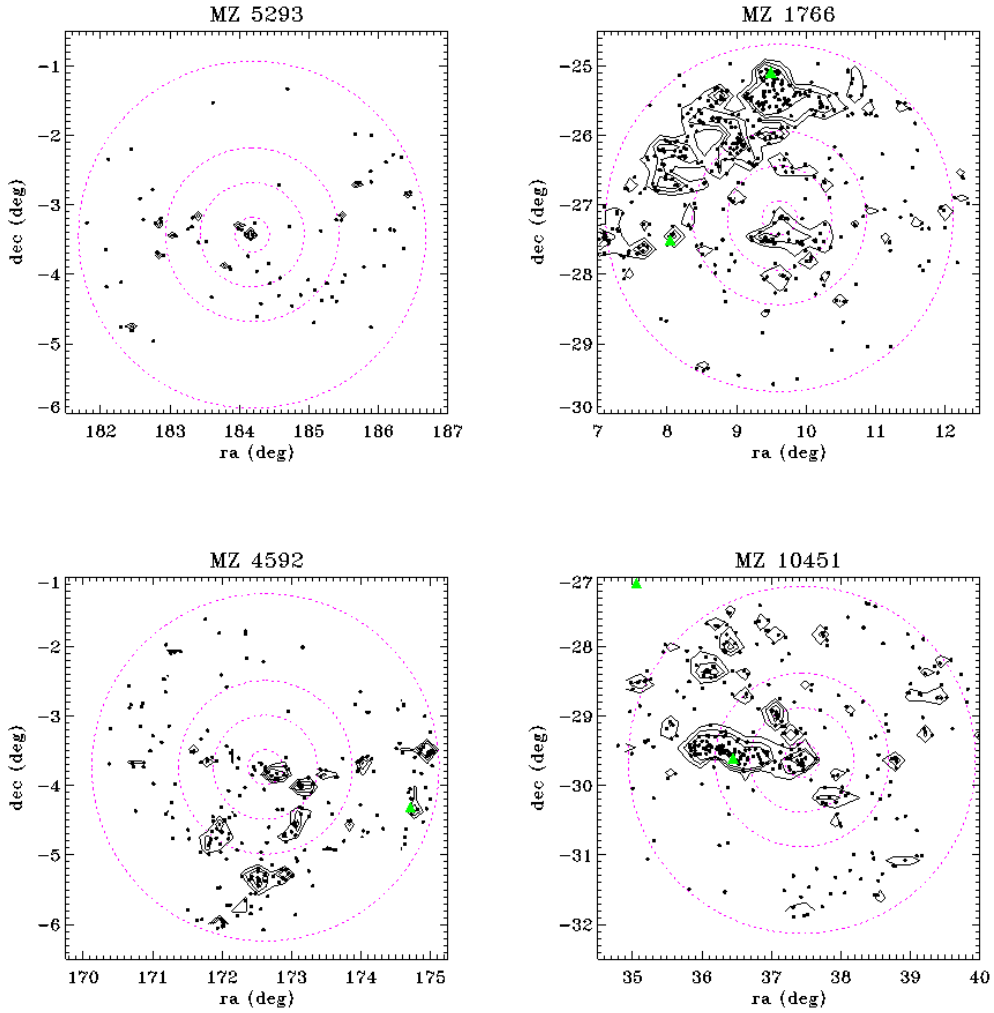

Figure 4.3: Example of four groups in the different categories: an isolated group in the top left corner, a group offset from a cluster in the top right, a group part of a sparse supercluster in the bottom left panel, and a group part of a supercluster in the bottom right. The contours show the density of points on the plot; the dashed circles are the radii at 1, 3, 5 and 10 Mpc respectively. The group members are contained within 1 Mpc (inner dashed line), the green triangles are known Abell clusters. See Appendix 1 for full sample plots.

notation	name	definition	min value	max value	units	no. of groups	log
σ	velocity dispersion	Calculated using bisquare weighting, galaxies beyond 3-σ were excluded	64	509	km/s	25	yes
M_{200}	characteristic mass	see Eq.3.2	$4.44 \cdot 10^{11}$	$2.21 \cdot 10^{14}$	$M_\odot$	25	yes
R_{200}	characteristic radius	see Eq.3.3	0.15	1.22	Mpc	25	
$intL_R$	integrated R-band luminosity	integrated within R_{200}	$3.18 \cdot 10^{10}$	$8.33 \cdot 10^{11}$	$L_\odot$	25	yes
$intL_{FUV}$	integrated far ulta-violet luminosity	integrated within R_{200}	$2.14 \cdot 10^{12}$	$4.10 \cdot 10^{14}$	$L_\odot$	22	yes
$intSM$	integrated stellar mass	integrated within R_{200}	$4.09 \cdot 10^{10}$	$1.41 \cdot 10^{12}$	$M_\odot$	25	yes
N	richness	No. of galaxies within 1 Mpc from the group centroid with $M_R < -16.5$	6	36	-	25	yes
$intSFR_{UV}$	integrated ultra-violet star-formation rate	integrated within R_{200}	0.175	20.748	$M_\odot ye^{-1}$	22	yes
$intSFR_{IR}$	integrated infra-red star-formation rate	integrated within R_{200}	0.0	13.07	$M_\odot ye^{-1}$	25	yes
$sSFR_{UV}$	ultra-violet specific star-formation rate	$intSFR_{UV}/intSM$	$2.94 \cdot 10^{-12}$	$3.18 \cdot 10^{10}$	yr^{-1}	22	yes
$sSFR_{IR}$	infra-red specific star-formation rate	$intSFR_{IR}/intSM$	0.0	$1.94 \cdot 10^{-10}$	yr^{-1}	25	yes
$SMfract$	stellar mass fraction	$intSM/M_{200}$	0.00151	0.16869	-	25	yes
ET	early-type fraction	Number of early-type galaxies ($Sersic > 3$) / total number of galaxies within R_{200}	0.0	0.5	-	25	no
AGN_{OI}	active galactic nuclei fraction	Total number of AGNs / number of galaxies within R_{200} (Eq.4.1,4.2)	0.0	0.5	-	25	no
AGN_{NII}	active galactic nuclei fraction	Total number of AGNs / number of galaxies within R_{200} (Eq.4.3,4.4)	0.0	0.5	-	25	no
$composite_{NII}$	composite galaxies fraction	Total number of composite galaxies / number of galaxies within R_{200} (Eq.4.5,4.6)	0.0	0.75	-	25	no
ell	projected ellipticity of the group	projected ellipticity of the group	0.19	0.85	-	25	no
R^+	correlation between projected major axis and redshift distributions	correlation between projected major axis and redshift distributions	0.02	0.94	-	25	no
Vir	virial ratio	velocity dispersion independently calculated / effective radius of the group	0.35	28.41	2.5×10^{39} kg Mpc^{-3}	25	yes
BGG_{dist}	distance between the BGG and the second brightest galaxy	distance between the BGG and the second brightest galaxy within R_{200}	0.0	0.36	Mpc	25	yes
mag_{gap}	magnitude gap	magnitude gap between the first and the second brightest galaxies within $\frac{1}{2}R_{200}$	0.17	3.38	-	22	no
BGG_{L_R}	R-band luminosity of the BGG	from the data	$1.43 \cdot 10^{-10}$	$1.89 \cdot 10^{-11}$	$L_\odot$	25	yes
$Sersic$	Sersic index value of the BGG	2-D Sersic fit	1.0	9.75	-	25	yes
$B-R$	B - R colour of the BGG	from the data	1.40	2.36	-	25	no
$NUV-R$	near UV - R colour	from the data	0.0	6.34	-	25	no
Age	age	from the Lick indices fit	0.057	1.29	$Log(yr)$	22	yes
$[Fe/H]$	iron peak elements abundance	from the Lick indices fit	-0.7	0.4	-	22	no
$[E/Fe]$	α-enhancement	from the Lick indices fit	-0.30	0.33	-	22	no
$[Z/H]$	total metallicity	from the Lick indices fit	-0.954	0.448	-	22	no
LSS	large scale structure code	visually assigned (1=isolated, 2=offset from a cluster, 3=part of a sparse supercluster, 4=part of a supercluster)	1	4	-	25	no
$3Mpc$	average density at 3 Mpc from the group centroid	calculated up to 3 Mpc	0.28	2.67	Mpc^{-3}	25	no
$5Mpc$	average density at 5 Mpc from the group centroid	calculated up to 5 Mpc	0.34	2.18	Mpc^{-3}	25	no
$10Mpc$	average density at 10 Mpc from the group centroid	calculated up to 10 Mpc	0.24	1.95	Mpc^{-3}	25	no

Table 4.1: Definition of the 33 parameters: the first column is the abbreviation used for each parameter, second and third columns are name and definition, then the minimum and maximum values, and the units are shown, the last two columns show the number of groups for which the parameter was available and if the value is in logarithmic scale. Some of the parameters are not independent hence they have not been used in some parts of the analysis.

4.2 Multi-variate Data Analysis

4.2.1 Correlation Analysis

The first step of the analysis consisted in studying the correlation between variables to confirm known trends and to identify new ones. To do this a Spearman rank correlation test was performed on each pair of parameters (excluding M_{200} and R_{200} because they are directly derived from σ, see Equations 3.2 and 3.3), the results can be seen in Figure 4.4. The significance of the result, determined using the p-value, is indicated by the symbols; three stars are used for a p-value of 0, two stars for 0.001, one star for 0.01, the small square for 0.05, and no symbol for higher values.

Some of the parameters were correlated by construction as expected, for instance all the variables containing information about how massive the system is (i.e. σ, integrated far ultra-violet luminosity ($intL_{FUV}$), and other scaling properties). However, other correlations were found to be more interesting and/or surprising and will be discussed further.

The most straightforward observable related to the total system mass is the velocity dispersion, σ, so correlations with it are of particular interest. The velocity dispersion is anti-correlated with the stellar mass fraction (slope = -0.76 with p-value = 0), indicating that more massive systems contain more dark matter than stellar content, in agreement with previous studies [e.g. Giodini et al., 2009; Gonzalez et al., 2007]. Two other interesting correlations regarding σ are with BGG Sersic index and environmental parameters. The first one indicates that more massive systems have bulge dominated BGGs, and so could indicate that they are in a more advanced evolutionary state. Interestingly, the R band luminosity of the BGG does not correlate with σ, nor with Sersic, which rules out the potential that the σ-Sersic correlation was simply reflecting an underlying BGG luminosity trend.

Additionally, the correlation with environmental parameters shows that more massive

systems tend to populate denser regions. While the most significant correlation is with the 3 Mpc environmental parameter, there are still strong correlations on the scale of 10 Mpc. Intuitively, this means that groups have been able to grow accreting mass from their surroundings, this explanation is consistent with a standard picture of hierarchical growth in which the most massive systems reside in more massive locations.

UV sSFR is anti-correlated with the luminosity of the BGG (slope = -0.54 with p-value = 0.001), thus the star formation is quenched in systems with a high mass BGG, which is a typical sign of an older structure. Notice that there is no similar correlation between UV sSFR and σ. While $intL_{FUV}$ and UV SFR and sSFR are all anti-correlated with the stellar mass fraction (slope = -0.55 with p-value = 0.001, slope = -0.60 with p-value = 0.001, slope = -0.64 with p-value = 0.001 respectively), only UV sSFR is uncorrelated with σ. This seems to indicate against a simple halo mass dependence, and may again point to sSFR being fundamentally linked with the state of the group.

The stellar mass fraction is anti-correlated with two environmental parameters: the LSS and the density at 3 Mpc (slope = -0.52 with p-value = 0.001, slope = -0.53 with p-value = 0.001 respectively). This could indicate that in less dense areas the dark matter haloes are smaller and, as expected for smaller haloes, they have a higher ratio of visible matter. Another interesting correlation of the stellar mass fraction is with the total metallicity ($[Z/H]$); low mass systems have higher metallicity. Notice that, if treating the galaxies as a whole, this is in the opposite direction to the standard galaxy mass-metallicity relation, which has higher metallicity for higher mass galaxies. This correlation does not have an obvious driver, but may reflect the more evolved state of the group.

The $NUV - R$ colour of the BGG correlates with the density parameters (i.e. 3, 5, 10 Mpc) (slope = 0.53 with p-value = 0.001, slope = 0.52 with p-value = 0.001, slope = 0.63 with p-value = 0 respectively) suggesting that the star formation is somewhat

linked to the large scale environment (i.e. suppressed in denser large scale environment). However, the BGG colour does not correlate with σ and this might again reflect that there are fundamental correlations that are not only governed by the system mass.

Indicators of the formation history of a group are always powerful as probes of the growth of structure. As might be expected, the magnitude gap (mag_{gap}) between the first and second brightest galaxies in the group correlates weakly with the *Age* of the BGG (slope = 0.41 with p-value = 0.05). Similarly, the mag_{gap} anti-correlates with the distance between the BGG and the center of the group (slope = -0.57 with p-value = 0.001). This would suggest a natural scenario where mag_{gap} reflects how evolved the system is.

Although also the absence of correlation could be significant, given the high number of parameters it was not possible to infer it.

Most of the correlations observed show some sort of dependence on the mass of the system, and they support the idea that more massive structures are older, hence in a more advanced evolutionary state. This is probably the case in dense large-scale environments, where lots of material is available for accretion and, as time go on, a group grows. However, this may not be the case for isolated systems, which could be in a relaxed dynamical state, but stay small since there is nothing to accrete from the surrounding regions.

4.2.2 Multivariate Data Analysis

In the previous analysis, there can be a concern that the correlation between two parameters is reflective of a third driving parameter, or that such an analysis will miss correlations that more parameters have in common. In an attempt to do a fully multi-dimensional analysis which looks for the common origin of the correlations, the second stage of the analysis consisted of identifying different classes of groups using all the parameters available. To do this, a statistical clustering analysis was performed using

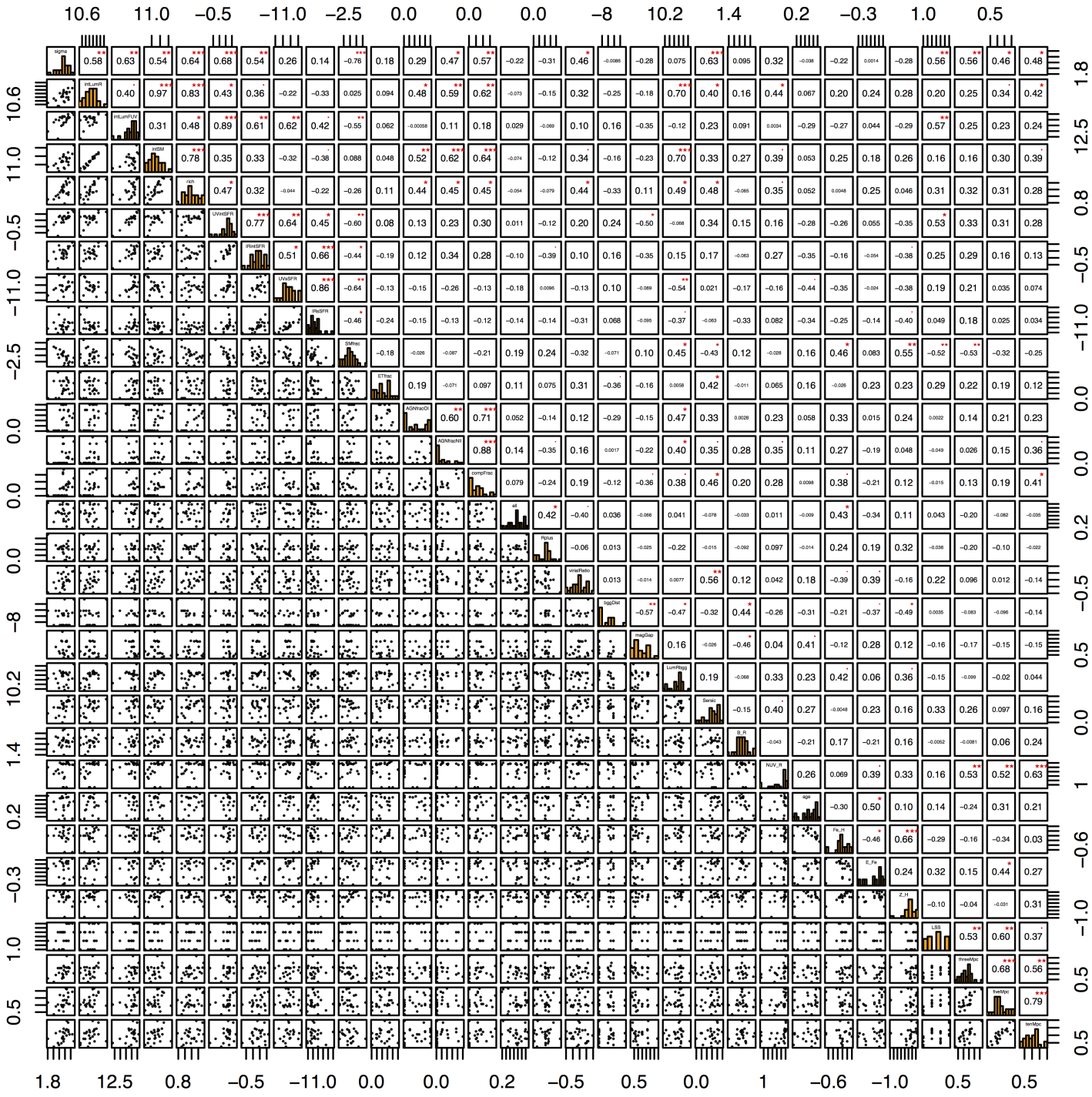

Figure 4.4: Correlation plot: in the lower left triangle the scatter plot for each pair of parameters are shown; on the diagonal there are the histograms showing the distribution of each variable; in the upper right triangle it is shown the result of the Spearman correlation test, highlighting the significance of the result obtained using the p-value (three stars for p=0, two stars for p=0.001, one star for p=0.01, and one small square for p=0.05). The numbers shown on the four sides are the lower values for each variable. This plot is solely shown with the purpose of displaying the large number of parameters available and analysed, the results are discussed in the text.

X-means [Dan Pelleg, 2000].

X-means

X-means is an algorithm used to find statistical clustering of points in n-dimensions. It is an extension of a previously existing algorithm called k-means [Bishop, 1995; Duda and Hart, 1973].

The original algorithm, k-means, divides the input data points into k subsets, called clusters[1], where k is given by the user. To do this, it defines k random centroids and calculates the distance of all points to each centroid, assigning membership according to the minimum distance obtained. Once the membership is determined the new centroids are calculated averaging the n-dimensional coordinates of all the points, the process is iterated until the result converges (i.e. the algorithm always finds the same centroid and assigns the same membership).

The main improvement of X-means is that it optimises the number of classes found, requiring only a lower bound to start with. Figure 4.5 schematically shows how the optimisation process works. After k-means has found a stable result for the lower bound set by the user (4.5a), it splits the centroids in two random and opposite direction within the boundary, and at a distance proportional to the size of the class (4.5b). Then k-means is run again within the 'parent' distribution for each pair of new centroids (i.e. k-means with k=2) (4.5c). The algorithm uses the Schwarz criterion to determine whether the new result (4.5d) models the distribution better than the previous one (4.5a) or not, and kills either the old 'parent' centroid or the new 'children' centroids (4.5e). If the new classes better describe the data distribution, the same procedure is repeated until the 'parent' centroid is chosen as best result. For more details see Dan Pelleg [2000].

[1] In the rest of this work a cluster will be referred to as a class, to avoid confusion with the term cluster of galaxies.

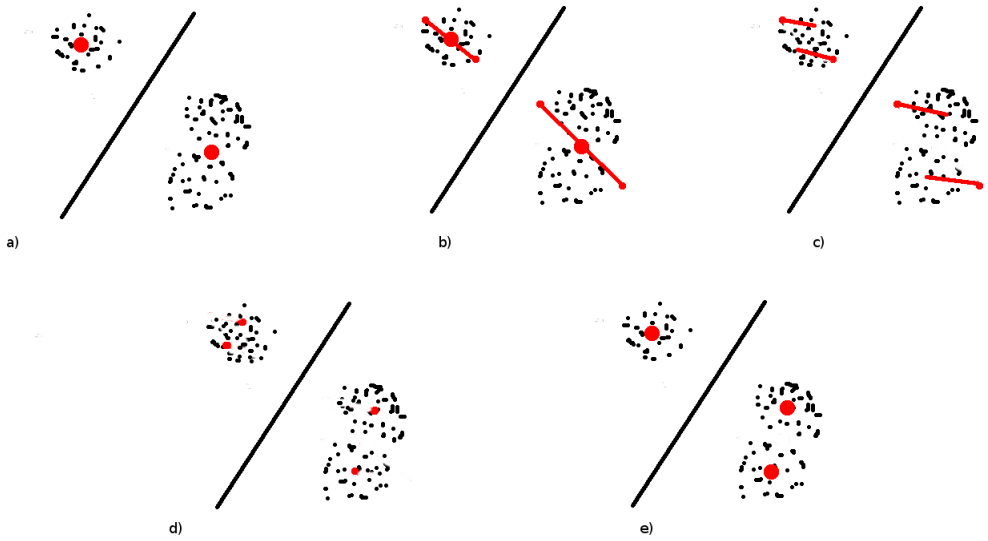

Figure 4.5: Cartoon explaining the optimisation of the number of classes k performed by X-means. The black lines represent the boundary between the classes, in red are shown the centroids. The number of cluster optimisation start after k-means has found a stable result for the lower bound set by the user a). Then it splits the centroids in two in a random and opposite direction within the boundary, and at a distance proportional to the size of the class b). k-means is run again within the 'parent' distribution for each pair of new centroids (i.e. k-means with k=2) c). A model selection criterion determines whether the new result d) models the distribution better than the previous one a) or not, and kills either the old 'parent' centroid or the new 'children' centroids e). If the new classes better describe the data distribution, the same procedure is repeated until the 'parent' centroid is chosen as best result.

Originally, due to missing data this analysis was performed on 17 groups. Before the clustering analysis, the set of data containing all the parameters available were normalised using the standard deviation of their distribution. Then the data were fed to the algorithm, setting the initial minimum class number to 2 and allowing 100 iterations per run and a total of a hundred runs.

A stable result was obtained, finding 2 classes with constant membership, a low mass groups class and a high mass groups one. Not surprisingly, these classes were dominated by mass dependence which prevailed over any other property. In Figure 4.6, it is shown a plot of NUV-R vs Sigma where the groups were divided according to their mass as shown by the two symbols, although there is an obvious visual grouping in NUV-R. This suggested that mass was not allowing a clustering based on any other property, effectively hiding any other classification.

Therefore, the next step was to exclude the mass dependent variables from the analysis. Furthermore, since in the following stage of the analysis the galaxy properties will be explored as a function of the group classes, they were excluded as well in order to remove any potential circularity. Variables dominated by low statistics were also discarded from the analysis in order to lower the noise introduced in the clustering analysis by unreliable, or in some way biasing, parameters. From this point onward also the density at 10 Mpc was excluded given its strong correlation with the density at 5 Mpc.

The exclusion of some of the parameters allowed to include more groups, thus the analysis was performed on 22. The final set of parameters used in the clustering analysis were: magnitude gap, stellar mass fraction, density at 3 and 5 Mpc, BGG distance from the centroid, ellipticity of the group, $R+$ parameter (described in section 4.1), and R-band luminosity, Sersic index and $NUV - R$ colour of the BGG.

X-means found a stable result, identifying 4 classes (see Table 4.2). In 20% of the

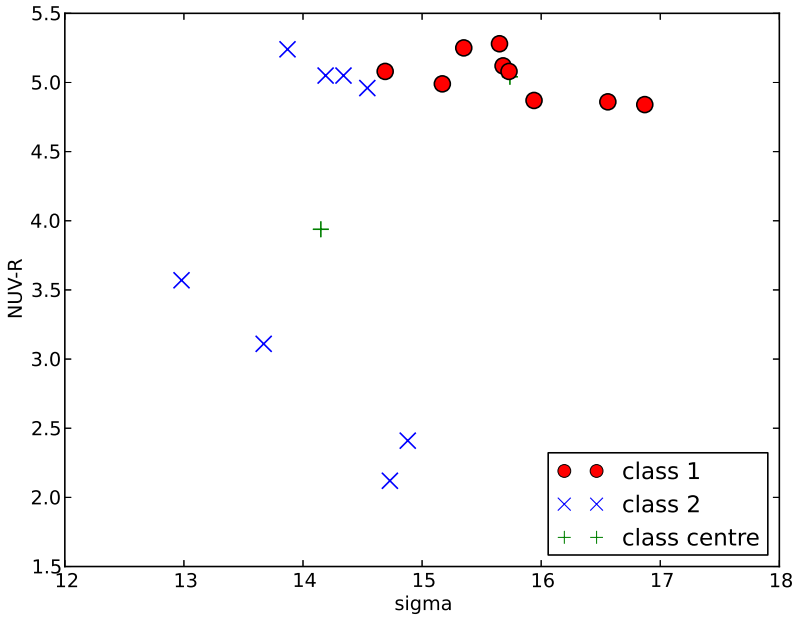

Figure 4.6: The plot shows how, in the first run of X-mean, the clustering is dominated by the mass of the systems. The two symbols represent the two classes obtained, the green crosses are the centroids of each class.

A	B	C	D
3182	770	1766	9137
3849	3541	3067	9307
4548	3698	4001	10451
4577	4592	4881	
	9994	5383	
	10167	8816	
		9014	
		9069	
		10300	

Table 4.2: This table shows the class memberships. The numbers are the groups ID (MZ*).

iterations two classes were joined, but they will be kept separated for the rest of the analysis and eventually rejoined if the galaxy properties will not show any difference. The stability of this result was confirmed by the fact that the final clustering was mostly consistent with that obtained in various check runs done excluding few variables at the time.

As a further check, the values for each of the ten parameters used in the clustering analysis were simulated in 30 iterations. The new points were distributed within each class according to the mean and standard deviation of the values in the class itself. The clustering analysis was re-run for each of the 30 iterations to check the new class assignment for each group.

The significance that a given group is in its class rather than another class is given by:

$$(No.\ in\ original\ group\ - No.\ in\ next\ group)\ /\sqrt{iterations}. \tag{4.7}$$

The result summarised in Table 4.3 and Figure 4.7 confirms that the reliability of the clustering is $> 3\ \sigma$ confidence level for all the groups hence confirming the robustness of the result.

After identifying the four classes, the value for every parameter was plotted for each

group	# in main group	# in next group	confidence level (σ)
MZ770	22	5	3.10
MZ1766	25	2	4.20
MZ3067	25	2	4.20
MZ3182	28	2	4.75
MZ3541	24	3	3.83
MZ3698	26	2	4.38
MZ3849	25	3	4.02
MZ4001	24	3	3.83
MZ4548	28	1	4.93
MZ4577	30	0	5.48
MZ4592	25	5	3.65
MZ4881	24	2	4.02
MZ5383	23	4	3.47
MZ8816	24	2	4.02
MZ9014	24	3	3.83
MZ9069	21	4	3.10
MZ9137	21	4	3.10
MZ9307	22	4	3.29
MZ9994	27	2	4.56
MZ10167	23	5	3.29
MZ10300	21	4	3.10
MZ10451	22	4	3.29

Table 4.3: Table showing the results obtained for the clustering analysis after the MC simulation of the points. The first column shows the name of the groups; the second the number of times the groups were classified in the same class as the main analysis; the third the number of times the groups were classified in the second most probable class; the fourth is the significance calculated as in Equation 4.7.

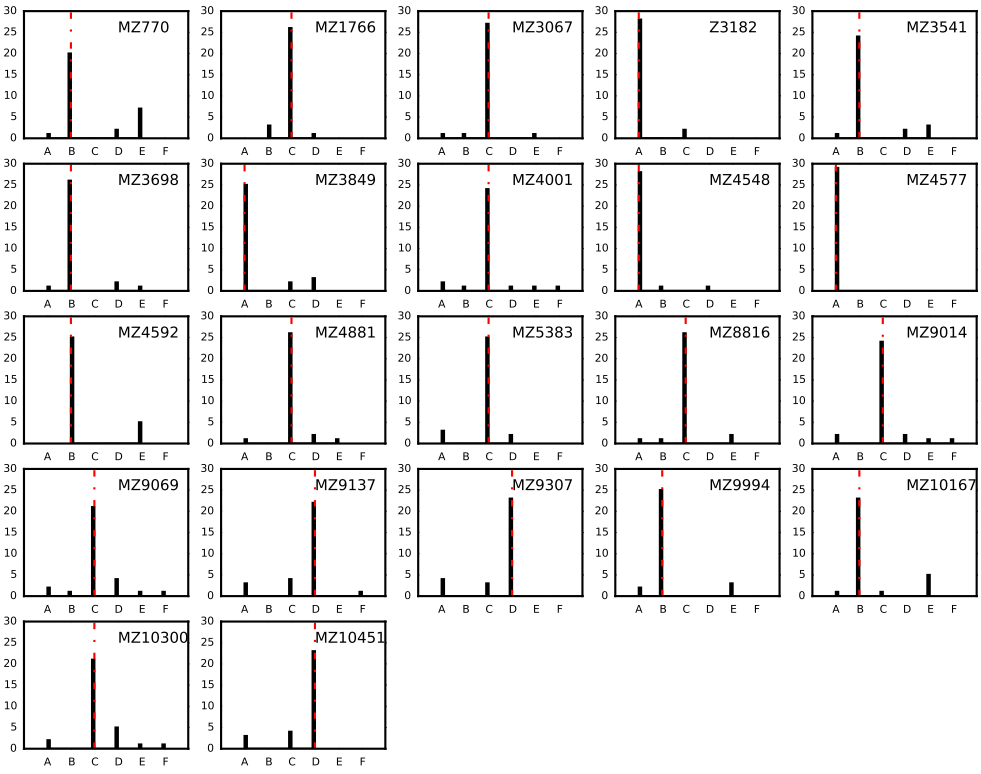

Figure 4.7: Each plot shows a histogram containing the classification of every group for each run of the clustering for the simulated points. The class assigned using the real data is shown by the dashed red vertical line.

group in the four classes (Figure 4.8), the parameters used in the multi-variate analysis are shown in red.

It can be observed in the plot that, despite the fact that none of the mass related parameters were included in the analysis, the clustering shows a separation in mass well visible in the sigma plot, where the left two classes are low mass systems (class A and B), whereas the other two are the high mass systems (class C and D).

One of the main differences between the two low mass systems is the UV sSFR which looks enhanced in class A. This same class appears also to have a peculiar behaviour in the stellar mass fraction parameter, which is lower than expected in that mass range. In fact as previously observed more massive systems contain more dark matter than stellar content and vice versa [e.g. Giodini et al., 2009; Gonzalez et al., 2007]. It can be expected that this value will increase thanks to the ongoing star formation, and, at a later stage, will be the same as that of class B, effectively making the groups in A and B part of the same class. The BGG distance of this highly star-forming class spans a wide range of values, as expect for systems in an early stage of formation, and $NUV - R$ colour and age are consistent with the UV sSFR. Another difference between the two low mass classes is the density at 3 Mpc, lower for class B than for class A. This might imply that galaxies are still accreting in class A groups, while class B groups are isolated.

4.3 Discussion

The aim of this work is to perform a systematic study of galaxy groups with the aim to find correlations within the multi-wavelength data available, and be able to divide the groups in different classes according to their evolutionary state.

From the correlation analysis it is clear that the main driver of the group properties is the mass. High σ groups, hence more massive groups, show the expected trend in

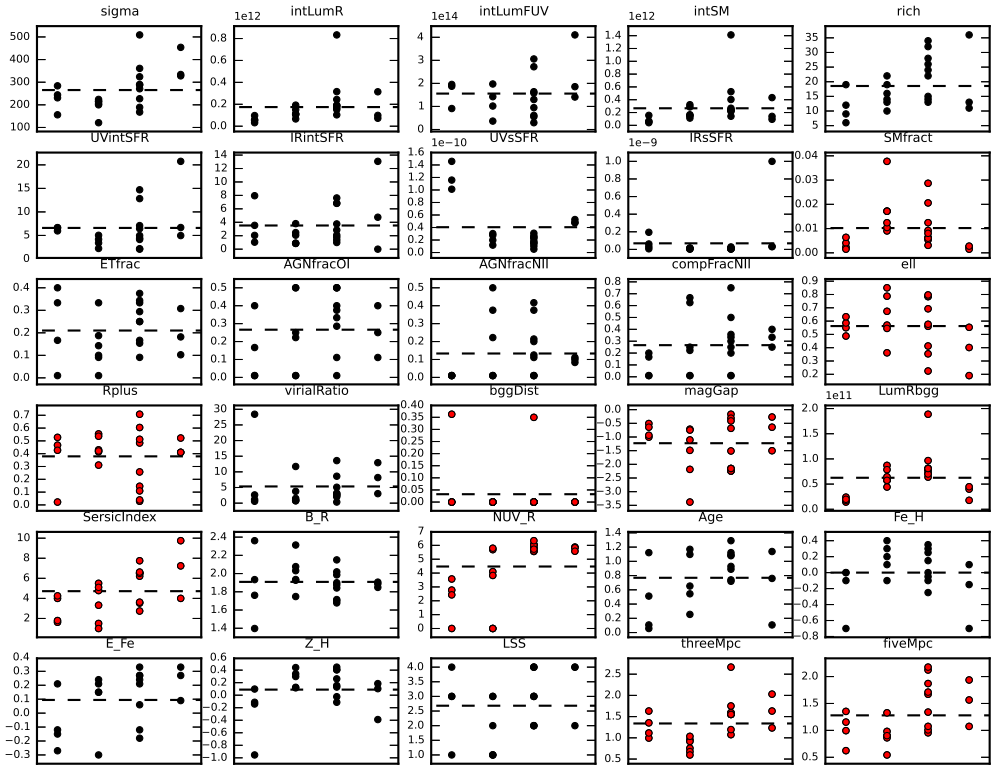

Figure 4.8: Each plot shows the value of every parameter for each group in the four classes. The dashed line shows the mean for that parameter calculated for all the groups. In red are plotted the variable used in the X-means clustering analysis.

stellar mass fraction, have bulge-dominated BGGs, and live in denser environments. The presence of an elliptical galaxy in the centre of the group is a clue of an evolved system, (i.e. the group looks like a small scale cluster), hence it is not expected to observe star formation getting closer to the centre, which is supported by the correlation with the UV properties. These results agree with the hierarchical growth of structures scenario: galaxies meet for the first time and are observed as a poor, not strongly bound, group of field-like galaxies. Then more galaxies accrete from the surrounding regions and the system slowly moves toward gravitational equilibrium with the formation of a larger dark matter halo. The group, whether relaxed or not, continues to accrete new members, eventually groups will merge or will be accreted by larger clusters.

However, because groups can be in a big variety of dynamical states, there is the chance to observe different stages of their evolution. Hence, it would be interesting to be able to separate these stages, classifying the groups according to their properties, other than their mass. Thanks to a statistical clustering analysis performed on selected parameters which describe different properties of the system, except for the total mass, four classes of groups are found.

Interestingly, the mass remains the dominant parameter in the characterization of a group evolutionary state. In fact the four groups can still be divided into two low mass (A and B) and two high mass (C and D) group classes.

C and D do not show many differences except for a few parameters, these are in fact the classes that are joined in some runs of the clustering analysis. The differences are in sSFR, R-band luminosity, age and metallicity of the BGG, which suggest ongoing star formation, hence younger stellar population, in class D despite the fact that this was expected to be in a more advanced evolutionary state given its mass. Also class D contains only three groups suggesting that these kind of groups are rare. It will be possible to better understand this with the study of the galaxy properties, but in the meantime assumptions can be made about the possibility of these being disturbed

systems, for example the BGG could be experiencing a merger, or the whole group could be in the process of infalling into a larger cluster.

Class A and B show more striking discrepancies. Given that these low mass classes were predicted to contain no relaxed groups, high SFR is expected to be seen in both, this is however only observed in class A, while class B simply looks like a small scale version of class C (e.g. the systems look in an advanced evolutionary state, but with smaller mass). This last point could be explained by the fact that class B groups reside in a low density environment, hence they are not surrounded by galaxies or gas to accrete. However, there is a large spread in stellar mass fraction which could indicate a wide range of dynamical states: some of the groups are small because they are isolated, others are still in an early stage of their evolution.

The most distinct class is A. Apart from the high UV sSFR, all the groups have low metallicity; SF metal poor galaxies are typical of the field and this suggests that they may be encountering each other for the first time, as it is also suggested by the large spread of BGG distances, since the brightest galaxy would be expected to occupy the centre of the halo in an evolved system. Furthermore, the stellar mass fraction is low compared to what expected for small haloes, thus it is reasonable to argue that the galaxies are not yet part of the same dark matter halo. If it was possible to observe the groups in this class in a later evolutionary stage, the star formation would be expected to have increased the stellar mass fraction to a value comparable to that of class B, and had been quenched by interaction with the evolved intra-group medium (IGM) and with the other group members.

After observing the different properties of these four classes, the galaxy properties and their relation with the different evolutionary state of groups will be studied. Ultimately, the aim is to be able to find new insights in the galaxy evolution process, what affects

it and on what time scale, and in the formation of large structures in the Universe.

Chapter 5

Properties of Galaxies within Classes of Groups

The aim of this chapter is to study the properties of galaxies belonging to the four different group classes defined in Chapter 4, with the aim to disentangle the different evolutionary states of the groups and to determine the effect these have on the evolution of galaxies.

The group classification showed that mass, both the halo mass and the mass traced by the luminous matter, is a key parameter in the characterisation of a system, so by studying the galaxy properties in the different classes a different trends reflecting the system state is expected. Several key diagnostics for the star formation, morphology and metallicity of these galaxies will be investigated in an attempt to unravel the connections between evolutionary state and galaxy property.

The generally accepted mass-metallicity relation [Tremonti et al., 2004] states that high mass galaxies have high metallicity. More recently the metallicity have been studied in the context of environment. Cooper et al. [2008] studied SDSS galaxies and observed that galaxies in high density environment have higher metallcity. Similarly Ellison et al. [2009], also using SDSS galaxies, observed that galaxies in denser local

environment had higher metallicity, whether they were cluster members or not. Conversely, Hughes et al. [2013] observed no dependence of the mass-metallicity relation with environment. Mannucci et al. [2010] uncovered a relation between metallicity and stellar mass: low-mass galaxies have lower metallicity the higher the SFR, while no dependence is observed for high-mass galaxies. In relation to this study, Peng and Maiolino [2014] studied the mass-metallicity dependence with environment using SDSS galaxies and distinguishing between central and satellite galaxies. Similarly to Mannucci et al. [2010] they observed that satellites in denser environment, thus with less star-formation have higher metallicity, while centrals, more massive show no such dependence. Furthermore the differences between the two populations are smaller at higher masses.

The galaxies studied in this work, independent of the class, follow the general mass-metallicity trend [Tremonti et al., 2004], as shown in Figure 5.1, in spite of the smaller mass range analysed in this study. The larger plot shows all the classes together plotted in different colours (class A in black, B in red, C in blue, and D in green), two different symbols have been used for galaxies within R_{200} (circles) and outside R_{200} (crosses). The smaller plots on the right represent each class, where the same general trend is followed by all the distributions, but the range in mass and metallicity varies, with class A having the smallest distribution in both parameters. The number of galaxies in the plots reflect the number of spectra for which it was possible to perform a Lick indices analysis. The outliers (i.e. highly scattered low-metallicity high-mass galaxies and high-metallicity low-mass galaxies) could be due to the high uncertainty in the determination of the metallicity, as shown by the size of the errobars, but may also reflect unique galaxy properties and should be further investigated. The galaxies outside R_{200} do not show any difference in their distribution on the plot, except in class A and B where they appear to be systematically at lower metallicity. This could reflect the fact that they are field galaxies in the process of being accreted by the groups, but this

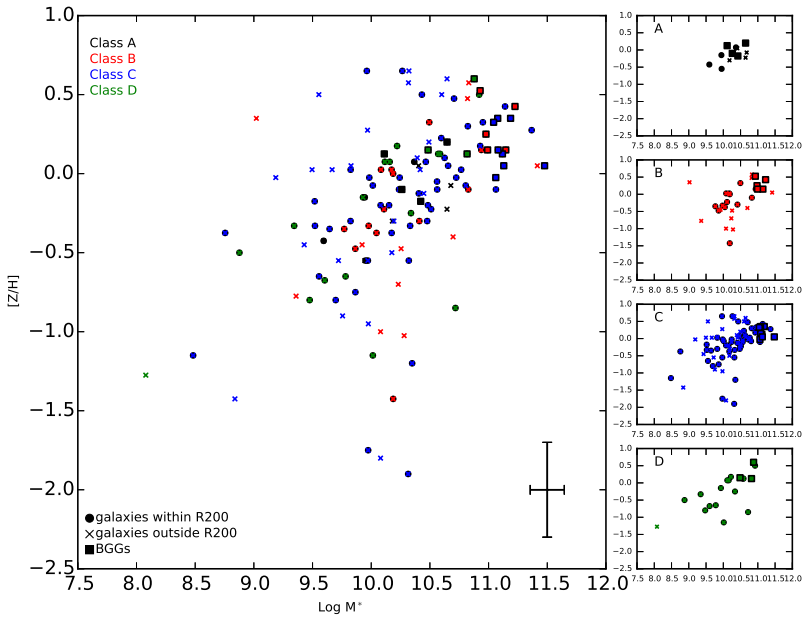

Figure 5.1: These plots show the mass-metallicity relation: on the x-axis is plotted the stellar mass, on the y-axis the metallicity. The bigger plot on the left shows all the classes together represented in different colours: class A in black, B in red, C in blue, and D in green. The circles are used for galaxies within R_{200}, the crosses for galaxies outside R_{200}, the squares show the BGGs. The smaller plots on the right show the same relation for each class. In the bottom right corner of the main plot the typical size of the errorbars is illustrated.

hypothesis needs further investigation. Strangulation, or stripping, processes is likely to move galaxies at fixed stellar mass to higher metallicity.

Exploiting the availability of multi-wavelength data, another general relation studied is between NUV-R colour and R-band magnitude, previously analysed by [Rasmussen et al., 2012] using the FUV-NUV coulour. Similarly to this previous work, the trend observed confirms that passive galaxies are the brightest in the R-band (see Figure 5.2). However, faint passive galaxies are not included in this study because their UV luminosity is lower than the detection threshold. The plot, similarly to the previous one, shows the classes in different colours (A in black, B in red, C in blue, and

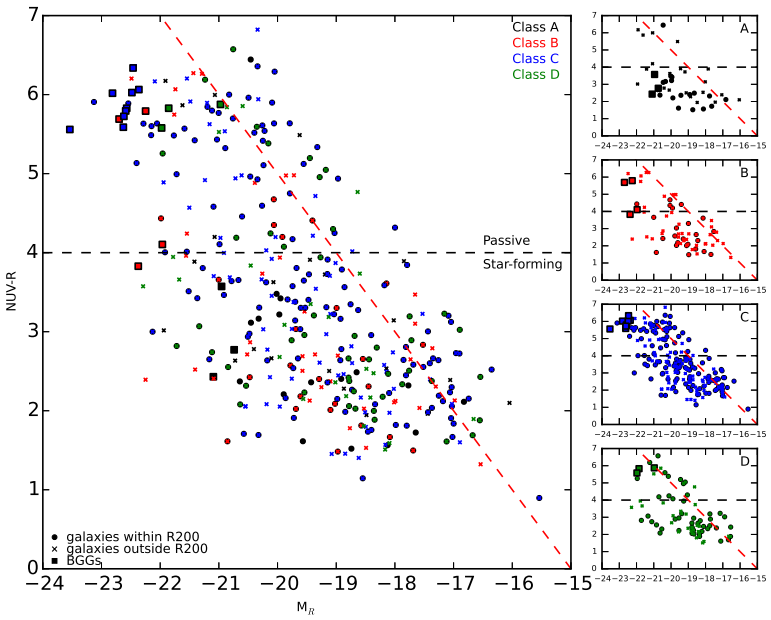

Figure 5.2: These plots show the NUV-R colour-magnitude relation: on the x-axis is plotted the absolute R-band magnitude, on the y-axis the NUV-R colour. The horizontal dashed line at NUV - R = 4 divides passive from star-forming galaxies, while the diagonal red dashed line shows the detection threshold. The bigger plot on the left shows all the classes together represented in different colours: class A in black, B in red, C in blue, and D in green. The circles are used for galaxies within R_{200}, the crosses for galaxies outside R_{200}, the squares show the BGGs. The smaller plots on the right show the same relation for each class.

D in green) and the galaxies within and outside R_{200} are represented with two different symbols, circles and crosses respectively. The dashed line at NUV-R = 4 separates the passive from the star forming galaxies [Salim et al., 2007], the red diagonal dashed line shows the detection threshold. The same plot split into classes does not show any substantial difference, neither does the distribution of galaxies within and outside R_{200}.

As it was obvious from the plots showing the single classes, the distribution of galaxies are very different from one class to the other. To better quantify this, Figure 5.3 shows the luminosity function for each class, as described in Chapter 3 the catalogue is 100% spectroscopically complete down to M_R = -20, with an even deeper photometric

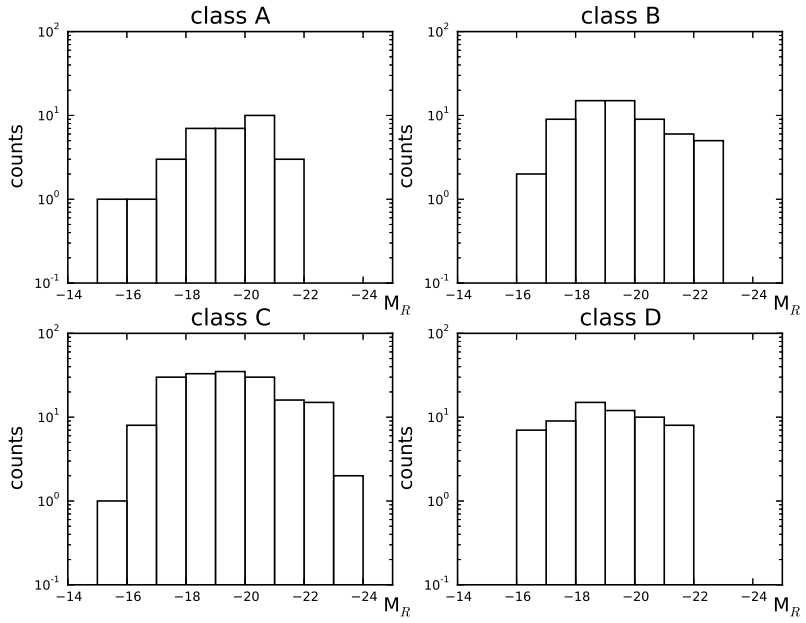

Figure 5.3: Plots showing the luminosity function for each class: the absolute R-band magnitude is on the x-axis, while the number of counts in logarithmic scale is on the y-axis.

completeness as in 2dF, and with no slit collision thanks to the multiple pointings in the group central regions. Classes A and B contain small mass groups hence the small number of galaxies, class D small number reflect the fact that it only contains three groups. The most noticeable characteristic of the luminosity functions is that class A and D lack bright galaxies compared to the other two. For class A this could be explained by the small mass of the groups, on the contrary class D contains massive groups, however they appear to be disturbed hence not virialised, this implies that the velocity dispersion could have been overestimated and so the mass. Additionally, the almost flat distribution could be explained by the absence, in galaxy groups, of galaxies comparable to the most massive galaxies in the Universe as seen in big clusters.

To study the galaxies in each class separately, it is interesting to plot the projected phase-space diagram showing the radial dependence of the velocity of each galaxy. This

is useful to deduce the infalling history of galaxies in groups and clusters, in fact, as shown by Haines et al. [2012] galaxies accreted at different epochs occupy different regions of the diagram: passive galaxies accreted early are found at small radii and velocities, while recently accreted objects occupy all the radial and velocity regions. A third important class is made of the so-called backsplash galaxies, namely those galaxies which have crossed the cluster core once, hence have interacted with the environment, but have not yet set in the virialised region [Balogh et al., 2000]. These galaxies occupy an intermediate region at high radii and small velocities compared to the recently accreted ones. A study by Noble et al. [2013] quantified the regions on the phase-space diagram using lines of constant $(R/R_{200}) \times (\Delta v/\sigma)$, called caustic lines, the three population of galaxies are now defined as follows: virialised galaxies are found within 0.1 $(R/R_{200}) \times (\Delta v/\sigma)$, backsplash galaxies between 0.1 and 0.4 $(R/R_{200}) \times (\Delta v/\sigma)$, and recently accreted galaxies reside outside 0.4 $(R/R_{200}) \times (\Delta v/\sigma)$. Muzzin et al. [2014] confirmed that quiescent galaxies are found at small radii and velocities, while post-starburst galaxies occupy a ring on the diagram at small radii, but high velocities, avoiding the cluster core, similarly to backsplash galaxies. This might suggest that post-starburst have crossed the cluster core once and have experienced a fast quenching mechanism. A similar results is also found by Jaffé et al. [2015] which studied the HI deficiency of galaxies in cluster and observed that they appear to occupy the same region as backsplash galaxies suggesting that the environmental effects, such as stripping, are experienced by a galaxy during its first crossing.

Despite galaxy groups not being well studied in phase-space because of the small number of members which makes the centroid definition highly uncertain, it can be assumed that they are small-scale clusters. Thus the study of their phase-space diagram should give some insight on their dynamical state. For instance more massive groups with a bright elliptical galaxy in the centre can be expected to be relaxed in the core similarly to clusters, hence have a similar phase-space galaxy distribution. Galaxies in less

massive groups or at an early stage of their formation can be expected to populate areas of the diagram at higher radii and velocities, typically populated by infalling or backsplash galaxies in clusters.
In this work different phase-space diagrams were studied, each one colour coded according to some of the most meaningful galaxy properties: morphology (i.e. Sersic index), R-band magnitude (i.e. mass), and NUV-R (i.e. star formation activity). We expect the diagram to be similar to that of massive clusters if the groups are virialised, or we expect to see the regions at high redius and velocity to be the most populated if the group is in its formation phase.

The first diagram shown is colour coded according to the Sersic index value for each galaxy (see Figure 5.4). We decided not to assign a morphology to a certain Sersic value due to the uncertainty in this measurement, moreover the Sersic index for BGGs could be due to extended emission and not indicative of its morphology. Thus the Sersic continuum was used, as it was for the clustering analysis, being a direct measurement and not a derived quantity. However in some studies Sersic values > 2.5 are considered to describe bulge-like galaxies [Patel et al., 2012].
In this plot and all the following phase-space diagrams the BGG is shown with a square symbol, the galaxies withing R_{200} are circles and those outside are crosses. Simply looking at the distribution of points on the plot, a few differences between the classes can be observed:

- Class A shows an asymmetric distribution of galaxies, supporting the hypothesis that the groups are not relaxed, as suggested by the study of phase-space diagrams indicating that galaxies at higher radii and velocities are likely in the process of being accreted by a larger halo;

- Class B and D seem to lack galaxies at small radii, suggesting that the groups are either not virialised, or disturbed, for example some galaxies might have moved in

the phase-space diagram because they were experiencing mergers and thus have high velocity offsets. Another possibility for class B is that, given the small mass of the groups, there are simply not many galaxies overall, nor new ones to accrete, this explanation does not hold for class D which contains high mass groups;

- Class C shows a concentration of bulge-like BGGs (i.e. high Sersic index value) at small radius and velocity, suggesting that this class contains the most evolved systems in the sample, again this is supported by previous studies of phase-space diagrams showing that the galaxies residing at small radii and velocities are in virial equilibrium.

In classes A and B some of the BGGs are late-type galaxies giving a further evidence that these groups are not yet relaxed. Globally, the colour coding shows that bulge-like galaxies, including the BGGs, tend to be concentrated at small radii, it also shows that apart from class C, the groups do not have a large population of these morphological types. This might indicate that these groups have not reached densities that affect the morphology type of the galaxies, meaning that they are still in a collapsing phase, similarly to what was observed by Oemler [1974] .

The second interesting quantity to study in the phase-space diagram is the absolute magnitude in the R-band (Figure 5.5), since it is strongly correlated with the galaxy mass. The R-band magnitude was chosen instead of the mass because it is a direct measurement and does not add uncertainty deriving from assumptions in the mass calculation. Brighter galaxies in R-band are displayed in a darker shade of red. The larger number of galaxies at higher radii compared to the previous plot is due to a higher R-band completeness thanks to the available data from 2dF for which a Sersic index analysis was not performed. The brightest galaxies are concentrated at small radii and, in class C, also at small velocity. This result is somewhat expected given that bulge-like galaxies are usually also the most massive. Class A seem to be the only

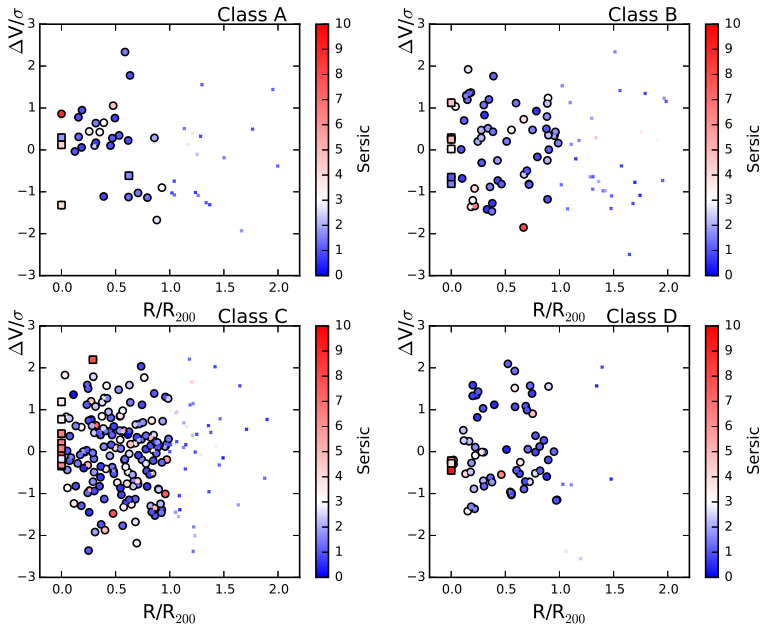

Figure 5.4: Phase-space diagram colour-coded according to the Sersic index value plotted for each class: on the x-axis is shown the radius in units of R_{200}, on the y-axis the difference between the galaxy velocity (cz) and the average group velocity, normalised by the velocity dispersion of the group. The circles are used for galaxies within R_{200}, the crosses for galaxies outside R_{200}, the squares show the BGGs.

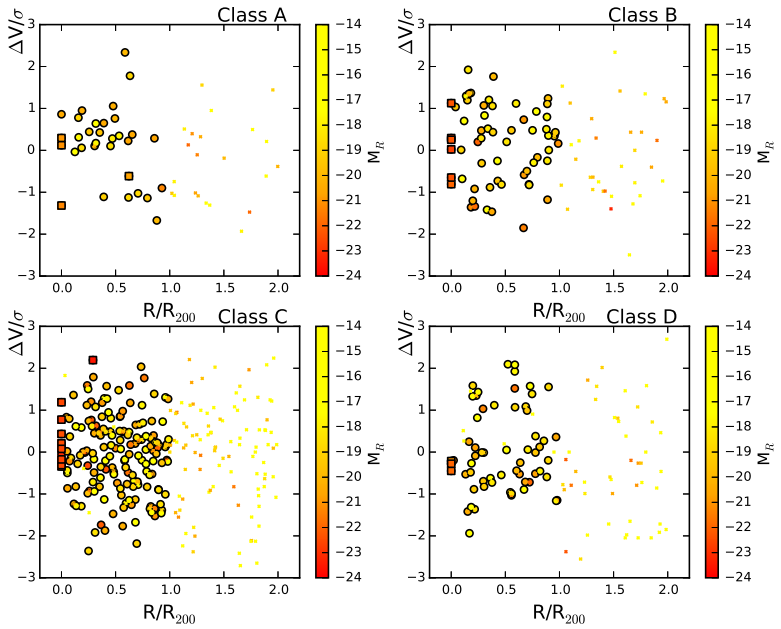

Figure 5.5: Phase-space diagram colour-coded according to the absolute R-band magnitude plotted for each class: on the x-axis is shown the radius in units of R_{200}, on the y-axis the difference between the galaxy velocity (cz) and the average group velocity, normalised by the velocity dispersion of the group. The circles are used for galaxies within R_{200}, the crosses for galaxies outside R_{200}, the squares show the BGGs. The brighter the galaxy the darker the colour.

one lacking bright galaxies at all radii. As expected the BGGs are the most massive members of the groups.

Since the star formation rate is one of the most interesting variable in the environmental study of galaxy properties, a useful parameter to exploit is the NUV-R colour. The choice of using the colour instead of the SFR was dictated by the fact that the former is a direct measurement, also the SFR is a combination of different physical quantities and in a multi-variate analysis can introduce a redundancy. A work done by Salim et al. [2007] showed that the distinction between star-forming and passive galaxies occurs at NUV-R = 4, higher values are typical of passive galaxies (in red in the plot), while below resides the star-forming population (in blue and white in the plot).

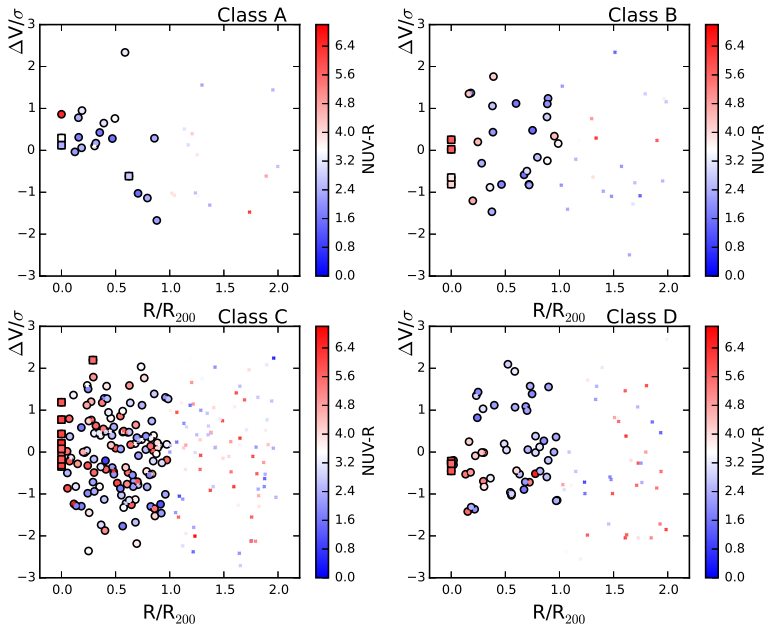

Figure 5.6: Phase-space diagram colour-coded according to the NUV-R colour plotted for each class: on the x-axis is shown the radius in units of R_{200}, on the y-axis the difference between the galaxy velocity (cz) and the average group velocity, normalised by the velocity dispersion of the group. The circles are used for galaxies within R_{200}, the crosses for galaxies outside R_{200}, the squares show the BGGs.

The phase-space diagrams showed in Figure 5.6 has a smaller number of data points than the previous two due to the availability of UV data for less galaxies. However the distribution of passive galaxies is coherent with the morphology and mass of the galaxies as observed in the previous plots, in fact passive galaxies tend to be concentrated toward the centre of the groups. Particular attention needs to be paid to classes A and C, the former lacks passive galaxies (apart from an isolated case), the latter reveals a more uniform distribution of passive galaxies at all radii which may indicate that the galaxies have experienced some sort of quenching, supporting the idea that this class contains the most evolved systems.

To better study the star-forming and passive galaxy population, it was useful to plot the radial dependence of the NUV-R colour and, using the colour coding, directly

relate it to the other two parameters just studied: Sersic index value (Figure5.7) and absolute R-band magnitude (Figure5.8).

Both the plots show somewhat similar results despite the different number of data points as described above:

- class A shows no passive bright bulge-like galaxies;
- class B and D have few passive bright and bulge-like galaxies mainly concentrated at small radii;
- class C has many passive galaxies, the bright ones are found mostly in this area of the plot and distributed out to R_{200}, the bulge-like galaxies are passive as well, but are mainly concentrated at small radii.

A direct comparison between NUV-R colour and Sersic index values is shown in Figure 5.9. As expected bulge-like galaxies tend to be passive, however the passive region of the plot is also populated by low Sersic index galaxies, this is more evident if the single classes are plotted. As previously noted, class A has no passive galaxies, class B and D have passive galaxies all above Sersic = 2, while class C has a large population of low Sersic passive galaxies that could be associated with the known population of passive spirals observed by [Masters et al., 2010; Wolf et al., 2009].

To study in more detail the star-forming properties of the galaxies in the different classes of groups it is interesting to look directly at the stellar population properties (i.e. age, [Fe/H], [E/Fe]) using the results obtained in the Lick indices analysis (see 3.5).

Figure 5.10 shows a plot of age and iron-elements abundance colour coded according to the α-enhancement (yellow shows low α-enhancement, red high). The symbols are used as before to indicate galaxies within R_{200} (circles) and outside R_{200} (crosses), the BGGs are plotted as squares. The stellar population light-weighted age roughly spans

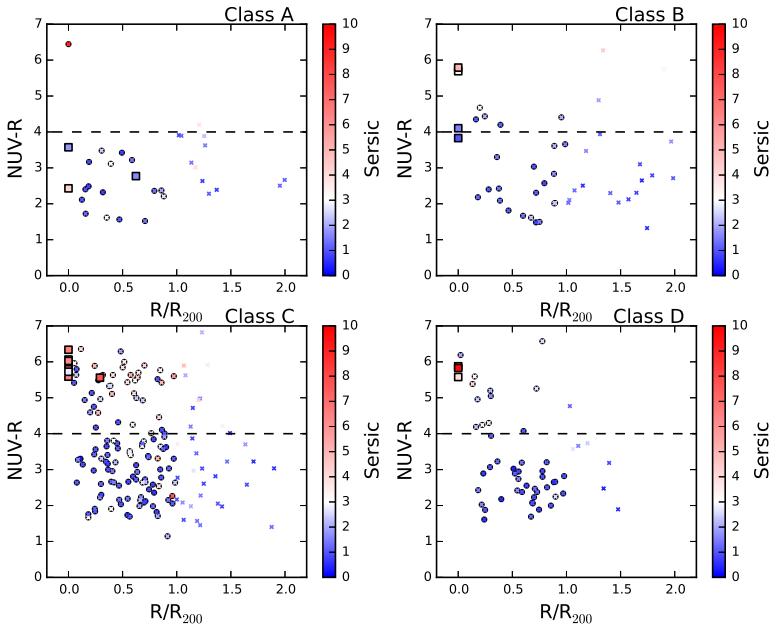

Figure 5.7: Plot showing the radial dependence of the star formation activity based on the NUV-R colour and colour coded according to the Sersic index value: the x-axis shows the radius in units of R_{200}, the y-axis the NUV-R colour. The circles are used for galaxies within R_{200}, the crosses for galaxies outside R_{200}, the squares show the BGGs. The dashed lines separates the star-forming from the passive region.

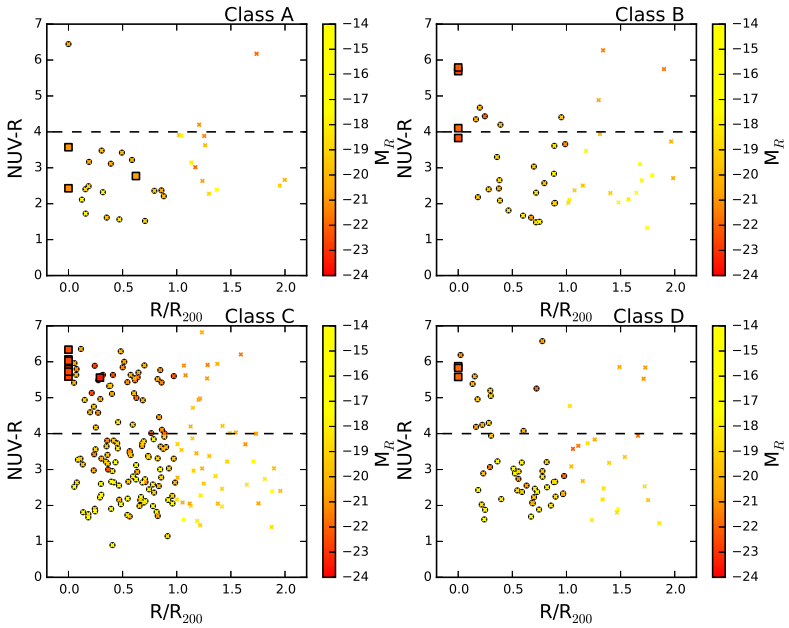

Figure 5.8: Plot showing the radial dependence of the star formation activity based on the NUV-R colour and colour coded according to the absolute R-band magnitude: the x-axis shows the radius in units of R_{200}, the y-axis the NUV-R colour. The circles are used for galaxies within R_{200}, the crosses for galaxies outside R_{200}, the squares show the BGGs. Brighter galaxies are shown in darker colours.. The dashed lines separates the star-forming from the passive region.

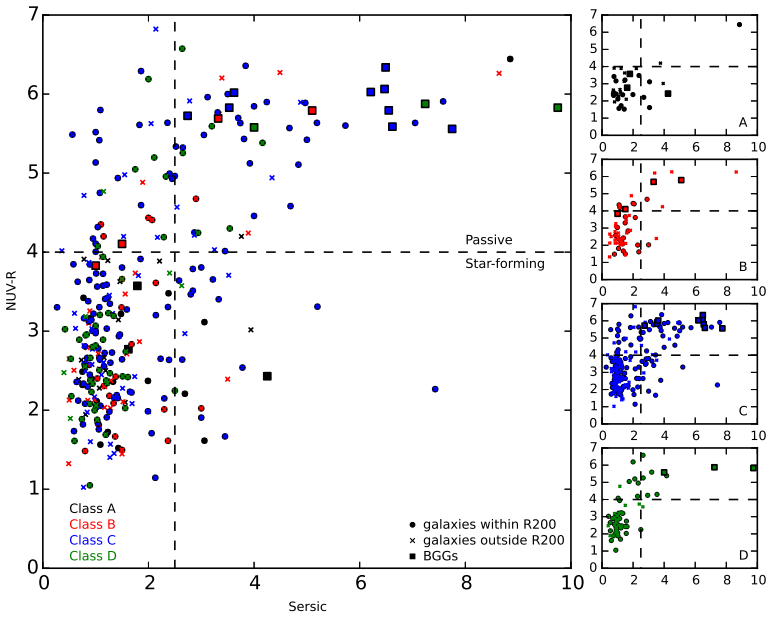

Figure 5.9: NUV-R colour (y-axis) plotted over the Sersic index value (x-axis). The bigger plot on the left shows all the classes together represented in different colours: class A in black, B in red, C in blue, and D in green. The circles are used for galaxies within R_{200}, the crosses for galaxies outside R_{200}, the squares show the BGGs. The smaller plots on the right show the same relation for each class. The horizontal dashed line separates the star-forming region from the passive one, the vertical one separates disc-like galaxies (left) and bulge-like (right).

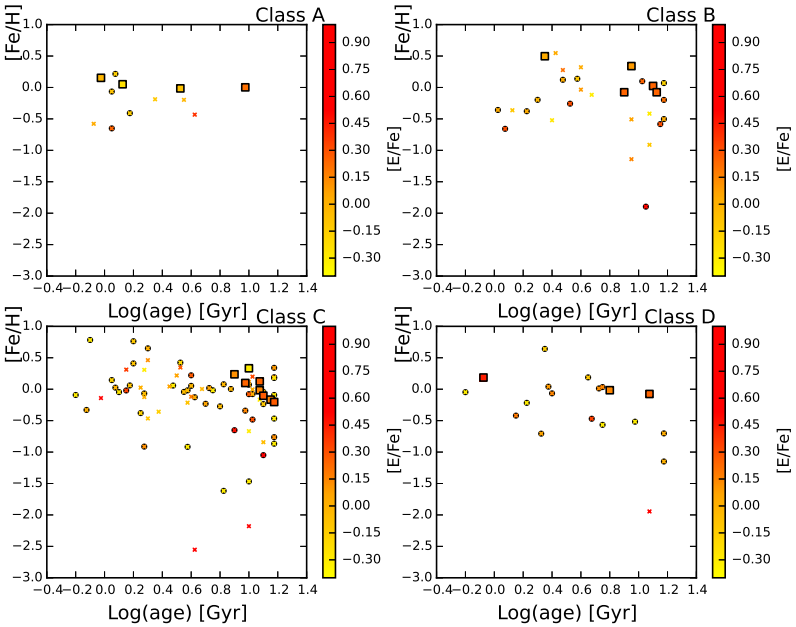

Figure 5.10: Plot of light weighted age against iron-element abundance ([Fe/H]) colour-coded according to the α-element abundance ([E/Fe]) shown for each class: the logarithm of the age is on the x-axis, [Fe/H] on the y-axis. The symbols are circles for the galaxies within R_{200} and crosses outside, the squares show the BGGs.

from 1 Gyr to the age of the Universe in all classes, while the metallicity varies from class to class. Class A spans a small metallicity range around solar values or slightly less, the BGGs span the entire age renge but have high metallicity. Old galaxies in class B, $\sim$ 10 Gyrs, span a broad metallicity range going well below solar metallicity, while the younger galaxies are distributed similarly to those in class A, but they can be slightly metal richer. In this class, apart from one exception, the BGGs are old and metal rich. Class C and D have a similar distribution, however class C galaxies extend to lower ages and metallicity and in class D the BGGs have a distribution similar to class A. The α-enhancement does not show any particular trend.

Figure 5.11 and 5.12 shows the age-metallicity plot colour coded by R-band absolute magnitude and Sersic index respectively to be able to compare with the results obtained

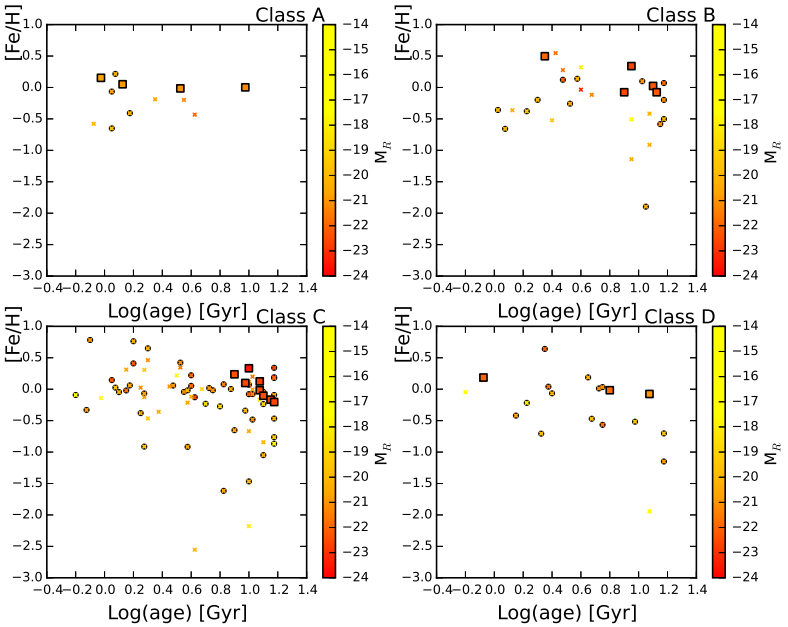

Figure 5.11: Plot of light weighted age against iron-element abundance ([Fe/H]) colour-coded according to the absolute R-band magnitude shown for each class: the logarithm of the age is on the x-axis, [Fe/H] on the y-axis. The symbols are circles for the galaxies within R_{200} and crosses outside, the squares show the BGGs.

in the previous plots, again the symbols used are circles within R_{200} and crosses outside, BGGs are shown as squares. In the Sersic index colour coded plot, it is interesting to notice that bulge-like galaxies are old and with high metallicity in class B and C, while the few in class A and D have younger age. Looking at the R-band magnitude colour-coded plot the reddest galaxies, hence most massive, are the oldest and those with higher metallicity in class B and C, while they are lacking in class A and D as previously observed. The BGG properties also show the same trend observed before. Figure 5.13 and 5.14 shows that old galaxies have high α-enhancement and are the brightest in the R-band and more bulge-like in class B and C. Class A and D do not have bright galaxies, A also lacks bulge-like galaxies. This confirms the hypothesis that these groups are still in a building phase, hence the galaxies are field-like galaxies. Class

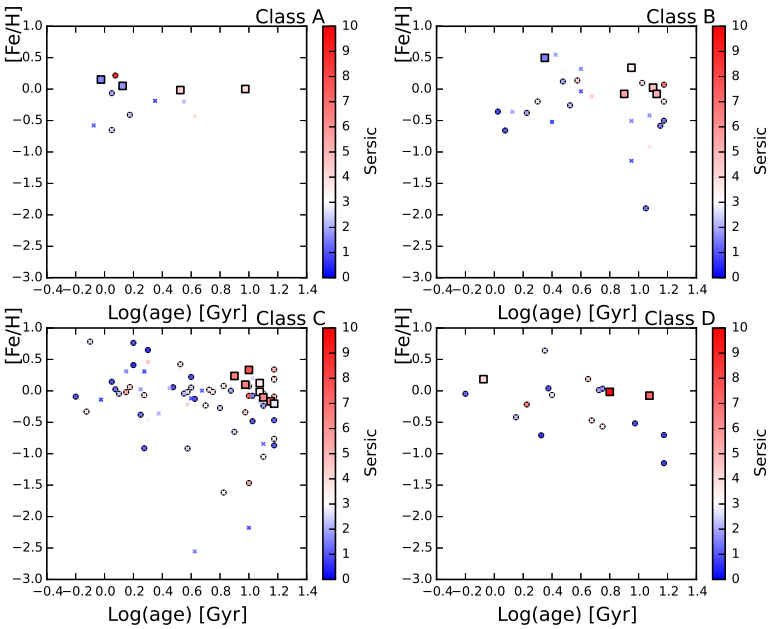

Figure 5.12: Plot of light weighted age against iron-element abundance ([Fe/H]) colour-coded according to the Sersic index value shown for each class: the logarithm of the age is on the x-axis, [Fe/H] on the y-axis. The symbols are circles for the galaxies within R_{200} and crosses outside, the squares show the BGGs.

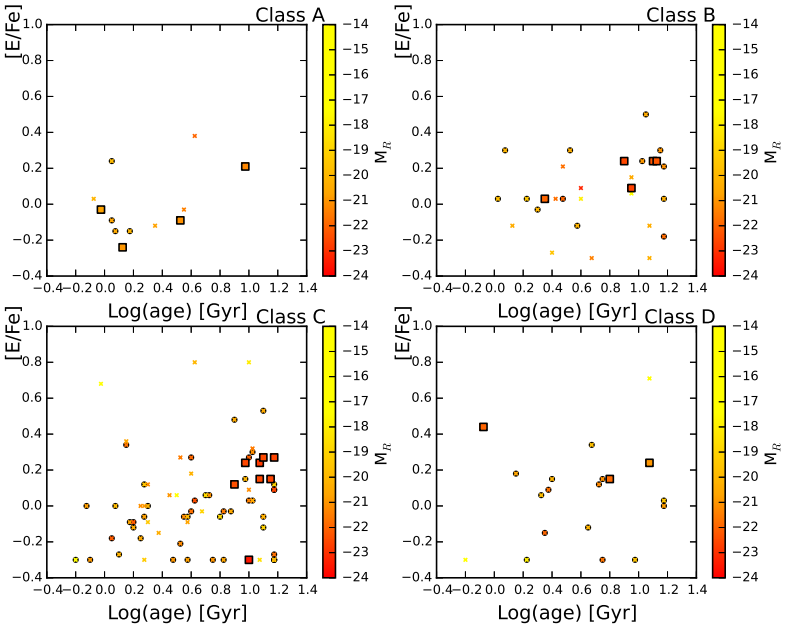

Figure 5.13: Plot of light weighted age against α-element abundance ([E/Fe]) colour coded by the absolute R-band magnitude shown for each class: the logarithm of the age is on the x-axis, [Fe/H] on the y-axis. The symbols are circles for the galaxies within R_{200} and crosses outside, the squares show the BGGs.

D similarly to class A does not have bright red galaxies, however in this case this can be attributed to the ongoing star formation, despite the fact that most galaxies are bulge-dominated. This suggests that this group are going through some sort of dynamical perturbation (e.g galaxy mergers, infalling of the group into a larger structure).

The plot comparing the two families of metal abundances (i.e. Fe-peak elements and α-elements) in Figure 5.15 and 5.16 suggests that the brightest galaxies, belonging to class B and C, are more α-enhanced, while bulge-like galaxies span all the α-enhancement range. There are no clear differences among the classes: this could signify that the metal enrichment history of galaxies is independent on the environment in which the galaxy evolves.

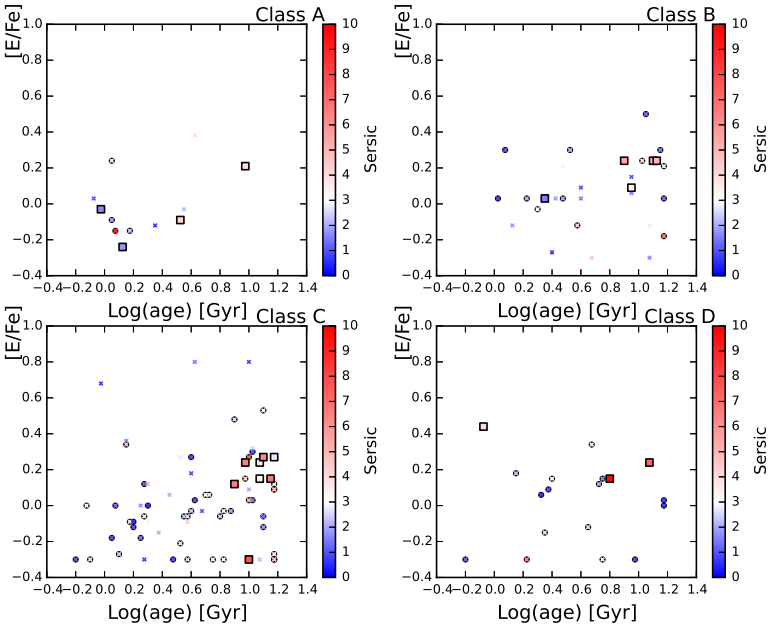

Figure 5.14: Plot of light weighted age against α-element abundance ([E/Fe]) colour coded by the Sersic index value shown for each class: the logarithm of the age is on the x-axis, [E/H] on the y-axis. The symbols are circles for the galaxies within R_{200} and crosses outside, the squares show the BGGs.

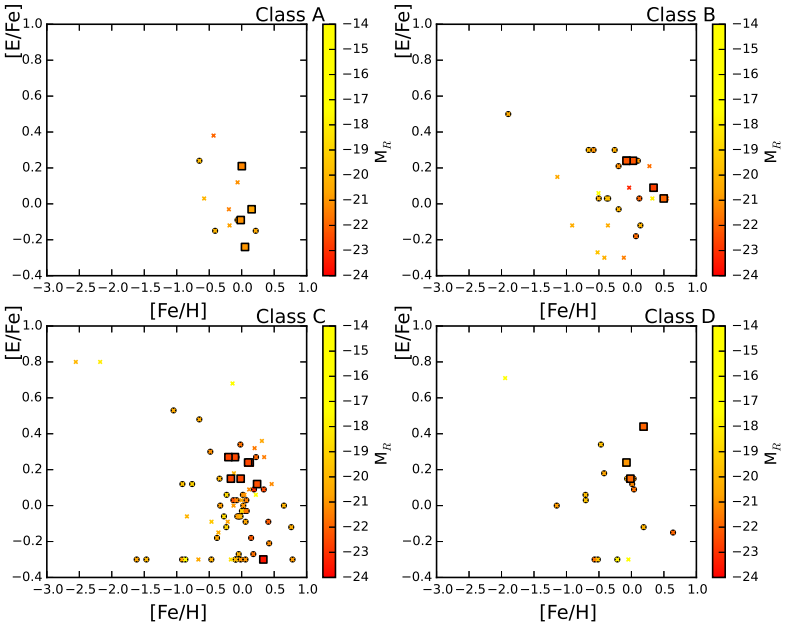

Figure 5.15: Plot of light weighted iron-element abundance ([Fe/H]) against α-element abundance ([E/Fe]) colour coded by the absolute R-band magnitude shown for each class: [Fe/H] is on the x-axis, [E/H] on the y-axis. The symbols are circles for the galaxies within R_{200} and crosses outside, the squares show the BGGs.

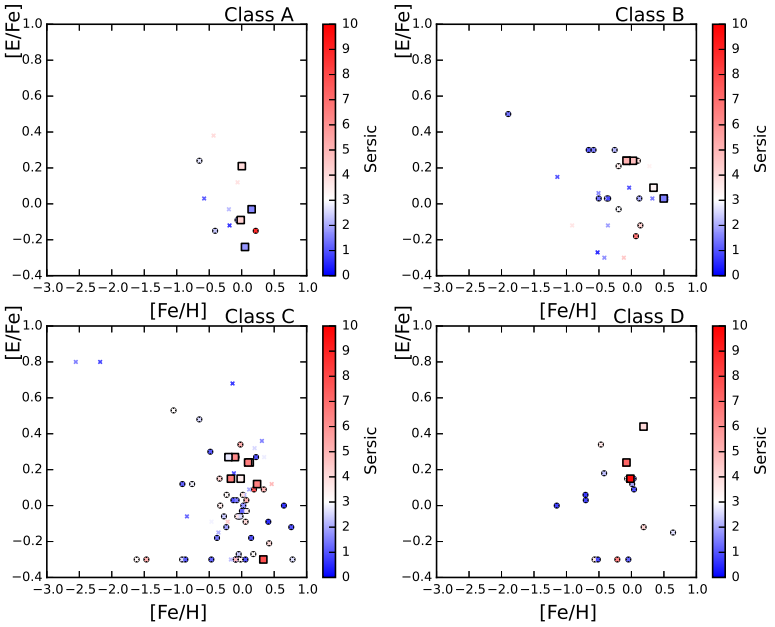

Figure 5.16: Plot of light weighted iron-element abundance ([Fe/H]) against α-element abundance ([E/Fe]) colour coded by the Sersic index value shown for each class: [Fe/H] is on the x-axis, [E/H] on the y-axis. The symbols are circles for the galaxies within R_{200} and crosses outside, the squares show the BGGs.

5.1 AGNs Properties

The environment can affect not only a galaxy stellar population and morphology, but also the activity of its central black hole. For this reason it is interesting to study AGN population related to the environment. With this purpose in mind two of the three diagnostic diagrams originally used by Baldwin et al. [1981] were plotted using Hα, Hβ, [OIII], [NII], and [OI] emission lines (see Figures 5.17 and 5.18). The third diagnostic diagram could not be studied because the [SII] line was not available due to the quality of the spectra at red wavelengths. The curves on the diagrams were empirically obtained by Kewley et al. [2006], and they divide the star-forming galaxies and the AGNs. The galaxies shown in the plots are all those for which the emission line measurements were available, hence the completeness reflects the spectroscopic completeness described in Chapter 3. The equivalent width errors are dominated by systematic effects dependent on the GANDALF emission line fit and are due to uncertainty in the kinematic of the gas, hence a Monte Carlo simulation would be required to properly estimate them.

The first diagnostic diagram (Figure 5.17) uses the [NII] and [OIII] lines together with two Balmer lines, Hα and Hβ, the solid line divides the AGNs (above) from the star-forming galaxies (below), the dashed line further divides the star-forming galaxies from those galaxies which are both star-forming and show some signs of AGN activity (i.e. composite). Again galaxies within and outside R_{200} are shown with two different symbols (circles and crosses respectively), the BGGs are shown as squares.
All the classes have similar distribution of star-forming galaxies, passive galaxies are not shown in this plot because they do not have any emission line, as expected. Class A lacks AGNs within R_{200}, the AGNs outside R_{200} likely do not depend on the environment. Class B has a few AGNs, but appear to lack composite galaxies which could be an indication of internal quenching where the AGN feedback is responsible for stopping the star formation. Class C shows a uniform distribution of star-forming galaxies,

composite galaxies and AGNs, suggesting again that this class is in a more evolved evolutionary state; class D has mainly star-forming galaxies and very few AGNs. The small number of BGGs in the plot confirms that these are passive galaxies or, in some cases the host an AGN. However as previously inferred using other parameters class A contains star-forming BGGs supporting the conclusion of this being a class of galaxies interacting for the first time.

The second AGN diagnostic diagram (Figure 5.18) uses [OI], [OIII], Hα and Hβ, the solid line is the boundary between the star-forming galaxies region (below) and the AGNs region (above), the symbols are used to discriminate between BGGs (squares), galaxies within (circles) and outside R_{200} (crosses). In disagreement with the previous result, class A has a few AGNs, class B and C do not show substantial differences from the results of the previous plot, and class D seems to have more galaxies classified as AGNs in this diagnostic. The BGGs have the same classification in both diagrams for classes B and C, in class A one previously classified as star-forming is now in the AGN region and class D BGG has no [OI] emission and does not appear in this plot.

Figure 5.19 shows the AGN fraction in each class for the two different diagnostic diagrams and the composite fraction (i.e. star-forming galaxies which also host an AGN). The diagnostic diagram comparing [OIII]/Hβ vs [NII]/Hα makes a distinction between galaxies hosting an AGN and galaxies both star-forming and with an active nucleus, the 'purely' AGN fraction is lowest in class A (~ 0.05), roughly the same in class B and C (~ 0.3) suggesting that the groups in these two classes might be in the same evolutionary state, and has a value between the other two in class D (~ 0.13). The composite fraction slightly increase from A to C (from ~ 0.10 to ~ 0.15), with a steep increase for class D (~ 0.22). The second diagnostic diagram shows an increase in the AGN fraction from class A to C, going from ~ 0.25 to ~ 0.45, to decrease again in class to a value close to class B (~ 0.40)

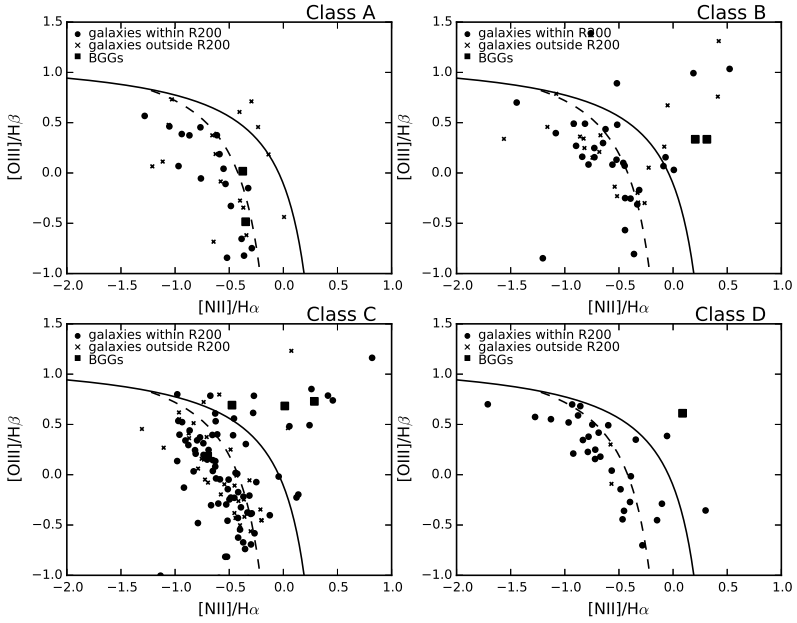

Figure 5.17: BPT diagnostic diagram [Baldwin et al., 1981; Kewley et al., 2006]: on the x-axis it is shown the ratio [NII]/Hα, on the y-axis the ratio [OIII]/Hβ. The symbols represent galaxies within R_{200} (circles) and outside R_{200} (crosses), the squares show the BGGs. The solid line divides the star-forming galaxies (below) from the AGNs (above), the region between the solid and the dashed line contains the composite galaxies (star-forming galaxies showing signs of AGN activity).

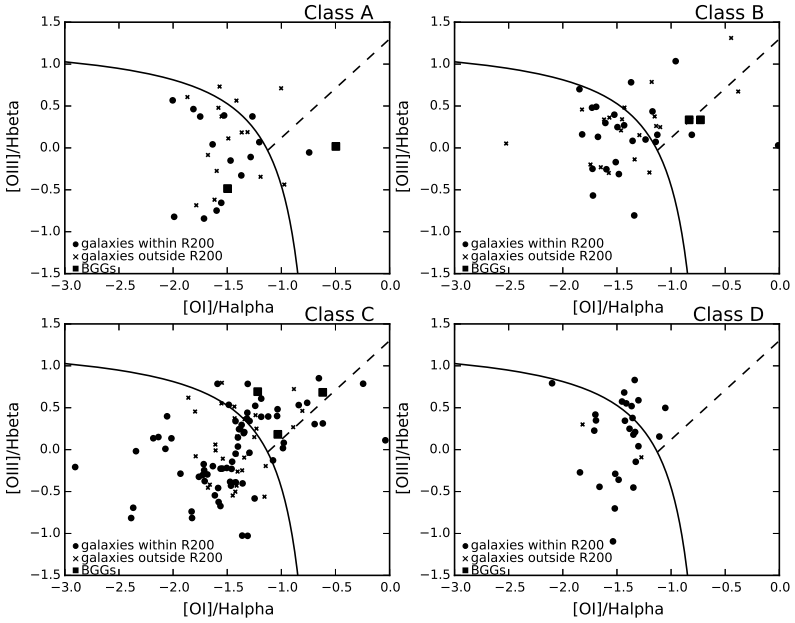

Figure 5.18: BPT diagnostic diagram [Baldwin et al., 1981; Kewley et al., 2006]: on the x-axis it is shown the ratio [OI]/Hα, on the y-axis the ratio [OIII]/Hβ. The symbols represent galaxies within R_{200} (circles) and outside R_{200} (crosses), the squares show the BGGs. The solid line divides the star-forming galaxies (below) from the AGNs (above), the dashed line divide Seyfert galaxies (above) and LINERs (below).

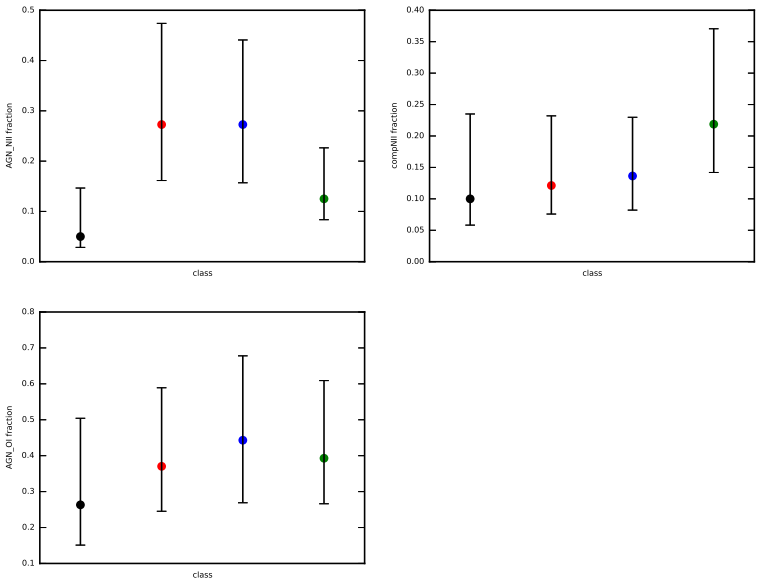

Figure 5.19: Plot showing the AGN and composite fraction with errors for each diagnostic diagram: on the x-axis is shown the class, on the y-axis the AGN fraction obtained using the [NII] line (top left), the AGN fraction obtained using the [OI] line (bottom left), and the composite fraction (top right).

5.2 Conclusion

This section summarises the results obtained from the study of the galaxy properties in the four group classes.

- Galaxies in class A appear to be very similar: they have a small range of masses ($\sim 10^{9.5}$ - 10^{11}), metallicity ($\sim$ solar), morphology (late-type), and they are all classified as star-forming. Furthermore none (or very few depending on the diagnostic used) of the galaxies hosts an AGN. These characteristics together with the asymmetric distribution of galaxies in the phase-space diagram and late-type star-forming BGGs are typical of field galaxies thus suggesting that the groups in this class are in the process of forming and are made of galaxies coming together for the first time.

- Galaxies in class B do not show any peculiarity, suggesting that these groups, despite being low mass groups, appear to be evolved systems. This could be justified by the fact that they are isolated groups, so they might be unable to accrete new galaxies from their surroundings. The only clues against this interpretation are the lack of galaxies at small radii and velocities in the phase-space diagram and the late-type star-forming BGGs, for this reason it would be interesting to further study these systems.

- Galaxies in class C have all the characteristics of galaxies living in evolved and relaxed structures, the major indication being the lack of star formation out to R_{200}.

- Galaxies in class D have some characteristics similar to galaxies in evolved clusters, however they show signs of star formation ongoing and dynamical disturbance from their distribution on the phase-space diagram, for this reason it would be interesting to further study these systems.

These results agrees with the hypothesis formulated studying the groups properties, suggesting that the galaxies are shaped by the environment in which they reside. However, the uncertainty on the measured quantities could introduce bias and compromise the clustering and any further study. For this reason a uniform data set obtained with in mind the purpose of the analysis and a larger statistical sample could increase the reliability of the results.

Chapter 6

Conclusion and Future Work

This study was aimed at understanding the properties of galaxy groups and how they affect the galaxy properties. The sample used was a set of 25 redshift selected groups in a very narrow redshift range ($0.060 < z < 0.062$) and with velocity dispersion $<$ 500 km/s. For each group, a multi-wavelength set of data was available: photometric, spectroscopic, UV and IR. Some data were directly used, some were analysed using dedicated tools to obtain the needed quantities, bringing the total number of parameters available for this study to 30.

The first step was to perform a Spearman rank correlation analysis on all the pairs of the 30 multi-wavelength parameters describing the group properties to investigate the existence of any correlation overlooked in previous studies, and to confirm the existence of widely accepted trends. To each correlation, a value was assigned a significance which indicated the strength of the correlation itself. The main picture arising from this analysis was that higher mass groups tend to be more evolved, hence they host a bulge-like galaxy in their centre and their galaxies have lower star formation ongoing, as expected.

The second analysis was a statistical clustering analysis performed on the 30 multi-wavelength parameters, with the aim to classify the groups according to their properties,

expecting the resulting classes to contain groups at different stages of the structure evolution. The 30 parameters clustering analysis appeared to be driven by the group mass, substantially dividing the groups in 2 classes, split in low mass and high mass groups. This result is somewhat similar to that obtained in the previous analysis, confirming that low mass and high mass systems are likely in two different evolutionary states. However, given the aim of the study that of studying the galaxy properties, it was interesting to separate the classes according to some other group properties other than mass, for this reason some of the parameters were excluded and the clustering analysis repeated. The parameters excluded were those related to the mass of the systems, the galaxy properties, and those dominated by low statistics. Finally, the analysis was performed on 10 parameters and 4 stable group classes were found. Surprisingly, the 4 classes still showed a mass dependence with 2 lower mass groups classes and 2 high mass group classes, the other striking differences for some classes where the UV sSFR and the stellar mass fraction.

The next step was to study the galaxy properties within each of the 4 classes examining different galaxy properties. From their distribution it was possible to physically interpret the meaning of the 4 classes. The outcome of this analysis allowed to physically interpret the four classes according to their evolutionary state as follows:

- a class of field-like galaxies in the early stage of structure formation;
- a class of low mass groups either still in formation phase, or unable to grow more mass because isolated;
- a class of massive groups with no, or very little, ongoing star formation, likely in a more evolved stage of structure formation;
- a class of massive groups showing signs of ongoing star formation, indicating possible interactions among the galaxies or between the groups and a larger structure.

This analysis reveals how the group classes appear to be tightly related to structure formation in the Universe, showing different stages of their evolution, and how galaxy properties trace the properties of the environment they reside in.
However the objective of this work was not only aimed at getting significant results, but also at developing a new method to study galaxy groups utilising all the available multi-wavelength data and not only focussing on few properties.

The XI sample was ideal for this purpose being a homogeneous sample of galaxy groups not biassed toward any evolutionary stare given the optical selection of the groups. Unfortunately, it was not possible to exploit all the potential of the survey since the X-ray data were not available for most of the groups. Also the spectral data quality was not ideal for most of the galaxies because the original purpose of the spectral observations was only to derive the galaxy redshift to determine the membership. Furthermore some of the parameters defined in this work should be reviewed and substituted with more quantifiable ones, for instance the large scale classification should be replaced by some objective way of determine the large scale environment properties. Similarly, the method to define the dynamical parameters used in this work should be tested on mock data in order to have a better physical understanding of the inferred quantities.
The results obtained are however robust, despite the data quality and the low statistics, although not conclusive. Anyhow, the method developed could be applied to other data sets after determining what parameters should be considered for the analysis.
The most straightforward application, also useful to refine the method, would be to apply it to a simulated mock group catalogue. This would help understanding how the data clustering works and how it is affected by data quality. A further step would also be to implement a clustering algorithm that takes into account the errors on the data and that gives a significance for the result.

The experience developed in this work made possible to plan future applications of

the method on data samples more adapt for the analysis.
The ideal characteristic of the data sample are:

- higher statistics with at least double the groups number (> 50 groups);
- uniform data and clear understanding of the data completeness in order to be able to apply corrections;
- good quality spectroscopic data which should be properly wavelength and flux calibrated in order to allow a continuum fitting to determine the stellar population properties and possibly identifying different stellar population (as opposite to light-weighted stellar population properties);
- availability of data in multiple optical bands, UV, IR, X-ray and radio observations.

Bearing in mind what stated, two already available group catalogues would be ideal for this kind of study: the CLoGS (Complete Local-volume Groups Survey Vrtilek et al. [2013]) and the GAMA (Galaxy And Mass Assembly [Robotham et al., 2011]) group samples.

CLoGS is a survey of 53 optically selected local groups ($z < 0.03$). Photometric and spectroscopic observations were carried out with the Wide Field Reimaging CCD Camera (WFCCD) on the DuPont telescope and IMACS on the Magellan telescope at Las Campanas Observatory, some of the data are extracted from HyperLEDA (originally used for the groups slection) and Sloan Digital Sky Survey (SDSS). Radio observations were performed with the Giant Metrewave Radio Telescope (GMRT) at 601 and 235 MHz, but the groups were also selected to be observables with the Very Large Array telescopes (VLA). XMM-Newton and Chandra satellites were used to acquire X-ray data. The Complete H-Alpha imaging of Nearby Group EnvironmentS (CHANGES) provided Hα observations. UV and IR data are also available from GALEX and Spitzer respectively.

The GAMA group catalogue contains 14,388 galaxy groups. The spectroscopic observations were carried out with the AAOmega multi-object spectrograph on the Anglo-Australian Telescope (AAT) and integrated with SDSS data. The United Kingdom Infrared Telescope (UKIRT) and Herschel were used for IR observations and GALEX for UV observations. Radio and X-ray data were acquired with the GMRT and XMM-Newton respectively.

These samples make ideal data sets to continue this work.

Appendix 1

The appendix summarises the group properties.

Large scale classification:

- isolated,
- offset from a cluster,
- part of a sparse supercluster,
- part of a supercluster.

The group classification after the clustering analysis:

- Class A: small groups in a collapsing phase.
- Class B: small and isolated groups.
- Class C: massive groups in an advanced evolutionary state.
- Class D: massive and disturbed groups.

The table shows the number of group members within R_{200}, the number of IR and UV luminous members, the number of members for which the emission lines measurement was possible and the number of members for which the Lick indices analysis was possible.

The first plot shows the spatial distribution of galaxies, RA on the x-axis and Dec on the y-axis. The source from which the photometry was extracted: galaxies observed with IMACS are shown as circles, while those extracted from the 2dF are shown as reverse triangles. Crosses denotes galaxies for which the R-band magnitude was not available, while the red cross is the BGG. The colour-coding shows the galaxy redshift, while the symbol size reflects the absolute R-band magnitude. The blue solid circle shows R_{200}, while the purple one the 1 Mpc radius. The bottom histogram shows the redshift distribution of the galaxies within R_{200}, the left side histogram shows the same thing for the absolute R-band magnitude. In both histogram the values for the BGG are shown by the red annotation. The name of the group is shown on top of the plot.

The second plot shows the large scale distribution of galaxies for each group and was used to define the large scale classification described above. The name of the group is above the plot, RA and Dec are shown on the x and y-axis respectively. The magenta dashed circles describe the radii at 1, 3, 5 and 10 Mpc, all the group members are within the 1 Mpc radius. The contours visually show the projected galaxy overdensities, the green triangles are known Abell clusters..

When extracting the groups from the [Merchán and Zandivarez, 2002] catalogue it was noticed that four of them showed a bi-modal redshift distribution. At an early stage of the project it was decided to consider only one of the two distribution as group. So for MZ4577, MZ5383, MZ5388 and MZ8816 the histogram showing the bi-modal distribution is shown and it is described which peak was used as group in this analysis. The member were determined with the same procedure described in Section 3.1.

MZ 770

Large scale classification: part of a sparse supercluster.

Group classification: B small and isolated groups.

members within R_{200}	IR luminous	UV luminous	line measurement	Lick indices
12	3	n/a	10	5

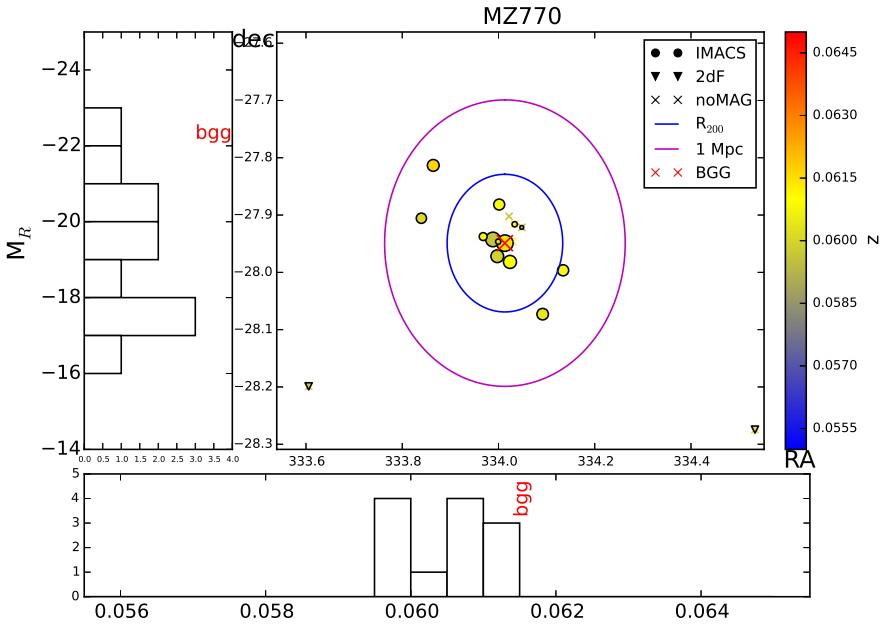

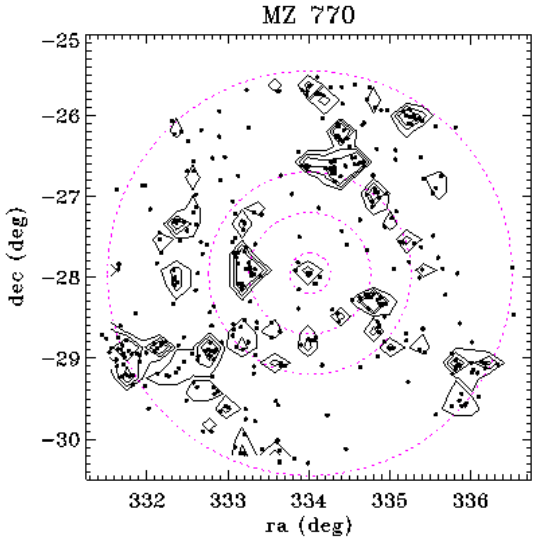

MZ 1766

Large scale classification: offset from a cluster.

Group classification: C massive groups in an advanced evolutionary state.

members within R_{200}	IR luminous	UV luminous	line measurement	Lick indices
13	7	10	12	6

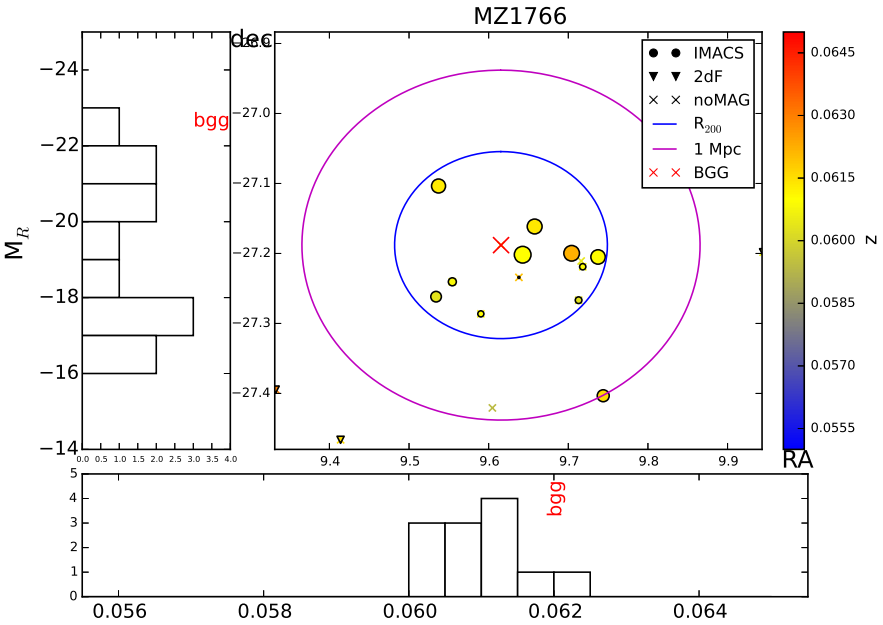

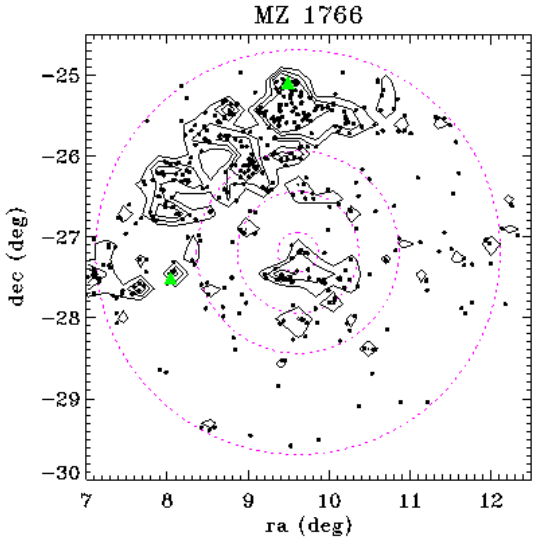

MZ 3067

Large scale classification: part of a sparse supercluster.

Group classification: C massive groups in an advanced evolutionary state.

members within R_{200}	IR luminous	UV luminous	line measurement	Lick indices
6	3	5	6	5

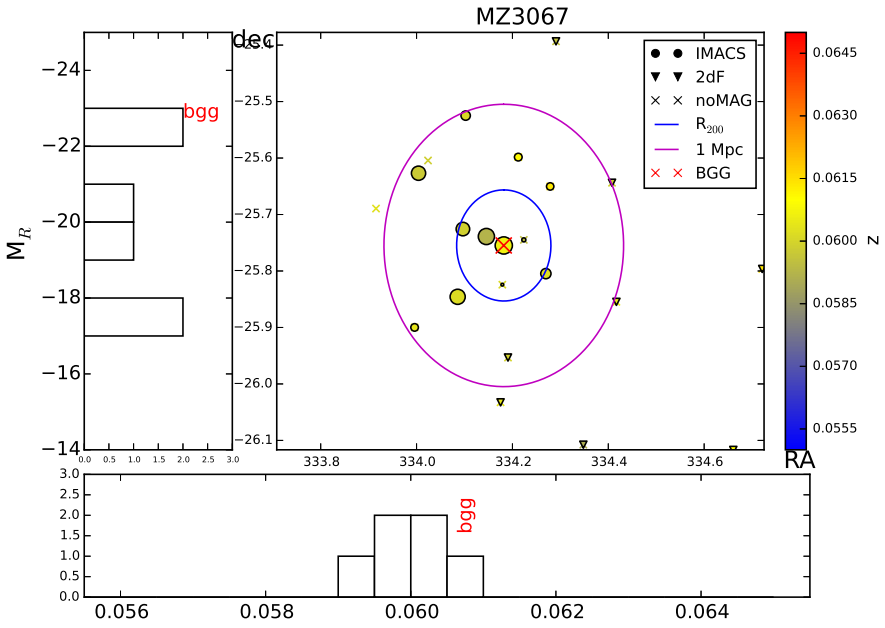

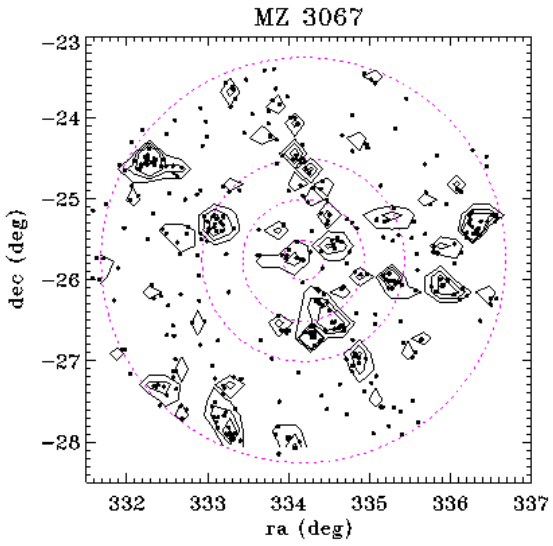

MZ 3182

Large scale classification: part of a sparse supercluster.

Group classification: A small groups in a collapsing phase.

members within R_{200}	IR luminous	UV luminous	line measurement	Lick indices
6	4	6	4	4

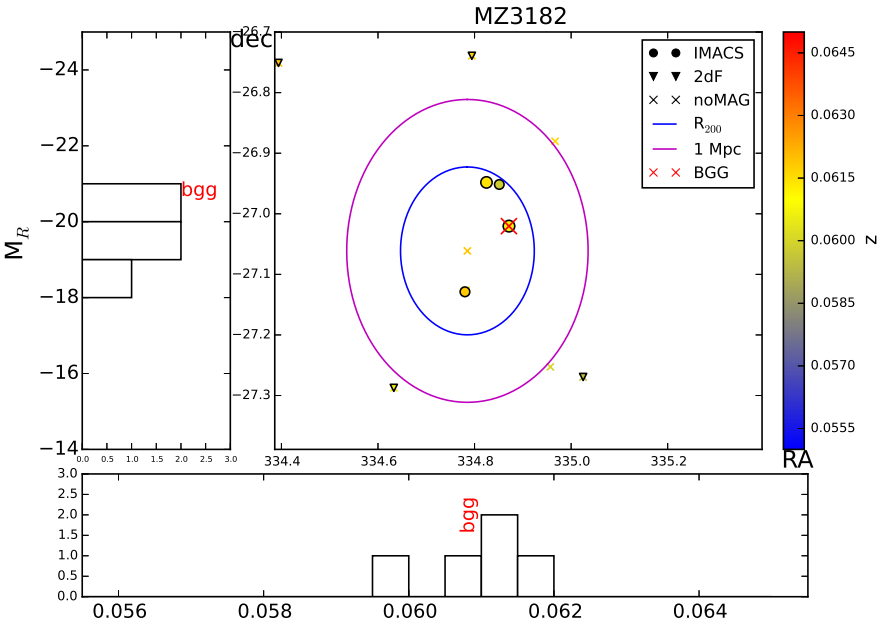

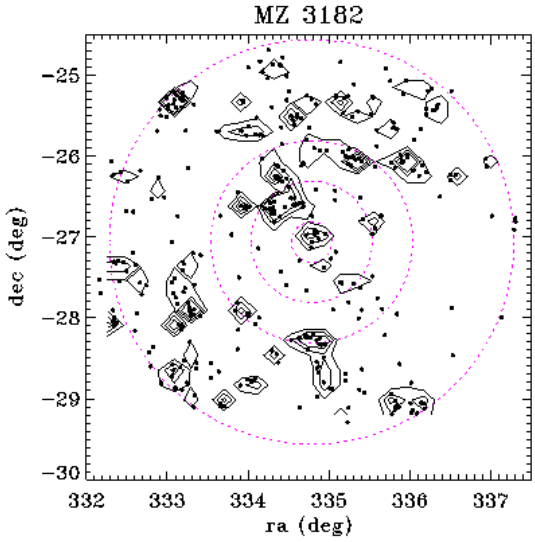

MZ 3541

Large scale classification: offset from a cluster.

Group classification: B small and isolated groups.

members within R_{200}	IR luminous	UV luminous	line measurement	Lick indices
5	4	4	3	2

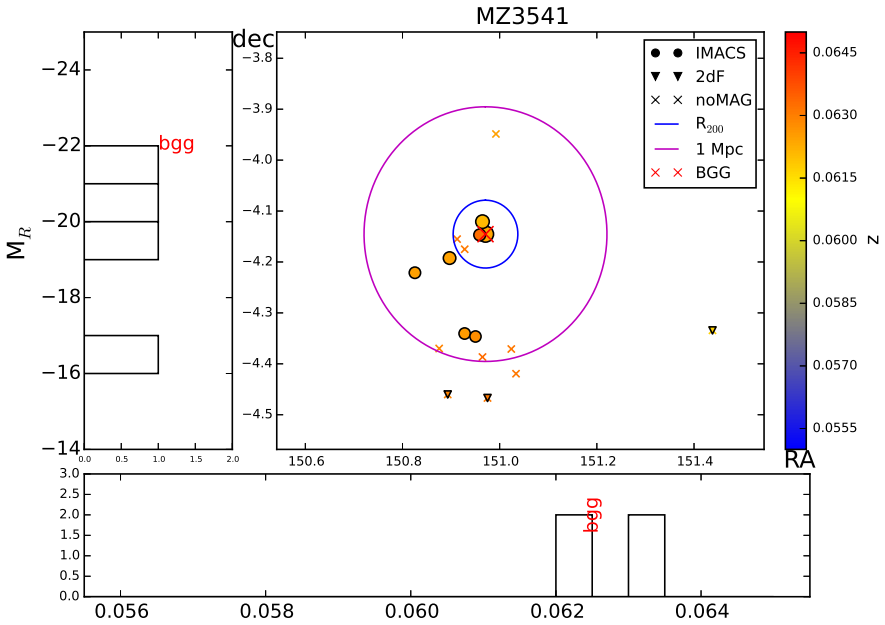

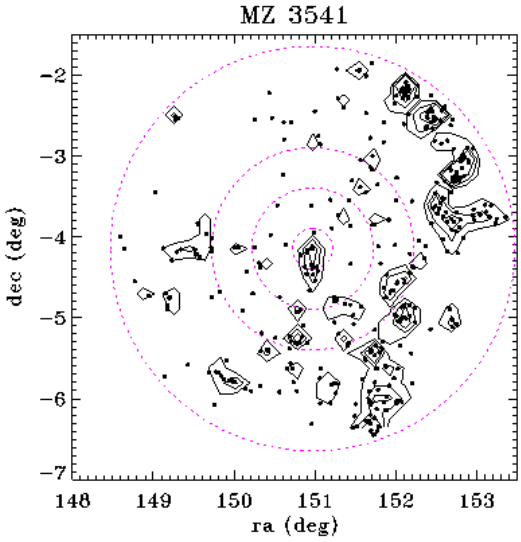

MZ 3698

Large scale classification: isolated.

Group classification: B small and isolated groups.

members within R_{200}	IR luminous	UV luminous	line measurement	Lick indices
8	3	5	7	3

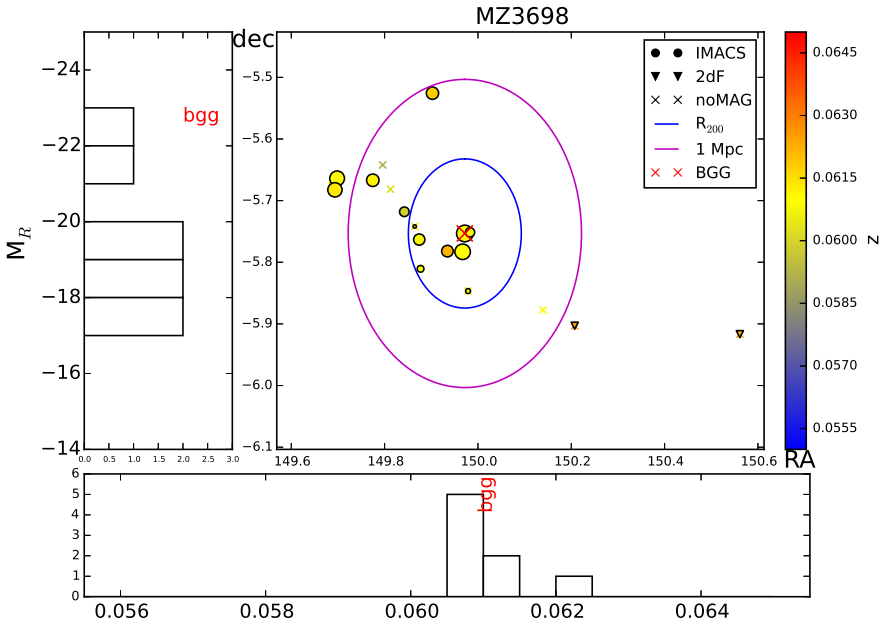

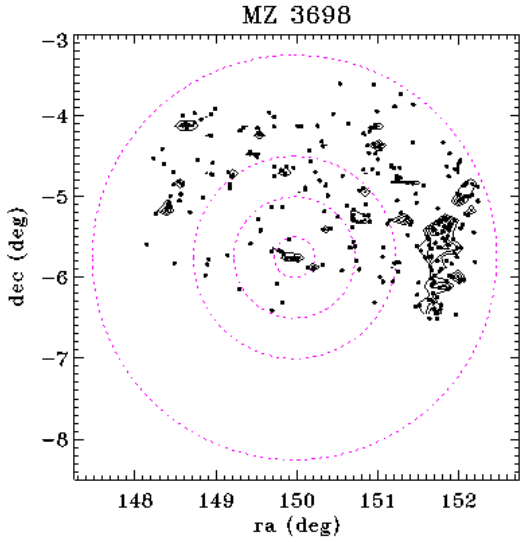

MZ 3849

Large scale classification: part of a supercluster.

Group classification: A small groups in a collapsing phase.

members within R_{200}	IR luminous	UV luminous	line measurement	Lick indices
11	2	n/a	10	1

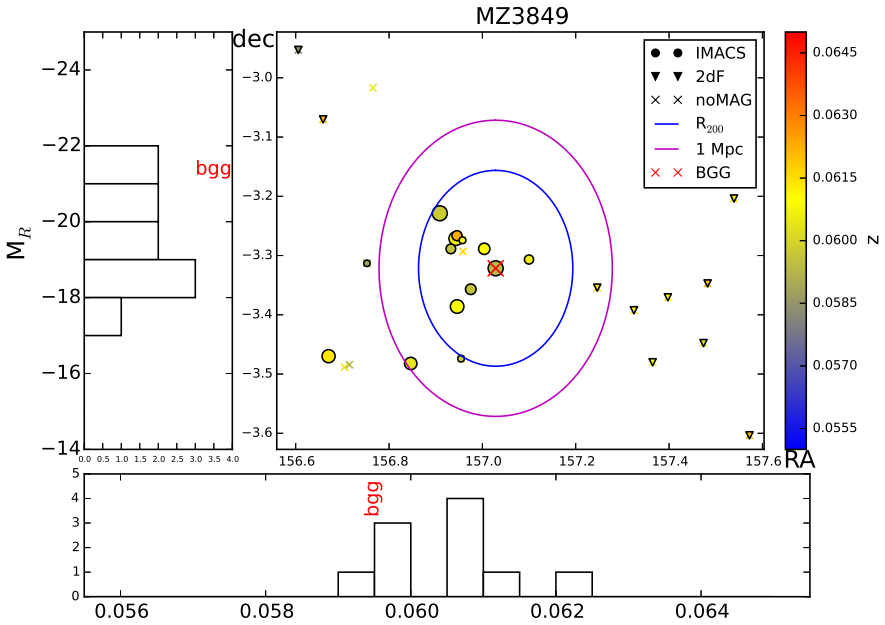

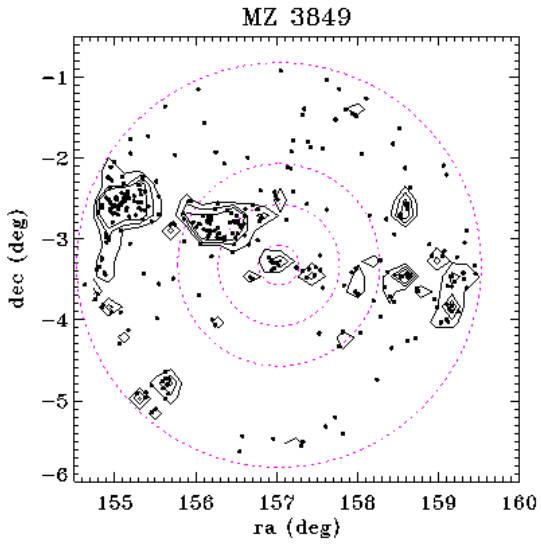

MZ 4001

Large scale classification: part of a supercluster.

Group classification: C massive groups in an advanced evolutionary state.

members within R_{200}	IR luminous	UV luminous	line measurement	Lick indices
34	14	27	21	9

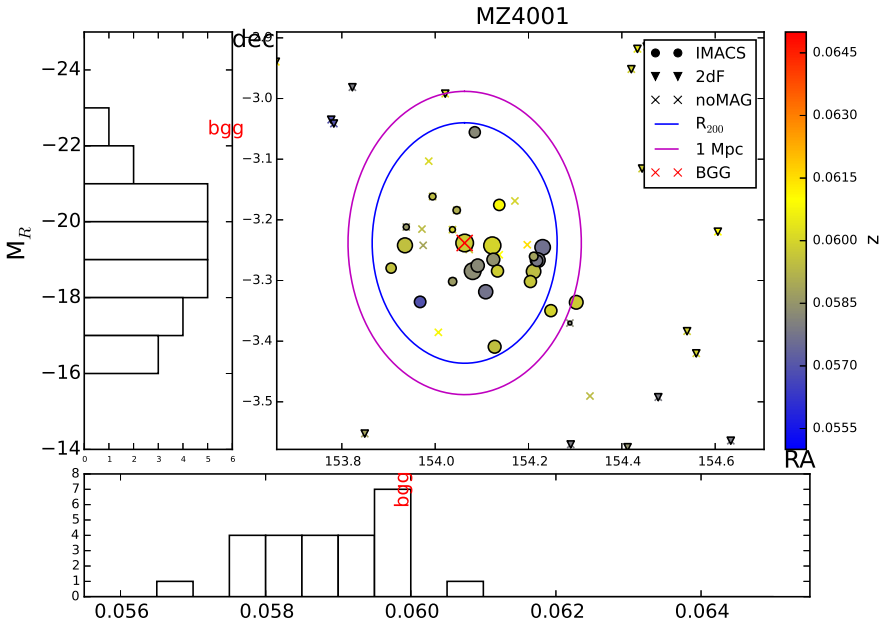

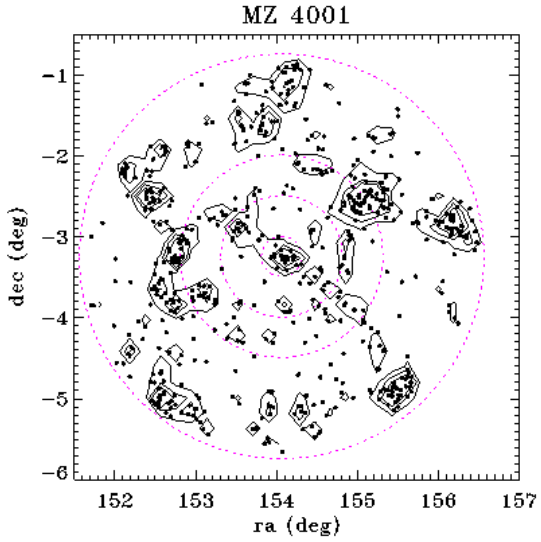

MZ 4548

Large scale classification: isolated.

Group classification: A small groups in a collapsing phase.

members within R_{200}	IR luminous	UV luminous	line measurement	Lick indices
6	4	5	5	2

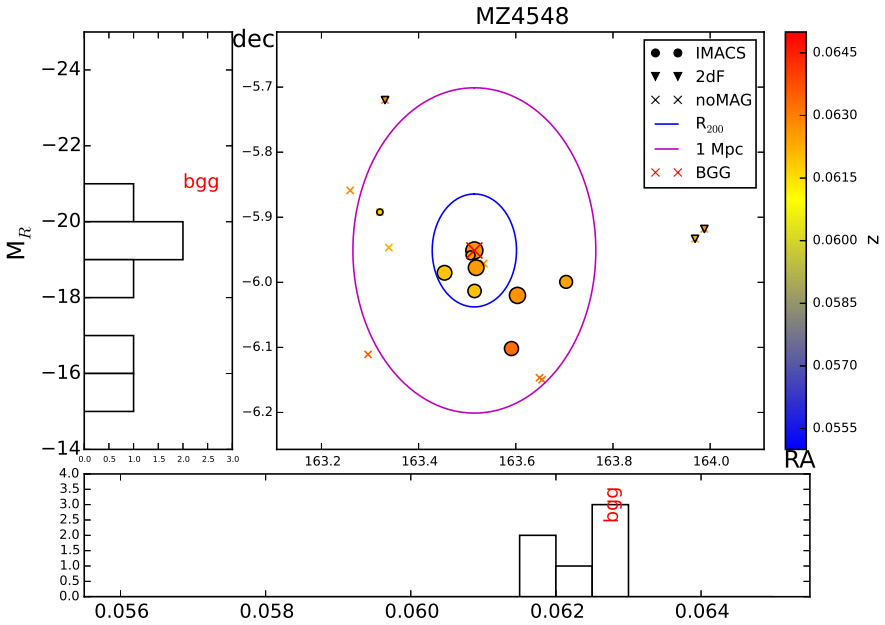

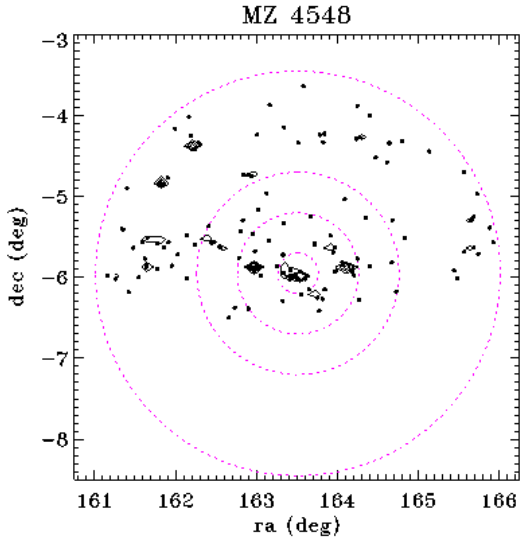

MZ 4577

Double group.

Large scale classification: part of a sparse supercluster.

Group classification: A small groups in a collapsing phase.

members within R_{200}	IR luminous	UV luminous	line measurement	Lick indices
9	4	9	7	1

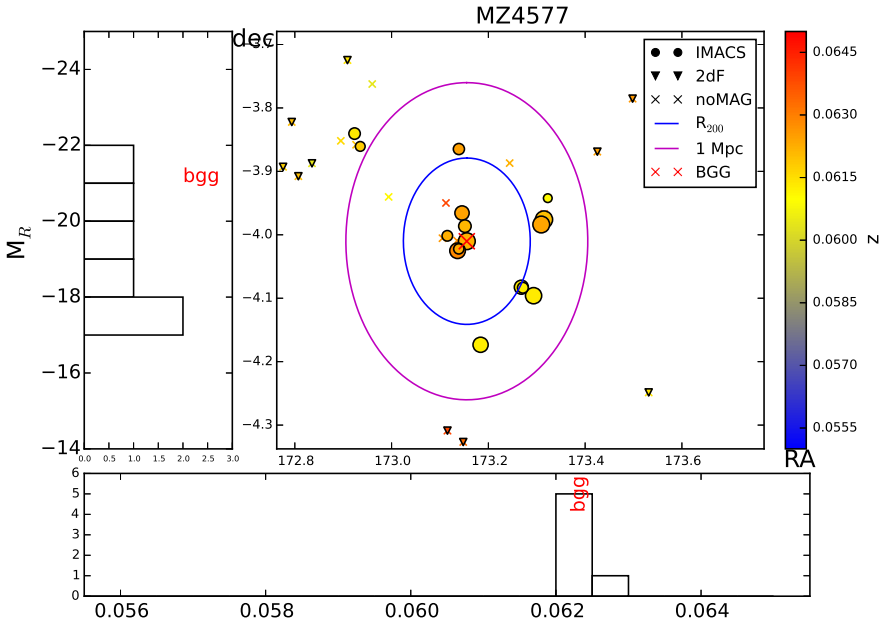

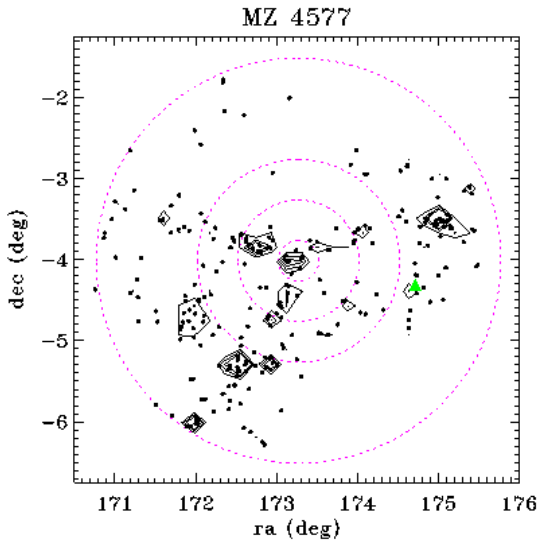

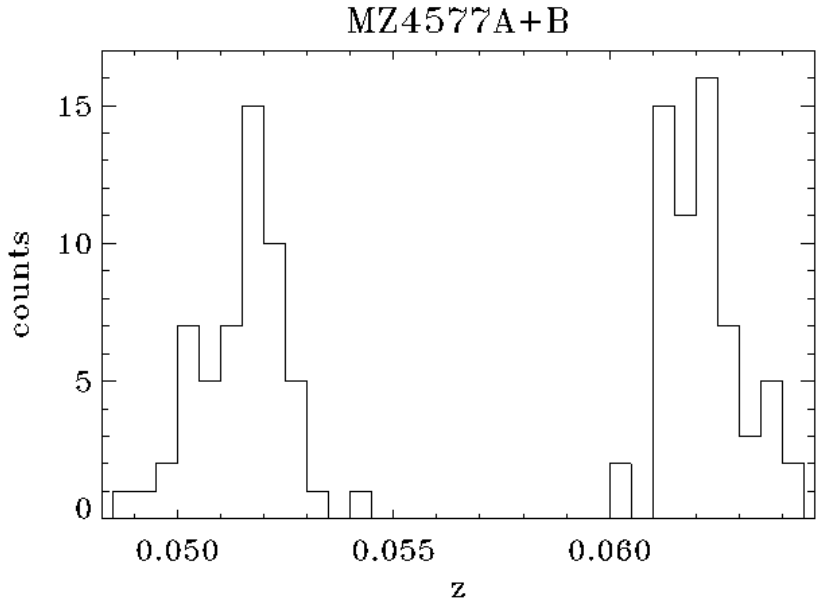

The histogram shows the redshift distribution on the x-axis and the number of galaxies in each redshift bin (counts) on the y-axis. For this work the peak at higher redshift was chosen to be studied.

MZ 4592

Large scale classification: part of a sparse supercluster.

Group classification: B small and isolated groups.

members within R_{200}	IR luminous	UV luminous	line measurement	Lick indices
9	5	7	6	1

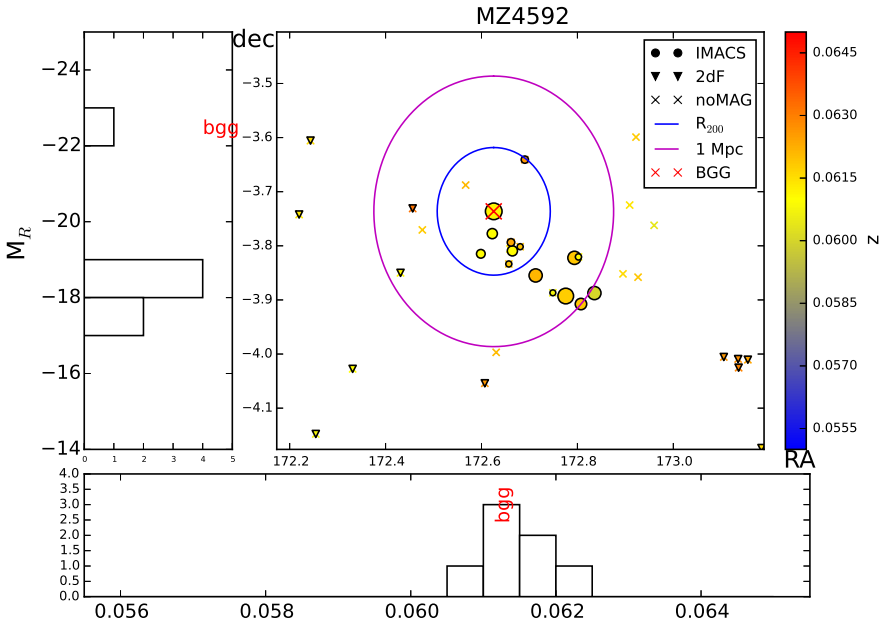

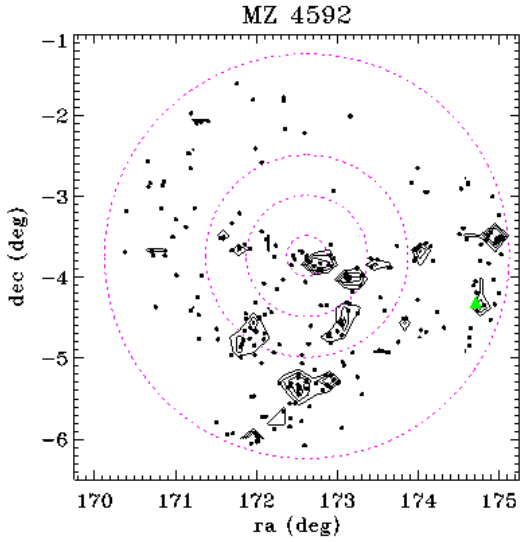

MZ 4881

Large scale classification: part of a sparse supercluster.

Group classification: C massive groups in an advanced evolutionary state.

members within R_{200}	IR luminous	UV luminous	line measurement	Lick indices
36	16	34	16	9

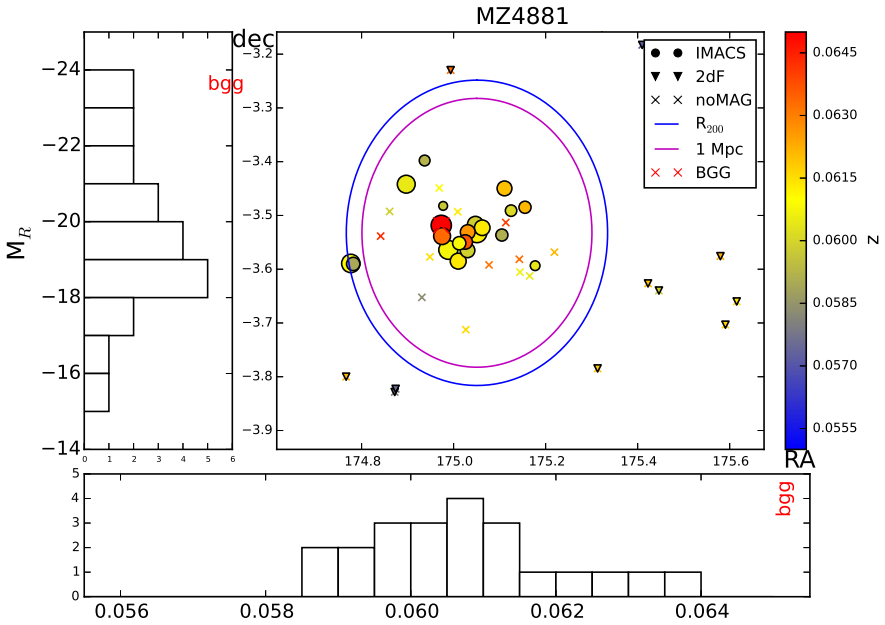

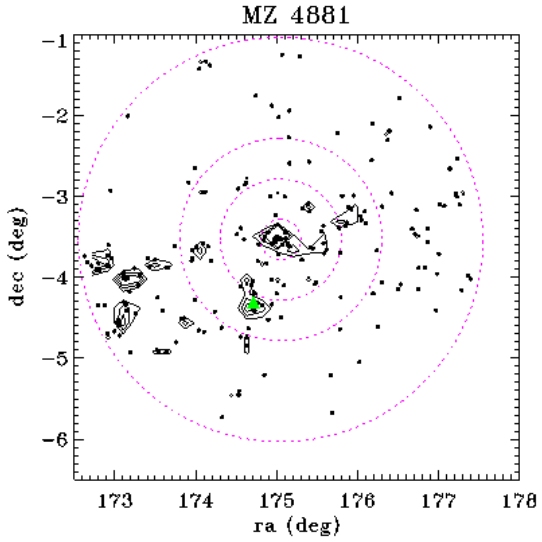

MZ 4940

Large scale classification: offset from a cluster.

Group classification: n/a

members within R_{200}	IR luminous	UV luminous	line measurement	Lick indices
2	1	2	1	1

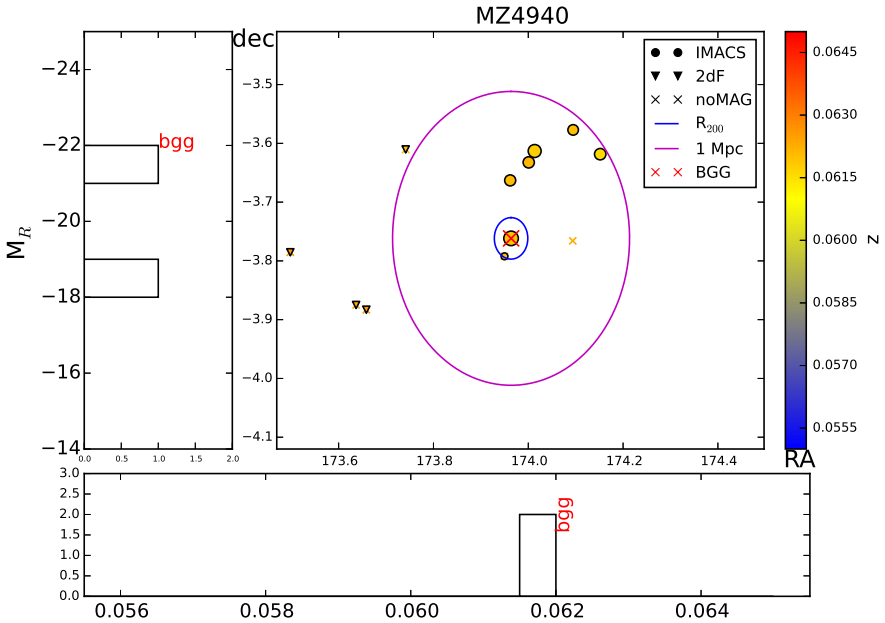

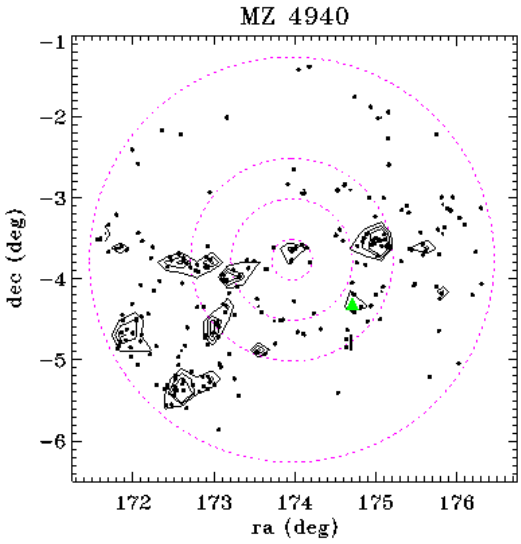

MZ 5293

Large scale classification: isolated.

Group classification: n/a

members within R_{200}	IR luminous	UV luminous	line measurement	Lick indices
3	2	2	3	2

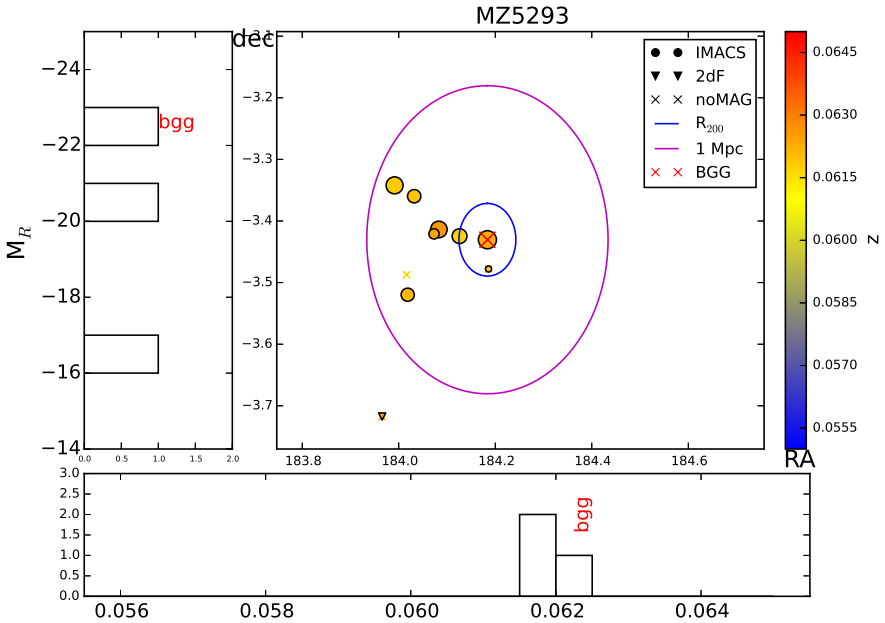

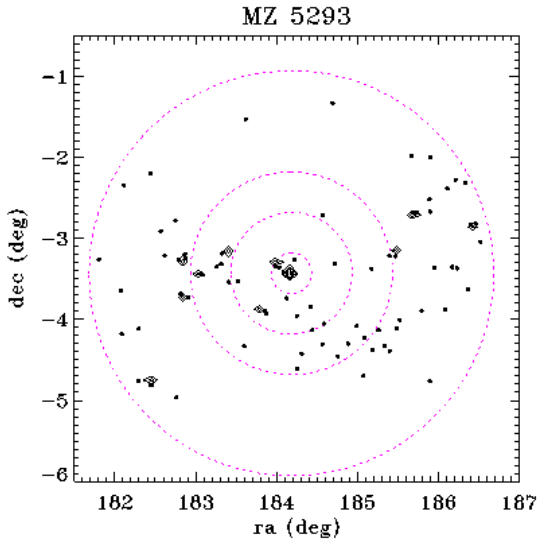

MZ 5383

Double group.

Large scale classification: part of a sparse supercluster.

Group classification: C massive groups in an advanced evolutionary state.

members within R_{200}	IR luminous	UV luminous	line measurement	Lick indices
8	1	6	5	4

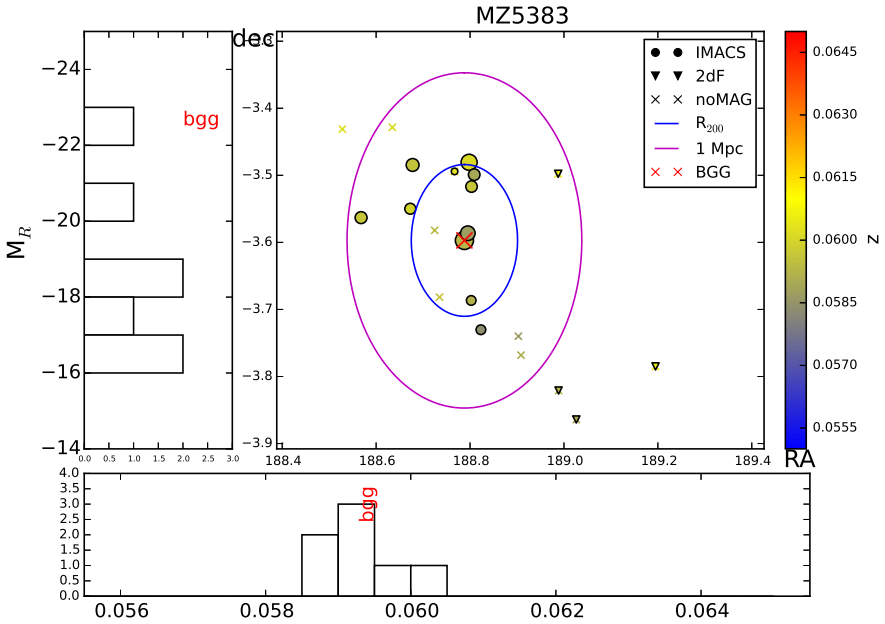

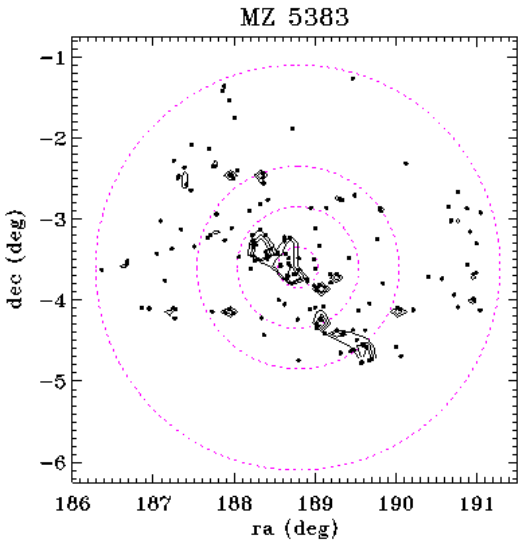

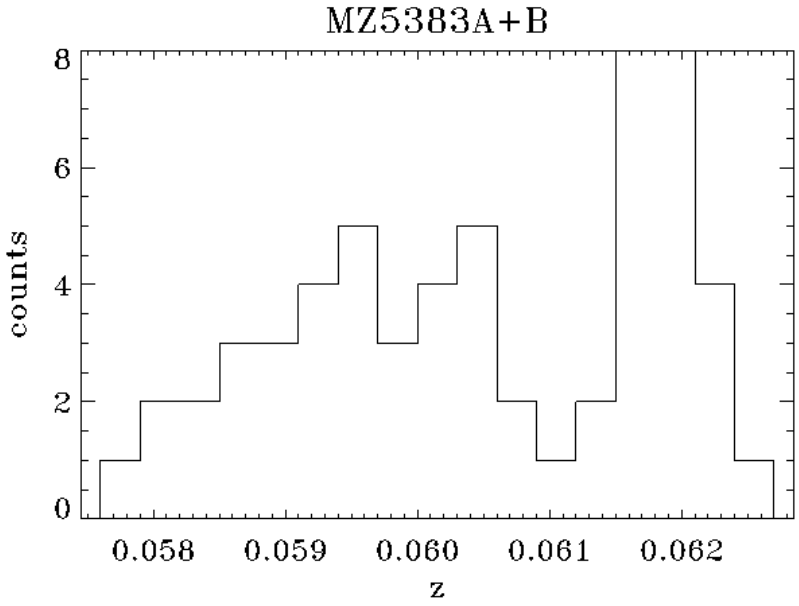

The histogram shows the redshift distribution on the x-axis and the number of galaxies in each redshift bin (counts) on the y-axis. For this work the wider peak at lower redshift was chosen to be studied.

MZ 5388

Double group.

Large scale classification: part of a sparse supercluster.

Group classification: n/a

members within R_{200}	IR luminous	UV luminous	line measurement	Lick indices
2	1	2	2	0

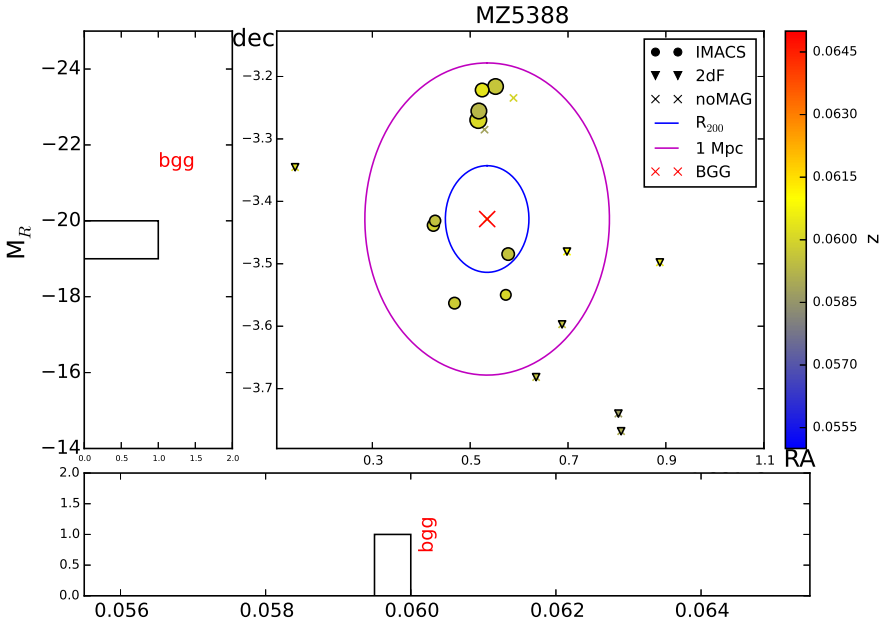

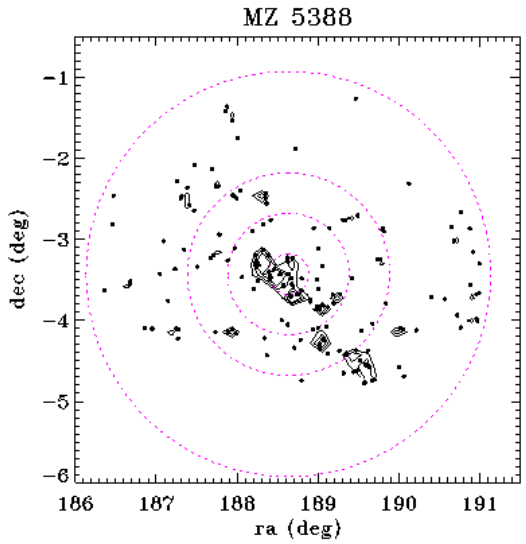

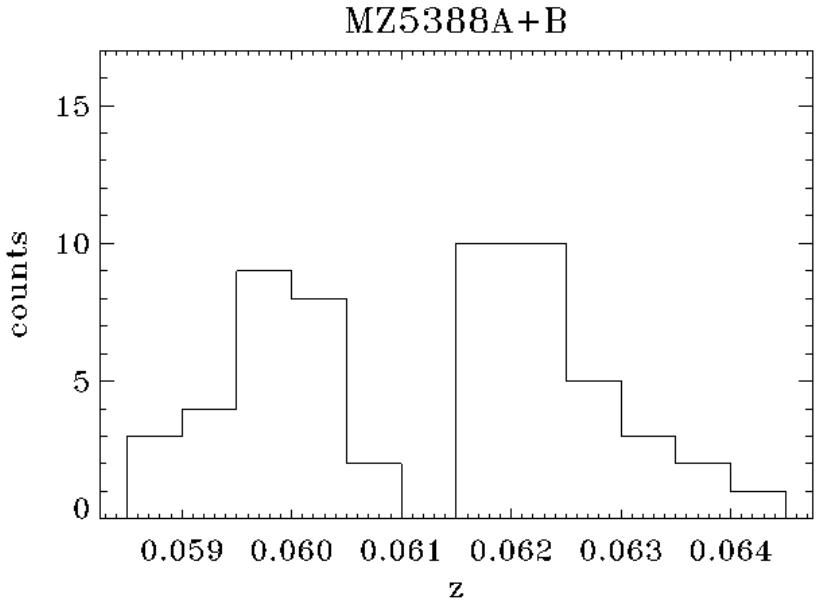

The histogram shows the redshift distribution on the x-axis and the number of galaxies in each redshift bin (counts) on the y-axis. For this work the peak at lower redshift was chosen to be studied.

MZ 8816

Double group.

Large scale classification: part of a supercluster.

Group classification: C massive groups in an advanced evolutionary state.

members within R_{200}	IR luminous	UV luminous	line measurement	Lick indices
16	5	10	11	4

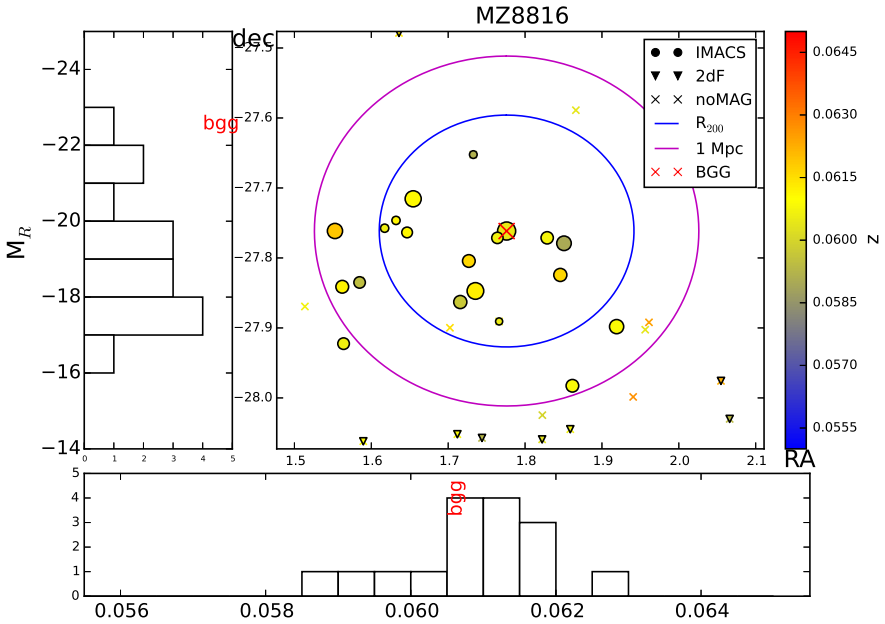

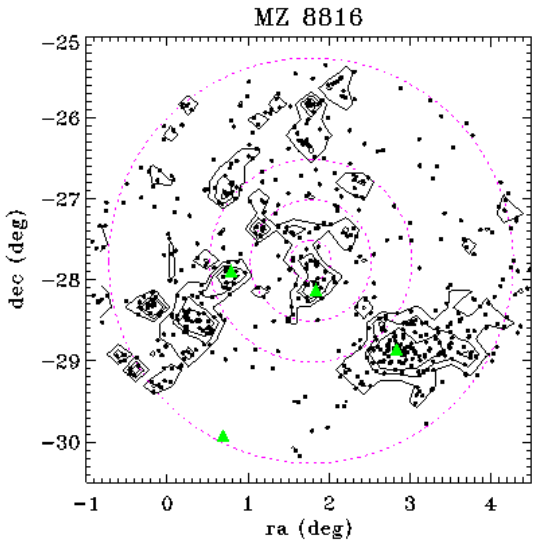

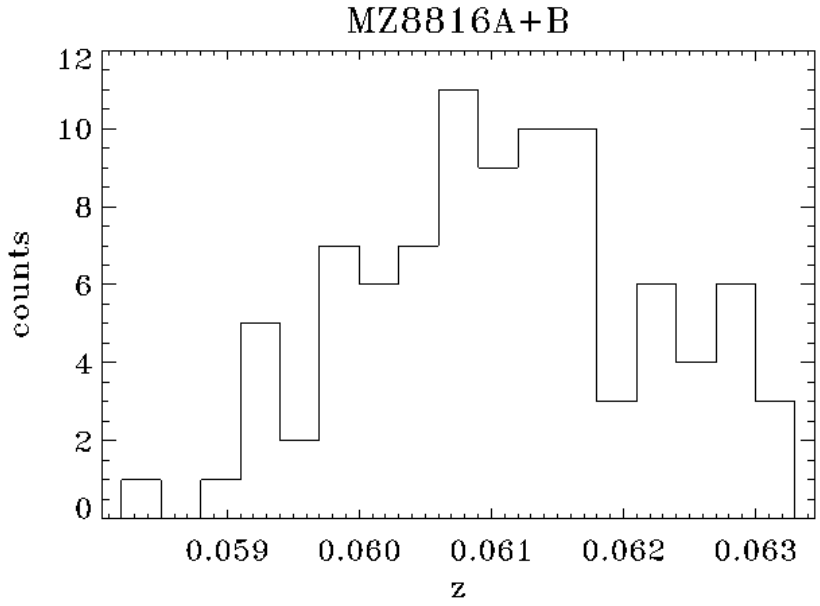

The histogram shows the redshift distribution on the x-axis and the number of galaxies in each redshift bin (counts) on the y-axis. For this work the wider and larger peak at lower redshift was chosen to be studied.

MZ 9014

Large scale classification: offset from a cluster.

Group classification: C massive groups in an advanced evolutionary state.

members within R_{200}	IR luminous	UV luminous	line measurement	Lick indices
15	3	15	11	5

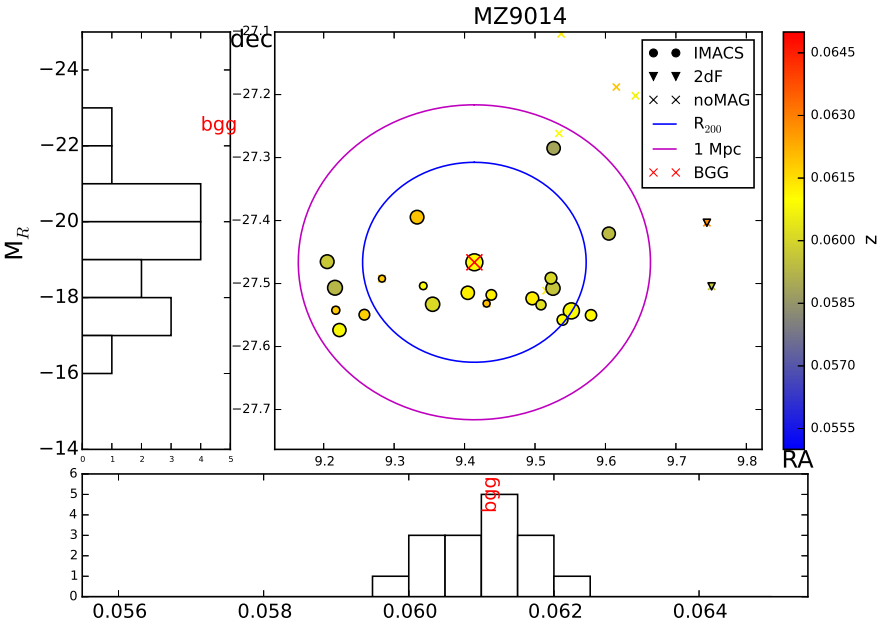

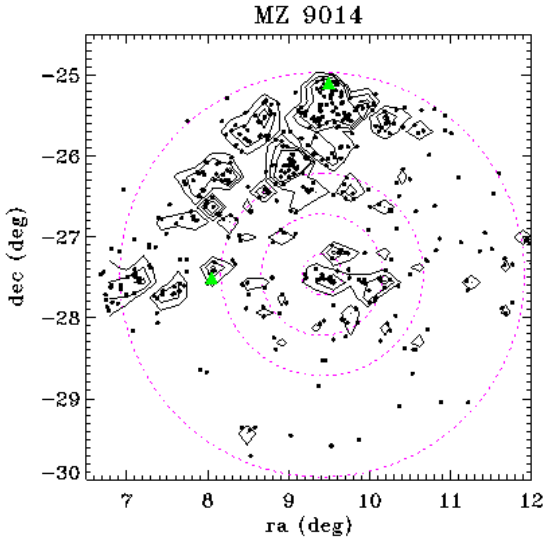

MZ 9069

Large scale classification: part of a supercluster.

Group classification: C massive groups in an advanced evolutionary state.

members within R_{200}	IR luminous	UV luminous	line measurement	Lick indices
22	11	17	17	4

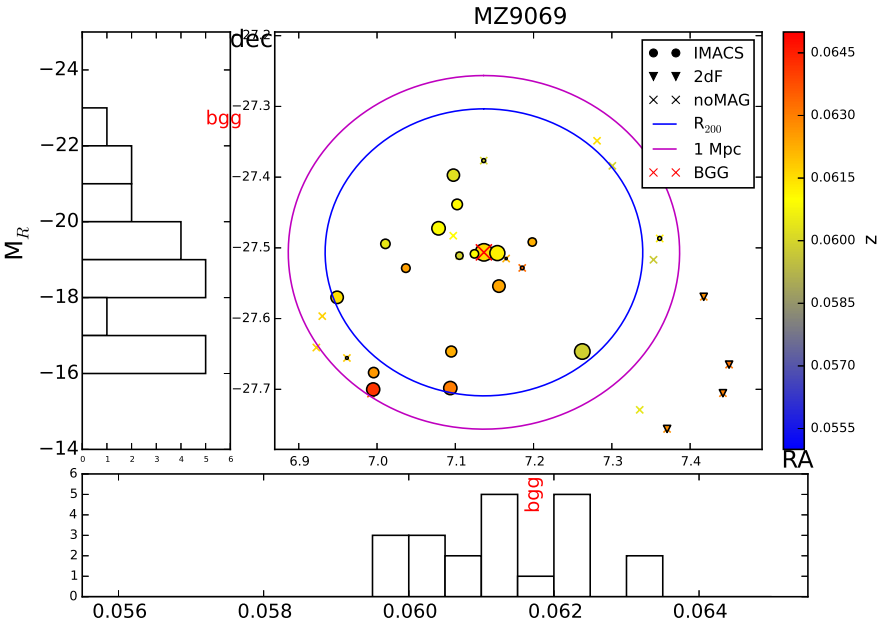

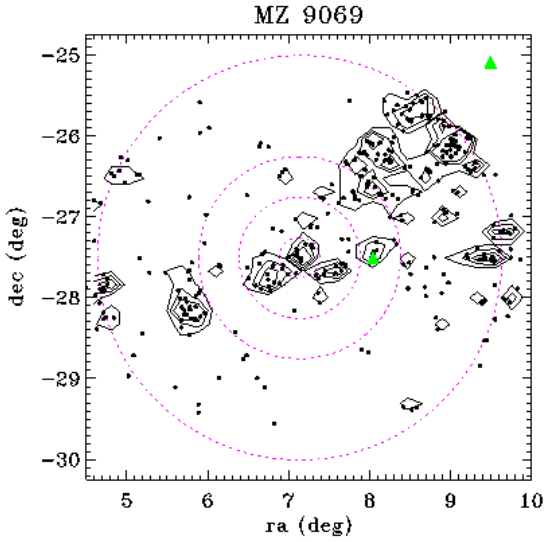

MZ 9137

Large scale classification: part of a supercluster.

Group classification: D massive and disturbed groups.

members within R_{200}	IR luminous	UV luminous	line measurement	Lick indices
13	5	13	10	6

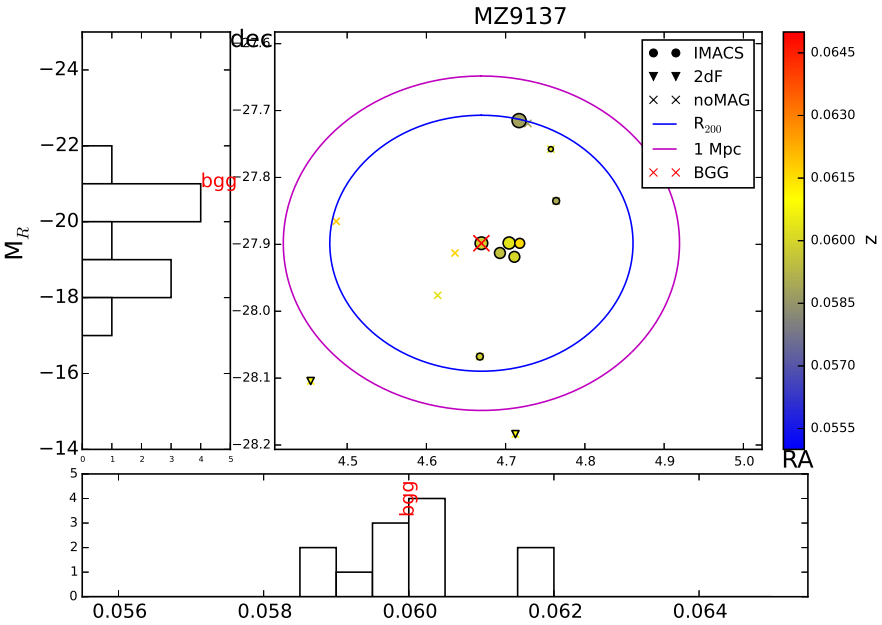

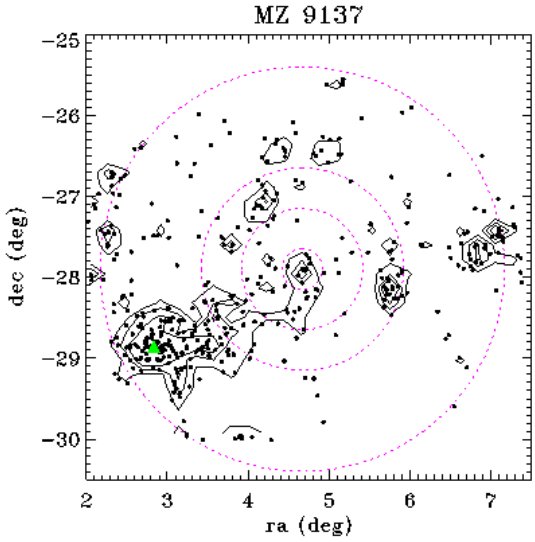

MZ 9307

Large scale classification: offset from a cluster.

Group classification: D massive and disturbed groups.

members within R_{200}	IR luminous	UV luminous	line measurement	Lick indices
15	0	12	13	3

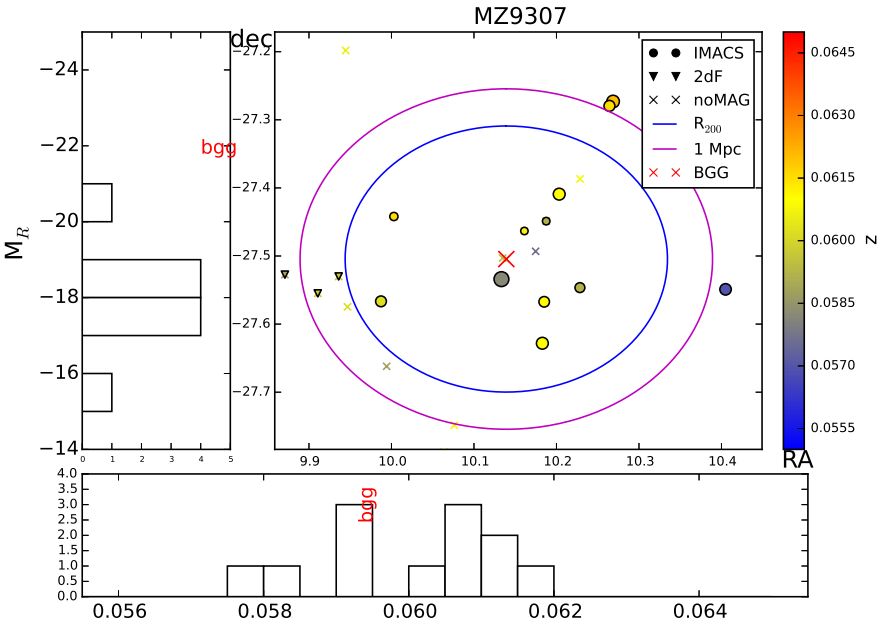

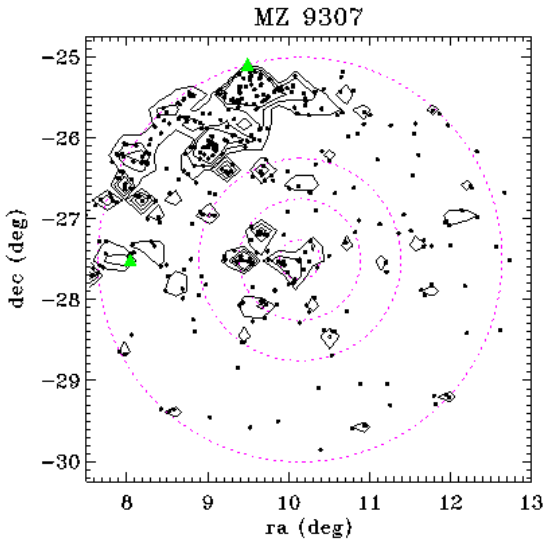

MZ 9994

Large scale classification: isolated.

Group classification: B small and isolated groups.

members within R_{200}	IR luminous	UV luminous	line measurement	Lick indices
16	3	n/a	9	3

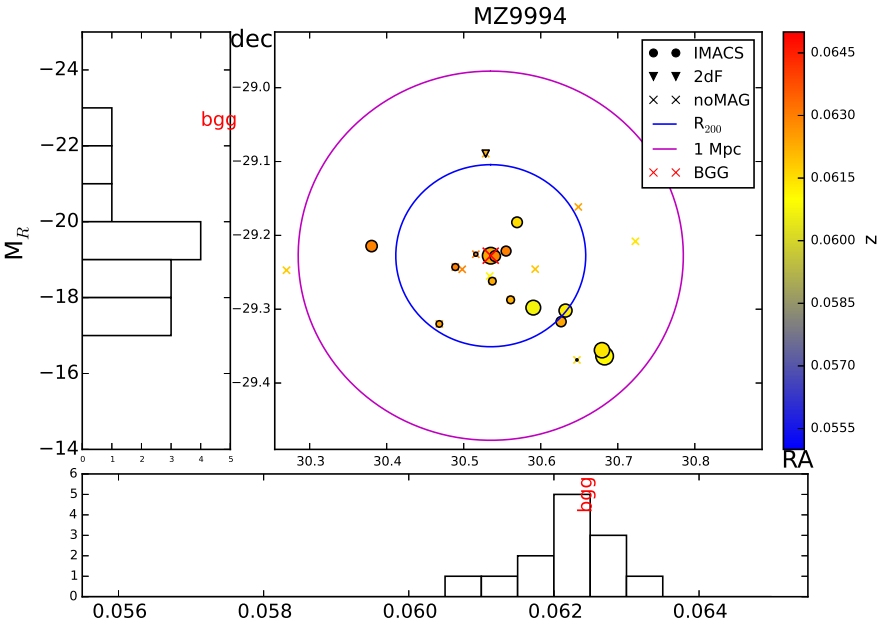

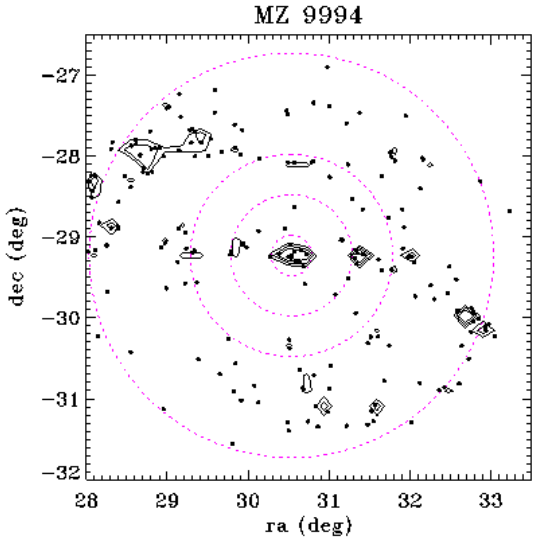

MZ 10167

Large scale classification: isolated.

Group classification: B small and isolated groups.

members within R_{200}	IR luminous	UV luminous	line measurement	Lick indices
12	7	11	12	4

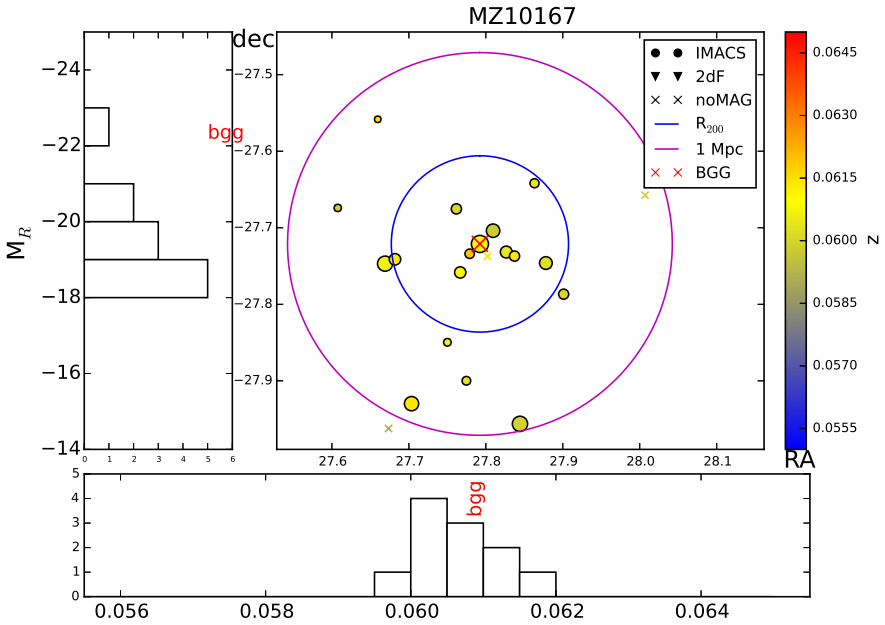

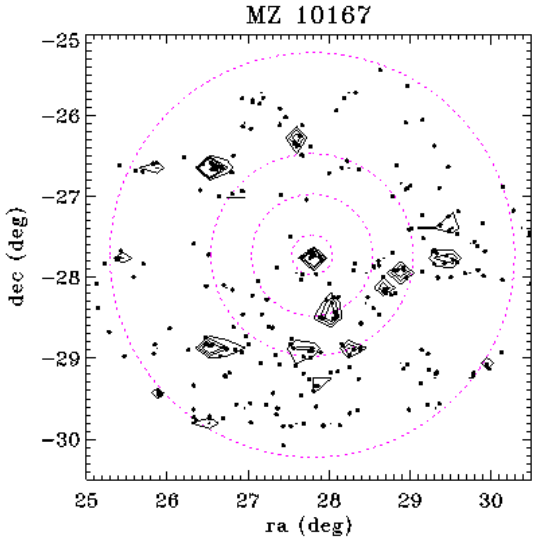

MZ 10300

Large scale classification: offset from a cluster.

Group classification: C massive groups in an advanced evolutionary state.

members within R_{200}	IR luminous	UV luminous	line measurement	Lick indices
24	6	14	18	8

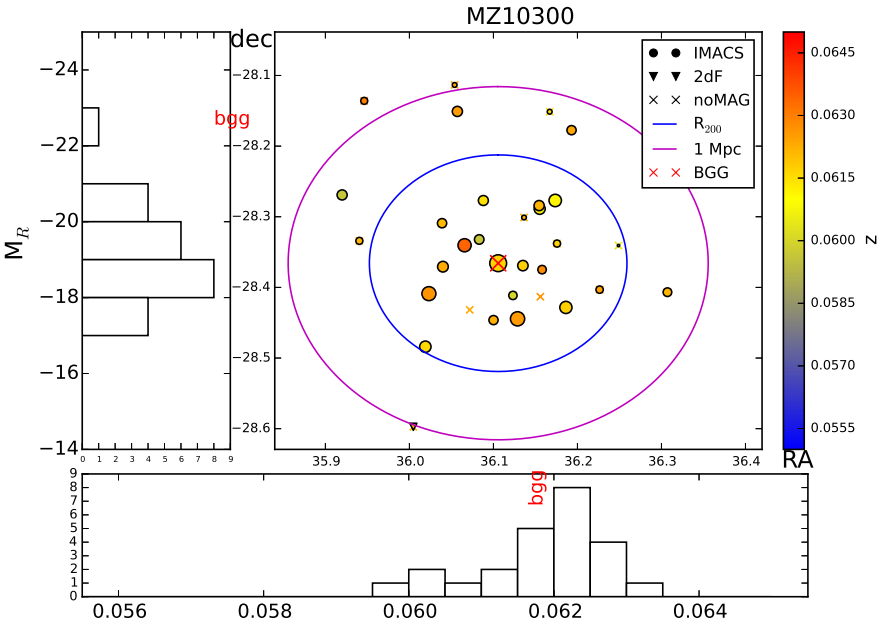

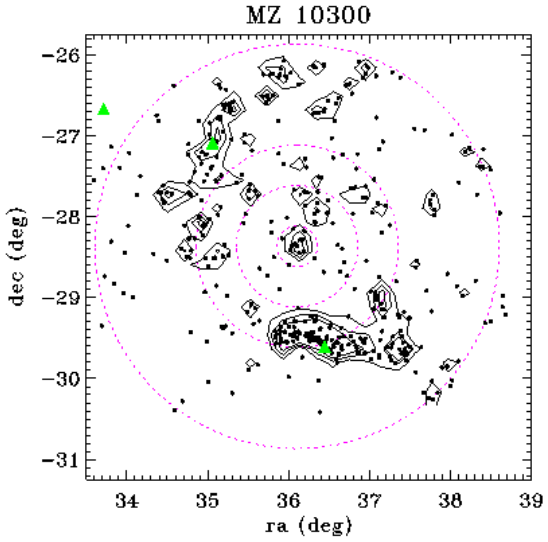

MZ 10451

Large scale classification: part of a supercluster.

Group classification: D massive and disturbed groups.

members within R_{200}	IR luminous	UV luminous	line measurement	Lick indices
40	13	32	23	9

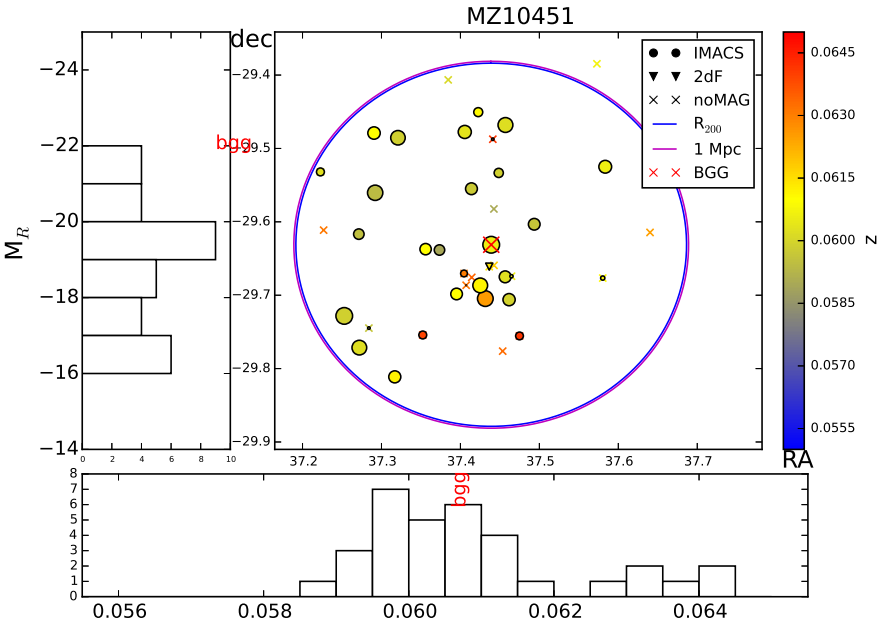

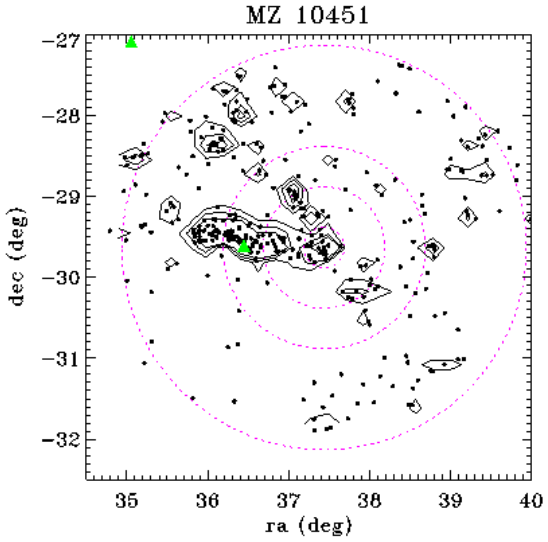

Appendix 2

Before performing the Lick indices analysis it was necessary to choose between the two available Single Stellar Population (SSP) models: KMT [Korn et al., 2005] and BC03 [Bruzual and Charlot, 2003]. The choice between them was not obvious so a test was performed in order to have an indication of which might be more suitable for the purpose.

The most striking difference between the two models is that the α-enhancement is not included in the BC03 models which only measure [Fe/H], but was manually added using Equation 3.14. Table 1 shows the value ranges for both models.

Models	Log age (yr)	[Z/H] (dex)	[Fe/H] (dex)	[E/H] (dex)
KMT	-1.0 – 1.175	-2.25 – +0.8	–	-0.3 – +0.8
BC03	-0.993 – 1.301	–	-2.25–+0.4	–

Table 1: In this table it is shown the parameter ranges for the fitting models. The KMT models give the total metallicity and the α-enhancement [Korn et al., 2005], while the BC03 models give only the iron abundance.

For the test 80 SDSS galaxies where selected in a narrow redshift range ($0.029 \leq z \leq 0.031$) and g-band magnitude range ($14 \leq g \leq 14.5$) with spectra available and morphological classification from Galaxy Zoo.

The process followed was the same as described in Section 3.5, the advantage in this case was the uniform spectral quality. Figure 5 shows the Lick indices position on one of the galaxy spectra used.

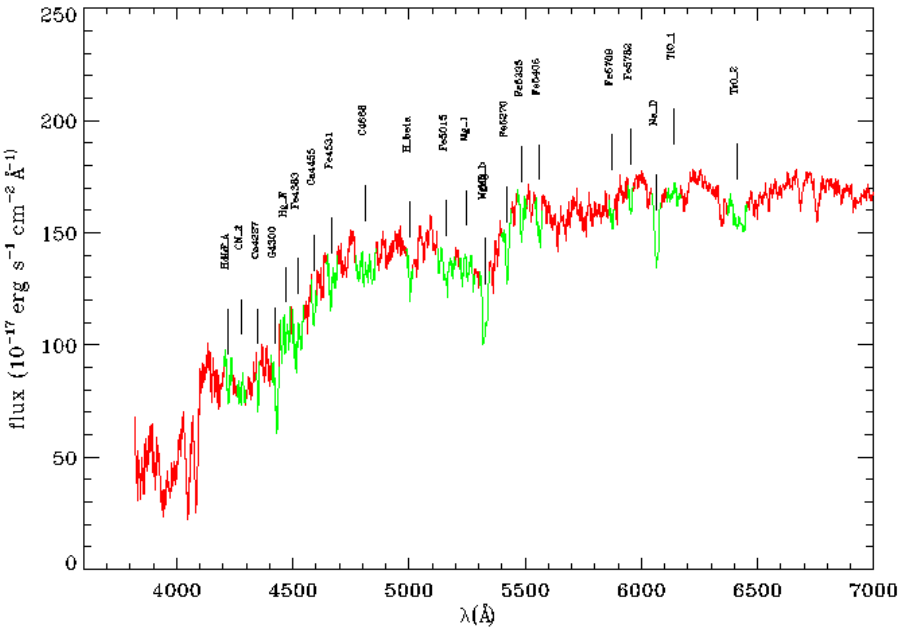

Figure 5: Spectrum of SDSS J090311.33+133756.4 (in red) cleaned from any emission line. In green is shown the central passband of all the 25 Lick indices for which the name is annotated in black. On the x-axis is shown the wavelength in Å, on the y-axis the flux in units of 10^{-17} erg s^{-1} cm^{-2} Å^{-1}.

The results obtained fitting the spectra with the two models are compared in Figure 6 where age, [Fe/H], α-enhancement and total metallicity are plotted, the galaxies are divided according to their morphology (i.e. ellipticals and spirals) as defined by Galaxy Zoo. The most striking result is the large size of the error bars, despite the good quality of the data, as obtained perturbing the Lick index values in a MC simulation. This is due to the large model uncertainty which does not allow to consider the absolute value but only the relative difference between the two model results. The age shows good agreement and elliptical galaxies are older as expected, however the major discrepancies seem to be at higher ages where the BC03 models overestimate the age with respect to the KMT models, this is surprising since we expect younger galaxies cleaned of emission lines to be more trivial to fit. The α-enhancement is also in good agreement and it shows the expected separation in morphology, similarly to the age plot since

α-enhancement is strongly correlated to the age of the stellar population. [Fe/H] and total metallicity are the most difficult to interpret due to both the intrinsic distribution and the size of the errors. They both show an outlier which should be investigated on its own, but it is not the purpose of the test. In this case it seems that the major discrepancies are on the determination of values for spiral galaxies.
The direct comparison of the results did not show any major problem with any of the models, hence a choice cannot be based on this.

A further investigation is done comparing the results with the galaxy velocity dispersion. Figure 7 shows the results obtained using both the models for the four stellar population parameters compared to the velocity dispersion. The data were fitted using the orthogonal method in the BCES (Bivariate Correlated Errors and Intrinsic Scatter, Akritas and Bershady [1996]) package. From the plots it is obvious that [Fe/H] does not depend on σ, similarly [Z/H] slightly depends on this quantity and the dependency is introduced by the α-enhancement which is included in [Z/H] according to Formula 3.14. Both age and α-enhancement depend on the velocity dispersion. The result of the Lick indices analysis do not show any anomaly in either model, however it is observed that the BC03 models over-estimate the age and α-enhancement of the stellar population (blue dashed line is above red solid line, and red dashed line is below blue solid line) and underestimate [Fe/H] and [Z/H] (blue dashed line is below red solid line, and red dashed line is above blue solid line). It is expected that [Fe/H] and [Z/H] show a similar behaviour, which also opposite to what observed for the α-enhancement, the latter is linked to the age by the stellar population properties. The fact that BC03 over-estimates the age could be simply a reflection of the higher age boundary of the models, however it is impossible to further infer from these results given that the real stellar population parameters are not known.

A similar approach is taken plotting the stellar population parameters as a function of colour u-r (Figure 8), bearing in mind that it is expected that a redder colour

corresponds to an older or more metal rich stellar population. In this study there is no [Fe/H]-colour dependence, possibly given the very large uncertainty on the determination of metallicity-related parameters, the age-colour relation is observed as expected. This analysis does not add any further information about the models behaviour since the same trends as before are observed: BC03 over-estimates age and α-enhancement while it under-estimates [Fe/H] and [Z/H] compared to the KMT models.

It is immediately clear from the plots that this kind of analysis is affected by very large errors and it is difficult to infer whether either model is better than the other one. The differences shown are clearly depending on the way the models were constructed, but neither seem to suffer from major instabilities or problems, however they cannot be used to infer an absolute value for the parameters, but only a relative one.

Thus, the choice between the two models was purely arbitrary, the KMT models were chosen because they included the α-enhancement by construction and because the top value for the stellar population age in the BC03 models was higher than the age of the Universe inferred by the Cosmology used in this work.

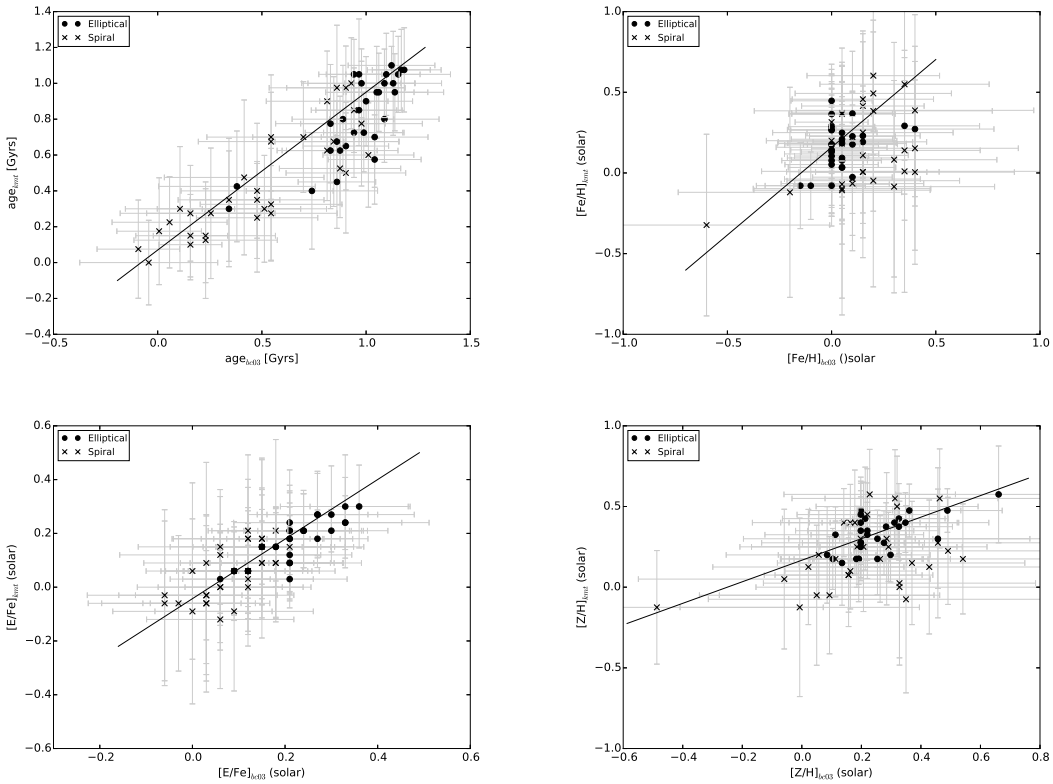

Figure 6: The four plots compare the results obtained fitting the spectra with the BC03 (x-axis) and KMT (y-axis) models. Circles represent elliptical galaxies while crosses are spirals, the solid line is the identity line. Log age (top left) and α-enhancement (bottom left) show good agreement between the two models and, as expected, elliptical galaxies tend to be older and have higher α-enhancement. The iron-abundance results (top right) are not consistent between the two models. The total metallicity (bottom right) being a combination of the previous two quantities, shows an agreement lead by the α-enhancement but weakened by the iron-element abundance. The size of the error bars does not allow to draw any definitive conclusion.

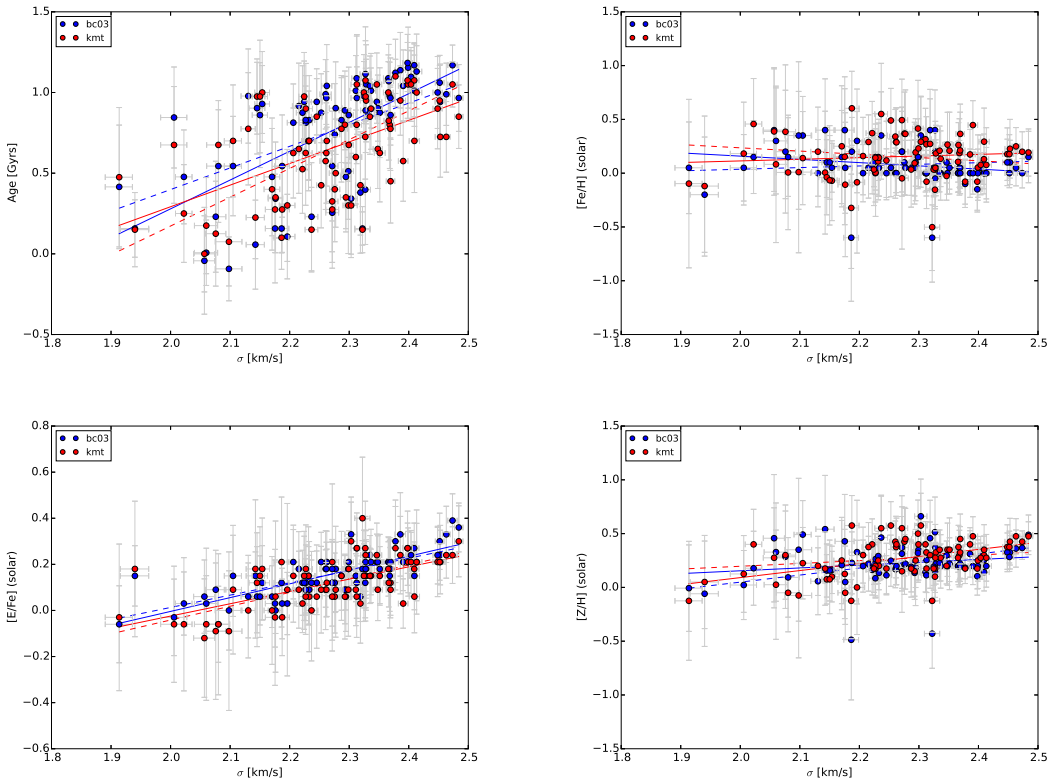

Figure 7: The four plots show the stellar population parameters (y-axis) plotted against the Log galaxy velocity dispersion (x-axis). BC03 results are shown in blue, KMT in red. The two solid lines are independent fits of the two point sets. The dashed lines are fits to the points with the slope set to match the opposite colour solid line (e.g blue dashed line has the same slope as red solid line, and vice versa) to allow for a direct comparison.

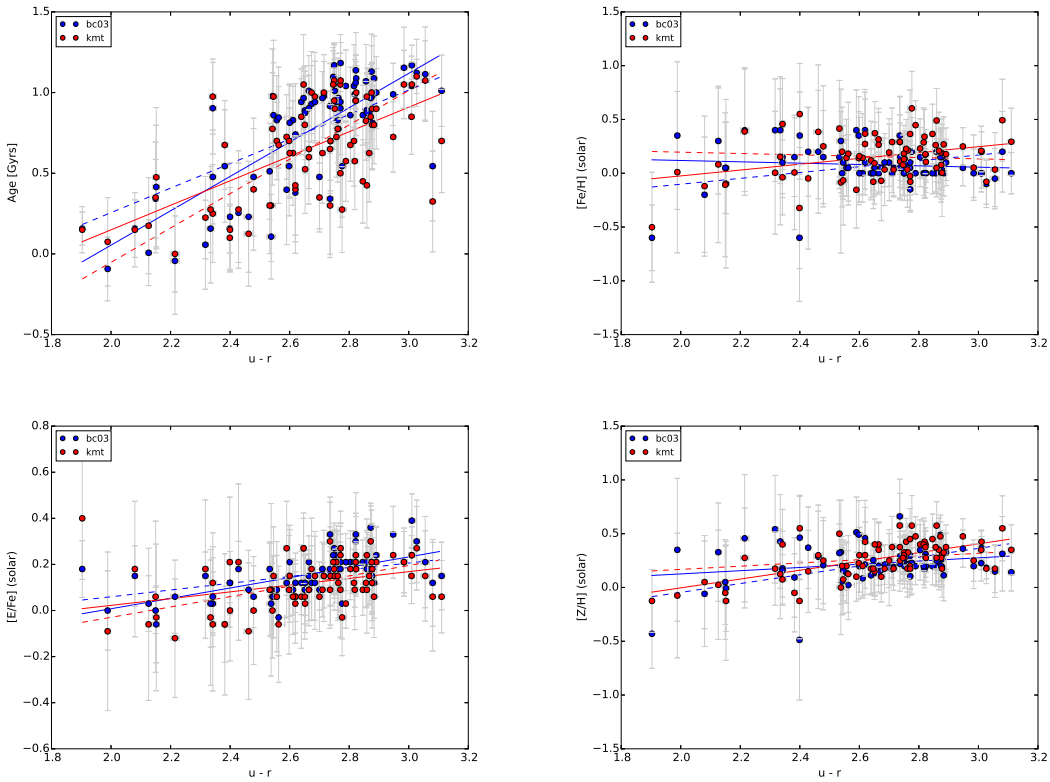

Figure 8: The four plots show the stellar population parameters (y-axis) plotted against the galaxy u-r colour (x-axis). BC03 results are shown in blue, KMT in red. The two solid lines are independent fits of the two point sets. The dashed lines are fits to the points with the slope set to match the opposite colour solid line (e.g blue dashed line has the same slope as red solid line, and vice versa) to allow for a direct comparison.

Bibliography

M. G. Abadi, B. Moore, and R. G. Bower. Ram pressure stripping of spiral galaxies in clusters. *MNRAS*, 308:947–954, October 1999. doi: 10.1046/j.1365-8711.1999.02715.x. 11, 14

M. G. Akritas and M. A. Bershady. Linear Regression for Astronomical Data with Measurement Errors and Intrinsic Scatter. *ApJ*, 470:706, October 1996. doi: 10.1086/177901. 154

Y. M. Bahé, I. G. McCarthy, M. L. Balogh, and A. S. Font. Why does the environmental influence on group and cluster galaxies extend beyond the virial radius? *MNRAS*, 430:3017–3031, April 2013. doi: 10.1093/mnras/stt109. 19

L. Bai, J. Rasmussen, J. S. Mulchaey, A. Dariush, S. Raychaudhury, and T. J. Ponman. The First Mid-infrared View of the Star-forming Properties of Nearby Galaxy Groups. *ApJ*, 713:637–650, April 2010. doi: 10.1088/0004-637X/713/1/637. 1, 37, 38, 40, 42, 43

I. K. Baldry, M. L. Balogh, R. Bower, K. Glazebrook, and R. C. Nichol. Color bimodality: Implications for galaxy evolution. In R. E. Allen, D. V. Nanopoulos, and C. N. Pope, editors, *The New Cosmology: Conference on Strings and Cosmology*, volume 743 of *American Institute of Physics Conference Series*, pages 106–119, December 2004. doi: 10.1063/1.1848322. 9

J. A. Baldwin, M. M. Phillips, and R. Terlevich. Classification parameters for the emission-line spectra of extragalactic objects. *PASP*, 93:5–19, February 1981. doi: 10.1086/130766. 63, 109, 111, 112

M. L. Balogh. *The recent star formation history of galaxies in X-ray clusters*. PhD thesis, UNIVERSITY OF VICTORIA (CANADA), 1999. 9, 10, 19

M. L. Balogh and S. L. McGee. Implications of the remarkable homogeneity of galaxy groups and clusters. *MNRAS*, 402:L59–L63, February 2010. doi: 10.1111/j.1745-3933.2009.00800.x. 19

M. L. Balogh, S. L. Morris, H. K. C. Yee, R. G. Carlberg, and E. Ellingson. Star Formation in Cluster Galaxies at 0.2 ¡ Z ¡ 0.55. *ApJL*, 488:L75–L78, October 1997. doi: 10.1086/310927. 9

M. L. Balogh, D. Schade, S. L. Morris, H. K. C. Yee, R. G. Carlberg, and E. Ellingson. The Dependence of Cluster Galaxy Star Formation Rates on the Global Environment. *ApJL*, 504:L75–L78, September 1998. doi: 10.1086/311576. 9

M. L. Balogh, J. F. Navarro, and S. L. Morris. The Origin of Star Formation Gradients in Rich Galaxy Clusters. *ApJ*, 540:113–121, September 2000. doi: 10.1086/309323. 10, 14, 20, 92

M. L. Balogh, I. K. Baldry, R. Nichol, C. Miller, R. Bower, and K. Glazebrook. The Bimodal Galaxy Color Distribution: Dependence on Luminosity and Environment. *ApJL*, 615:L101–L104, November 2004. doi: 10.1086/426079. 9

S. P. Bamford, B. Milvang-Jensen, and A. Aragón-Salamanca. The sizes of disc galaxies in intermediate-redshift clusters. *MNRAS*, 378:L6–L10, June 2007. doi: 10.1111/j.1745-3933.2007.00307.x. 20

J. E. Barnes. Evolution of compact groups and the formation of elliptical galaxies. *Nature*, 338:123–126, March 1989. doi: 10.1038/338123a0. 11

M. A. Beasley, J. P. Brodie, J. Strader, D. A. Forbes, R. N. Proctor, P. Barmby, and J. P. Huchra. The Chemical Properties of Milky Way and M31 Globular Clusters. I. A Comparative Study. *AJ*, 128:1623–1645, October 2004. doi: 10.1086/424000. 56

T. C. Beers, K. Flynn, and K. Gebhardt. Measures of location and scale for velocities in clusters of galaxies - A robust approach. *AJ*, 100:32–46, July 1990. doi: 10.1086/115487. 40

K. Bekki, W. J. Couch, and Y. Shioya. Passive Spiral Formation from Halo Gas Starvation: Gradual Transformation into S0s. *ApJ*, 577:651–657, October 2002. doi: 10.1086/342221. 15

E. F. Bell, D. H. McIntosh, N. Katz, and M. D. Weinberg. The Optical and Near-Infrared Properties of Galaxies. I. Luminosity and Stellar Mass Functions. *ApJS*, 149:289–312, December 2003. doi: 10.1086/378847. 42

J. C. Berrier, J. S. Bullock, E. J. Barton, H. D. Guenther, A. R. Zentner, and R. H. Wechsler. Close Galaxy Counts as a Probe of Hierarchical Structure Formation. *ApJ*, 652:56–70, November 2006. doi: 10.1086/507573. 2

E. Bertin and S. Arnouts. SExtractor: Software for source extraction. *A&AS*, 117: 393–404, June 1996. doi: 10.1051/aas:1996164. 37, 42, 43

B. C. Bigelow and A. M. Dressler. IMACS, the multiobject spectrograph and imager for Magellan: a status report. In M. Iye and A. F. M. Moorwood, editors, *Instrument Design and Performance for Optical/Infrared Ground-based Telescopes*, volume 4841 of *Society of Photo-Optical Instrumentation Engineers (SPIE) Conference Series*, pages 1727–1738, March 2003. doi: 10.1117/12.461870. 37

Christopher M. Bishop. *Neural Networks for Pattern Recognition*. Oxford University Press, Inc., New York, NY, USA, 1995. ISBN 0198538642. 75

M. R. Blanton and J. Moustakas. Physical Properties and Environments of Nearby Galaxies. *ARA&A*, 47:159–210, September 2009. doi: 10.1146/annurev-astro-082708-101734. 9

M. R. Blanton and S. Roweis. K-Corrections and Filter Transformations in the Ultraviolet, Optical, and Near-Infrared. *AJ*, 133:734–754, February 2007. doi: 10.1086/510127. 42

B. Bösch, A. Böhm, C. Wolf, A. Aragón-Salamanca, M. Barden, M. E. Gray, B. L. Ziegler, S. Schindler, and M. Balogh. Ram pressure and dusty red galaxies - key factors in the evolution of the multiple cluster system Abell 901/902. *A&A*, 549: A142, January 2013. doi: 10.1051/0004-6361/201219244. 13

A. Boselli and G. Gavazzi. Environmental Effects on Late-Type Galaxies in Nearby Clusters. *PASP*, 118:517–559, April 2006. doi: 10.1086/500691. 4, 9, 14

A. Boselli, S. Boissier, L. Cortese, A. Gil de Paz, M. Seibert, B. F. Madore, V. Buat, and D. C. Martin. The Fate of Spiral Galaxies in Clusters: The Star Formation History of the Anemic Virgo Cluster Galaxy NGC 4569. *ApJ*, 651:811–821, November 2006. doi: 10.1086/507766. 14

A. Boselli, S. Boissier, L. Cortese, and G. Gavazzi. The Origin of Dwarf Ellipticals in the Virgo Cluster. *ApJ*, 674:742–767, February 2008. doi: 10.1086/525513. 14

A. Boselli, S. Boissier, L. Cortese, and G. Gavazzi. The effect of ram-pressure stripping and starvation on the star formation properties of cluster galaxies. *Astronomische Nachrichten*, 330:904, December 2009. doi: 10.1002/asna.200911259. 14

R. G. Bower, A. J. Benson, R. Malbon, J. C. Helly, C. S. Frenk, C. M. Baugh, S. Cole, and C. G. Lacey. Breaking the hierarchy of galaxy formation. *MNRAS*, 370:645–655, August 2006. doi: 10.1111/j.1365-2966.2006.10519.x. 12

U. G. Briel, J. P. Henry, R. A. Schwarz, H. Bohringer, H. Ebeling, A. C. Edge, G. D. Hartner, S. Schindler, J. Trumper, and W. Voges. The X-ray morphology of the relaxed cluster of galaxies A2256. I - Evidence for a merger event. *A&A*, 246:L10–L13, June 1991. 8

M. Brüggen and G. De Lucia. Ram-pressure histories of cluster galaxies. *MNRAS*, 383: 1336–1342, February 2008. doi: 10.1111/j.1365-2966.2007.12670.x. 11, 14

G. Bruzual and S. Charlot. Stellar population synthesis at the resolution of 2003. *MNRAS*, 344:1000–1028, October 2003. doi: 10.1046/j.1365-8711.2003.06897.x. 35, 56, 152

V. Buat, J. Iglesias-Páramo, M. Seibert, D. Burgarella, S. Charlot, D. C. Martin, C. K. Xu, T. M. Heckman, S. Boissier, A. Boselli, T. Barlow, L. Bianchi, Y.-I. Byun, J. Donas, K. Forster, P. G. Friedman, P. Jelinski, Y.-W. Lee, B. F. Madore, R. Malina, B. Milliard, P. Morissey, S. Neff, M. Rich, D. Schiminovitch, O. Siegmund, T. Small, A. S. Szalay, B. Welsh, and T. K. Wyder. Dust Attenuation in the Nearby Universe: A Comparison between Galaxies Selected in the Ultraviolet and in the Far-Infrared. *ApJL*, 619:L51–L54, January 2005. doi: 10.1086/423241. 43

D. Calzetti, A. L. Kinney, and T. Storchi-Bergmann. Dust extinction of the stellar continua in starburst galaxies: The ultraviolet and optical extinction law. *ApJ*, 429: 582–601, July 1994. doi: 10.1086/174346. 34

M. Cappellari and E. Emsellem. Parametric Recovery of Line-of-Sight Velocity Distributions from Absorption-Line Spectra of Galaxies via Penalized Likelihood. *PASP*, 116:138–147, February 2004. doi: 10.1086/381875. 49

B. Catinella, D. Schiminovich, L. Cortese, S. Fabello, C. B. Hummels, S. M. Moran, J. J. Lemonias, A. P. Cooper, R. Wu, T. M. Heckman, and J. Wang. The GALEX Arecibo SDSS Survey - VIII. Final data release. The effect of group environment on the gas content of massive galaxies. *MNRAS*, 436:34–70, November 2013. doi: 10.1093/mnras/stt1417. 13

A. Cattaneo, S. M. Faber, J. Binney, A. Dekel, J. Kormendy, R. Mushotzky, A. Babul, P. N. Best, M. Brüggen, A. C. Fabian, C. S. Frenk, A. Khalatyan, H. Netzer, A. Mahdavi, J. Silk, M. Steinmetz, and L. Wisotzki. The role of black holes in galaxy formation and evolution. *Nature*, 460:213–219, July 2009. doi: 10.1038/nature08135. 12

G. Chabrier. Galactic Stellar and Substellar Initial Mass Function. *PASP*, 115:763–795, July 2003. doi: 10.1086/376392. 33

CISCO. Hickson compact group 40. URL `http://www.nao.ac.jp/`. vi, 6

M. Colless, G. Dalton, S. Maddox, W. Sutherland, P. Norberg, S. Cole, J. Bland-Hawthorn, T. Bridges, R. Cannon, C. Collins, W. Couch, N. Cross, K. Deeley, R. De Propris, S. P. Driver, G. Efstathiou, R. S. Ellis, C. S. Frenk, K. Glazebrook, C. Jackson, O. Lahav, I. Lewis, S. Lumsden, D. Madgwick, J. A. Peacock, B. A. Peterson, I. Price, M. Seaborne, and K. Taylor. The 2dF Galaxy Redshift Survey: spectra and redshifts. *MNRAS*, 328:1039–1063, December 2001. doi: 10.1046/j.1365-8711.2001.04902.x. 8, 36, 38

F. Combes. Secular Evolution of Galaxies. *ArXiv Astrophysics e-prints*, June 2005. 12

M. C. Cooper, C. A. Tremonti, J. A. Newman, and A. I. Zabludoff. The role of environment in the mass-metallicity relation. *MNRAS*, 390:245–256, October 2008. doi: 10.1111/j.1365-2966.2008.13714.x. 87

H. H. Crowl and J. D. P. Kenney. The Stellar Populations of Stripped Spiral Galaxies in the Virgo Cluster. *AJ*, 136:1623–1644, October 2008. doi: 10.1088/0004-6256/136/4/1623. 14

Andrew Moore Dan Pelleg. X-means: Extending k-means with efficient estimation of the number of clusters. In *Proceedings of the Seventeenth International Conference on Machine Learning*, pages 727–734, San Francisco, 2000. Morgan Kaufmann. 1, 75

A. A. Dariush, S. Raychaudhury, T. J. Ponman, H. G. Khosroshahi, A. J. Benson, R. G. Bower, and F. Pearce. The mass assembly of galaxy groups and the evolution of the magnitude gap. *MNRAS*, 405:1873–1887, July 2010. doi: 10.1111/j.1365-2966.2010.16569.x. 7

M. Davis, G. Efstathiou, C. S. Frenk, and S. D. M. White. The evolution of large-scale structure in a universe dominated by cold dark matter. *ApJ*, 292:371–394, May 1985. doi: 10.1086/163168. 8

G. De Lucia, S. Weinmann, B. M. Poggianti, A. Aragón-Salamanca, and D. Zaritsky. The environmental history of group and cluster galaxies in a Λ cold dark matter universe. *MNRAS*, 423:1277–1292, June 2012. doi: 10.1111/j.1365-2966.2012.20983.x. 20

R. De Propris, M. Colless, S. P. Driver, M. B. Pracy, and W. J. Couch. Internal colour gradients for E/S0 galaxies in Abell 2218. *MNRAS*, 357:590–598, February 2005. doi: 10.1111/j.1365-2966.2005.08662.x. 12

A. Dekel and J. Silk. The origin of dwarf galaxies, cold dark matter, and biased galaxy formation. *ApJ*, 303:39–55, April 1986. doi: 10.1086/164050. 12

Bruce T. Draine. *Phisics of the Interstellar and Intergalactic Medium.* Princeton University Press, first edition, 2011. 25, 34

A. Dressler. Galaxy morphology in rich clusters - Implications for the formation and evolution of galaxies. *ApJ*, 236:351–365, March 1980. doi: 10.1086/157753. 9

A. Dressler, I. B. Thompson, and S. A. Shectman. Statistics of emission-line galaxies in rich clusters. *ApJ*, 288:481–486, January 1985. doi: 10.1086/162813. 9

R. O. Duda and P. E. Hart. *Pattern Classification and Scene Analysis*. John Willey & Sons, New Yotk, 1973. 75

G. Efstathiou. A model of supernova feedback in galaxy formation. *MNRAS*, 317: 697–719, September 2000. doi: 10.1046/j.1365-8711.2000.03665.x. 12

V. R. Eke, C. M. Baugh, S. Cole, C. S. Frenk, P. Norberg, J. A. Peacock, I. K. Baldry, J. Bland-Hawthorn, T. Bridges, R. Cannon, M. Colless, C. Collins, W. Couch, G. Dalton, R. de Propris, S. P. Driver, G. Efstathiou, R. S. Ellis, K. Glazebrook, C. Jackson, O. Lahav, I. Lewis, S. Lumsden, S. Maddox, D. Madgwick, B. A. Peterson, W. Sutherland, and K. Taylor. Galaxy groups in the 2dFGRS: the group-finding algorithm and the 2PIGG catalogue. *MNRAS*, 348:866–878, March 2004a. doi: 10.1111/j.1365-2966.2004.07408.x. 5, 8

V. R. Eke, C. S. Frenk, C. M. Baugh, S. Cole, P. Norberg, J. A. Peacock, I. K. Baldry, J. Bland-Hawthorn, T. Bridges, R. Cannon, M. Colless, C. Collins, W. Couch, G. Dalton, R. de Propris, S. P. Driver, G. Efstathiou, R. S. Ellis, K. Glazebrook, C. A. Jackson, O. Lahav, I. Lewis, S. Lumsden, S. J. Maddox, D. Madgwick, B. A. Peterson, W. Sutherland, and K. Taylor. Galaxy groups in the Two-degree Field Galaxy Redshift Survey: the luminous content of the groups. *MNRAS*, 355:769–784, December 2004b. doi: 10.1111/j.1365-2966.2004.08354.x. 10

V. R. Eke, C. M. Baugh, S. Cole, C. S. Frenk, H. M. King, and J. A. Peacock. Where are the stars? *MNRAS*, 362:1233–1246, October 2005. doi: 10.1111/j.1365-2966.2005.09384.x. 5

S. L. Ellison, L. Simard, N. B. Cowan, I. K. Baldry, D. R. Patton, and A. W. McConnachie. The mass-metallicity relation in galaxy clusters: the relative importance of cluster membership versus local environment. *MNRAS*, 396:1257–1272, July 2009. doi: 10.1111/j.1365-2966.2009.14817.x. 87

S. Ettori, A. Morandi, P. Tozzi, I. Balestra, S. Borgani, P. Rosati, L. Lovisari, and F. Terenziani. The cluster gas mass fraction as a cosmological probe: a revised study. *A&A*, 501:61–73, July 2009. doi: 10.1051/0004-6361/200810878. 4

S. Fabello, G. Kauffmann, B. Catinella, C. Li, R. Giovanelli, and M. P. Haynes. ALFALFA H I data stacking - III. Comparison of environmental trends in H I gas mass fraction and specific star formation rate. *MNRAS*, 427:2841–2851, December 2012. doi: 10.1111/j.1365-2966.2012.22088.x. 13

S. M. Faber, E. D. Friel, D. Burstein, and C. M. Gaskell. Old stellar populations. II - an analysis of K-giant spectra. *ApJS*, 57:711–741, April 1985. doi: 10.1086/191024. 46

A. Faltenbacher and J. Diemand. Velocity distributions in clusters of galaxies. *MNRAS*, 369:1698–1702, July 2006. doi: 10.1111/j.1365-2966.2006.10421.x. 5

R. A. Finn, D. Zaritsky, and D. W. McCarthy, Jr. Hα-derived Star Formation Rates for the z = 0.84 Galaxy Cluster Cl J0023+0423B. *ApJ*, 604:141–152, March 2004. doi: 10.1086/381729. 40

M. Fossati, G. Gavazzi, A. Boselli, and M. Fumagalli. 65 kpc of ionized gas trailing behind NGC 4848 during its first crossing of the Coma cluster. *A&A*, 544:A128, August 2012. doi: 10.1051/0004-6361/201219933. 14

D. A. Gadotti. Secular evolution and structural properties of stellar bars in galaxies. *MNRAS*, 415:3308–3318, August 2011. doi: 10.1111/j.1365-2966.2011.18945.x. 12

A. Galametz, D. Stern, P. R. M. Eisenhardt, M. Brodwin, M. J. I. Brown, A. Dey, A. H. Gonzalez, B. T. Jannuzi, L. A. Moustakas, and S. A. Stanford. The Cosmic Evolution of Active Galactic Nuclei in Galaxy Clusters. *ApJ*, 694:1309–1316, April 2009. doi: 10.1088/0004-637X/694/2/1309. 11

A. Gallazzi, E. F. Bell, C. Wolf, M. E. Gray, C. Papovich, M. Barden, C. Y. Peng, K. Meisenheimer, C. Heymans, E. van Kampen, R. Gilmour, M. Balogh, D. H. McIntosh, D. Bacon, F. D. Barazza, A. Böhm, J. A. R. Caldwell, B. Häußler, K. Jahnke, S. Jogee, K. Lane, A. R. Robaina, S. F. Sanchez, A. Taylor, L. Wisotzki, and X. Zheng. Obscured Star Formation in Intermediate-Density Environments: A Spitzer Study of the Abell 901/902 Supercluster. *ApJ*, 690:1883–1900, January 2009. doi: 10.1088/0004-637X/690/2/1883. 10, 20

G. Gavazzi, A. Boselli, L. Mayer, J. Iglesias-Paramo, J. M. Vílchez, and L. Carrasco. 75 Kiloparsec Trails of Ionized Gas behind Two Irregular Galaxies in A1367. *ApJL*, 563:L23–L26, December 2001. doi: 10.1086/338389. 14

M. J. Geller and J. P. Huchra. Groups of galaxies. III - The CfA survey. *ApJS*, 52: 61–87, June 1983. doi: 10.1086/190859. 8

O. E. Gerhard. Line-of-sight velocity profiles in spherical galaxies: breaking the degeneracy between anisotropy and mass. *MNRAS*, 265:213, November 1993. 51

S. Giodini, D. Pierini, A. Finoguenov, G. W. Pratt, H. Boehringer, A. Leauthaud, L. Guzzo, H. Aussel, M. Bolzonella, P. Capak, M. Elvis, G. Hasinger, O. Ilbert, J. S. Kartaltepe, A. M. Koekemoer, S. J. Lilly, R. Massey, H. J. McCracken, J. Rhodes, M. Salvato, D. B. Sanders, N. Z. Scoville, S. Sasaki, V. Smolcic, Y. Taniguchi, D. Thompson, and COSMOS Collaboration. Stellar and Total Baryon Mass Fractions in Groups and Clusters Since Redshift 1. *ApJ*, 703:982–993, September 2009. doi: 10.1088/0004-637X/703/1/982. 71, 82

M. Girardi, P. Manzato, M. Mezzetti, G. Giuricin, and F. Limboz. Observational Mass-to-Light Ratio of Galaxy Systems from Poor Groups to Rich Clusters. *ApJ*, 569:720–741, April 2002. doi: 10.1086/339360. 10

P. L. Gómez, R. C. Nichol, C. J. Miller, M. L. Balogh, T. Goto, A. I. Zabludoff, A. K. Romer, M. Bernardi, R. Sheth, A. M. Hopkins, F. J. Castander, A. J. Connolly, D. P. Schneider, J. Brinkmann, D. Q. Lamb, M. SubbaRao, and D. G. York. Galaxy Star Formation as a Function of Environment in the Early Data Release of the Sloan Digital Sky Survey. *ApJ*, 584:210–227, February 2003. doi: 10.1086/345593. 9

A. H. Gonzalez, D. Zaritsky, and A. I. Zabludoff. A Census of Baryons in Galaxy Clusters and Groups. *ApJ*, 666:147–155, September 2007. doi: 10.1086/519729. 71, 82

R. M. González Delgado, M. Cerviño, L. P. Martins, C. Leitherer, and P. H. Hauschildt. Evolutionary stellar population synthesis at high spectral resolution: optical wavelengths. *MNRAS*, 357:945–960, March 2005. doi: 10.1111/j.1365-2966.2005.08692.x. 35

K. D. Gordon, G. H. Rieke, C. W. Engelbracht, J. Muzerolle, J. A. Stansberry, K. A. Misselt, J. E. Morrison, J. Cadien, E. T. Young, H. Dole, D. M. Kelly, A. Alonso-Herrero, E. Egami, K. Y. L. Su, C. Papovich, P. S. Smith, D. C. Hines, M. J. Rieke, M. Blaylock, P. G. Pérez-González, E. Le Floc'h, J. L. Hinz, W. B. Latter, T. Hesselroth, D. T. Frayer, A. Noriega-Crespo, F. J. Masci, D. L. Padgett, M. P. Smylie, and N. M. Haegel. Reduction Algorithms for the Multiband Imaging Photometer for Spitzer. *PASP*, 117:503–525, May 2005. doi: 10.1086/429309. 42

T. Goto, C. Yamauchi, Y. Fujita, S. Okamura, M. Sekiguchi, I. Smail, M. Bernardi, and P. L. Gomez. The morphology-density relation in the Sloan Digital Sky Survey. *MNRAS*, 346:601–614, December 2003. doi: 10.1046/j.1365-2966.2003.07114.x. 9

F. Governato, R. Bhatia, and G. Chincarini. A long-lasting compact group. *ApJL*, 371: L15–L18, April 1991. doi: 10.1086/185991. 11

Richard O. Gray, Christopher J. Corbally, and Adam J. Burgasser. *Stellar Spectral Classification*. Princeton University Press, first edition, 2009. 26

J. E. Gunn and J. R. Gott, III. On the Infall of Matter Into Clusters of Galaxies and Some Effects on Their Evolution. *ApJ*, 176:1, August 1972. doi: 10.1086/151605. 11, 13, 14

C. P. Haines, M. J. Pereira, A. J. R. Sanderson, G. P. Smith, E. Egami, A. Babul, A. C. Edge, A. Finoguenov, S. M. Moran, and N. Okabe. LoCuSS: A Dynamical Analysis of X-Ray Active Galactic Nuclei in Local Clusters. *ApJ*, 754:97, August 2012. doi: 10.1088/0004-637X/754/2/97. 92

N. C. Hambly, H. T. MacGillivray, M. A. Read, S. B. Tritton, E. B. Thomson, B. D. Kelly, D. H. Morgan, R. E. Smith, S. P. Driver, J. Williamson, Q. A. Parker, M. R. S. Hawkins, P. M. Williams, and A. Lawrence. The SuperCOSMOS Sky Survey - I. Introduction and description. *MNRAS*, 326:1279–1294, October 2001. doi: 10.1111/j.1365-8711.2001.04660.x. 37

S. H. Hansen and J. Sommer-Larsen. The Density Profiles of Hot Galactic Halo Gas. *ApJL*, 653:L17–L20, December 2006. doi: 10.1086/510450. 5

W. G. Hartley, C. J. Conselice, A. Mortlock, S. Foucaud, and C. Simpson. Galactic conformity and central / satellite quenching, from the satellite profiles of M$ˆ{\ast}$ galaxies at $0.4¡z¡1.9$ in the UKIDSS UDS. *ArXiv e-prints*, June 2014. 10

Y. Hashimoto and A. Oemler. Environmental Influence on Star Formation of Galaxies in the Las Campanas Redshift Survey. In J. E. Barnes and D. B. Sanders, editors, *Galaxy Interactions at Low and High Redshift*, volume 186 of *IAU Symposium*, page 411, 1999. 9

A. P. Hearin and D. F. Watson. The dark side of galaxy colour. *MNRAS*, 435:1313–1324, October 2013. doi: 10.1093/mnras/stt1374. 10

A. P. Hearin, D. F. Watson, and F. C. van den Bosch. Beyond Halo Mass: Galactic Conformity as a Smoking Gun of Central Galaxy Assembly Bias. *ArXiv e-prints*, April 2014. 10

HHT. Peculiar galaxies of arp 273. URL `http://heritage.stsci.edu/`. vii, 18

HLA. Stephan's quintet, a. URL `http://hla.stsci.edu/`. vi, 6

HLA. Merging ngc 2623, b. URL `http://hla.stsci.edu/`. vii, 17

M. Hoeft, J. P. Mücket, and S. Gottlöber. Velocity Dispersion Profiles in Dark Matter Halos. *ApJ*, 602:162–169, February 2004. doi: 10.1086/380990. 5

D. W. Hogg, M. R. Blanton, J. Brinchmann, D. J. Eisenstein, D. J. Schlegel, J. E. Gunn, T. A. McKay, H.-W. Rix, N. A. Bahcall, J. Brinkmann, and A. Meiksin. The Dependence on Environment of the Color-Magnitude Relation of Galaxies. *ApJL*, 601:L29–L32, January 2004. doi: 10.1086/381749. 9

P. F. Hopkins, L. Hernquist, T. J. Cox, T. Di Matteo, B. Robertson, and V. Springel. A Unified, Merger-driven Model of the Origin of Starbursts, Quasars, the Cosmic X-Ray Background, Supermassive Black Holes, and Galaxy Spheroids. *ApJS*, 163: 1–49, March 2006. doi: 10.1086/499298. 16

A. Hou, L. C. Parker, D. J. Wilman, S. L. McGee, W. E. Harris, J. L. Connelly, M. L. Balogh, J. S. Mulchaey, and R. G. Bower. Substructure in the most massive GEEC groups: field-like populations in dynamically active groups. *MNRAS*, 421:3594–3611, April 2012. doi: 10.1111/j.1365-2966.2012.20586.x. 5

J. P. Huchra and M. J. Geller. Groups of galaxies. I - Nearby groups. *ApJ*, 257:423–437, June 1982. doi: 10.1086/160000. 5

T. M. Hughes, L. Cortese, A. Boselli, G. Gavazzi, and J. I. Davies. The role of cold gas and environment on the stellar mass-metallicity relation of nearby galaxies. *A&A*, 550:A115, February 2013. doi: 10.1051/0004-6361/201218822. 88

Y. L. Jaffé, R. Smith, G. N. Candlish, B. M. Poggianti, Y.-K. Sheen, and M. A. W. Verheijen. BUDHIES II: a phase-space view of H I gas stripping and star formation quenching in cluster galaxies. *MNRAS*, 448:1715–1728, April 2015. doi: 10.1093/mnras/stv100. 92

D. H. Jones, M. A. Read, W. Saunders, M. Colless, T. Jarrett, Q. A. Parker, A. P. Fairall, T. Mauch, E. M. Sadler, F. G. Watson, D. Burton, L. A. Campbell, P. Cass, S. M. Croom, J. Dawe, K. Fiegert, L. Frankcombe, M. Hartley, J. Huchra, D. James, E. Kirby, O. Lahav, J. Lucey, G. A. Mamon, L. Moore, B. A. Peterson, S. Prior, D. Proust, K. Russell, V. Safouris, K.-I. Wakamatsu, E. Westra, and M. Williams. The 6dF Galaxy Survey: final redshift release (DR3) and southern large-scale structures. *MNRAS*, 399:683–698, October 2009. doi: 10.1111/j.1365-2966.2009.15338.x. 38

L. R. Jones, T. J. Ponman, A. Horton, A. Babul, H. Ebeling, and D. J. Burke. The nature and space density of fossil groups of galaxies. *MNRAS*, 343:627–638, August 2003. doi: 10.1046/j.1365-8711.2003.06702.x. 7

G. Kauffmann, T. M. Heckman, S. D. M. White, S. Charlot, C. Tremonti, J. Brinchmann, G. Bruzual, E. W. Peng, M. Seibert, M. Bernardi, M. Blanton, J. Brinkmann, F. Castander, I. Csábai, M. Fukugita, Z. Ivezic, J. A. Munn, R. C. Nichol, N. Padmanabhan, A. R. Thakar, D. H. Weinberg, and D. York. Stellar masses and star formation histories for 10^5 galaxies from the Sloan Digital Sky Survey. *MNRAS*, 341: 33–53, May 2003. doi: 10.1046/j.1365-8711.2003.06291.x. 64

G. Kauffmann, C. Li, and T. M. Heckman. The accretion of gas on to galaxies as traced

by their satellites. *MNRAS*, 409:491–499, December 2010. doi: 10.1111/j.1365-2966.2010.17337.x. 10

G. Kauffmann, C. Li, W. Zhang, and S. Weinmann. A re-examination of galactic conformity and a comparison with semi-analytic models of galaxy formation. *MNRAS*, 430:1447–1456, April 2013. doi: 10.1093/mnras/stt007. 10

D. Kawata and J. S. Mulchaey. Strangulation in Galaxy Groups. *ApJL*, 672:L103–L106, January 2008. doi: 10.1086/526544. 15

J. D. P. Kenney, J. H. van Gorkom, and B. Vollmer. VLA H I Observations of Gas Stripping in the Virgo Cluster Spiral NGC 4522. *AJ*, 127:3361–3374, June 2004. doi: 10.1086/420805. vii, 15

L. J. Kewley, M. A. Dopita, R. S. Sutherland, C. A. Heisler, and J. Trevena. Theoretical Modeling of Starburst Galaxies. *ApJ*, 556:121–140, July 2001. doi: 10.1086/321545. 64

L. J. Kewley, B. Groves, G. Kauffmann, and T. Heckman. The host galaxies and classification of active galactic nuclei. *MNRAS*, 372:961–976, November 2006. doi: 10.1111/j.1365-2966.2006.10859.x. 64, 109, 111, 112

C. Knobel, S. J. Lilly, J. Woo, and K. Kovač. Quenching of Star Formation in Sloan Digital Sky Survey Groups: Centrals, Satellites, and Galactic Conformity. *ApJ*, 800:24, February 2015. doi: 10.1088/0004-637X/800/1/24. 10

R. A. Koopmann and J. D. P. Kenney. The Trouble with Hubble Types in the Virgo Cluster. *ApJL*, 497:L75–L79, April 1998. doi: 10.1086/311283. 9

R. A. Koopmann and J. D. P. Kenney. Hα Morphologies and Environmental Effects in Virgo Cluster Spiral Galaxies. *ApJ*, 613:866–885, October 2004. doi: 10.1086/423191. 20

J. Kormendy. Observations of galaxy structure and dynamics. In L. Martinet and M. Mayor, editors, *Saas-Fee Advanced Course 12: Morphology and Dynamics of Galaxies*, pages 113–288, 1982. vii, 12

J. Kormendy and R. Bender. A Revised Parallel-sequence Morphological Classification of Galaxies: Structure and Formation of S0 and Spheroidal Galaxies. *ApJS*, 198:2, January 2012. doi: 10.1088/0067-0049/198/1/2. 14

John Kormendy and Rober C. Jr. Kennicut. *Annual Review Astron. Astrophys.* Annual Reviews, 2004. vii, 12

A. J. Korn, C. Maraston, and D. Thomas. The sensitivity of Lick indices to abundance variations. *A&A*, 438:685–704, August 2005. doi: 10.1051/0004-6361:20042126. xvi, xvii, 56, 61, 152

P. Kroupa. On the variation of the initial mass function. *MNRAS*, 322:231–246, April 2001. doi: 10.1046/j.1365-8711.2001.04022.x. 33

C. Lacey and S. Cole. Merger Rates in Hierarchical Models of Galaxy Formation - Part Two - Comparison with N-Body Simulations. *MNRAS*, 271:676, December 1994. doi: 10.1093/mnras/271.3.676. 8

R. B. Larson, B. M. Tinsley, and C. N. Caldwell. The evolution of disk galaxies and the origin of S0 galaxies. *ApJ*, 237:692–707, May 1980. doi: 10.1086/157917. 13, 15

E. Laurikainen, H. Salo, R. Buta, J. H. Knapen, and S. Comerón. Photometric scaling relations of lenticular and spiral galaxies. *MNRAS*, 405:1089–1118, June 2010. doi: 10.1111/j.1365-2966.2010.16521.x. 14

D. Le Borgne, B. Rocca-Volmerange, P. Prugniel, A. Lançon, M. Fioc, and C. Soubiran. Evolutionary synthesis of galaxies at high spectral resolution with the code PEGASE-

HR. Metallicity and age tracers. *A&A*, 425:881–897, October 2004. doi: 10.1051/0004-6361:200400044. 35

Y. Lee, T. C. Beers, C. Bailer-Jones, H. J. Newberg, M. Subbarao, and D. Surendran. Estimation of Stellar Atmospheric Parameters from SDSS ugriz Photometry. In *American Astronomical Society Meeting Abstracts*, volume 37 of *Bulletin of the American Astronomical Society*, page 131.04, December 2005. 47

C. Leitherer, P. A. Ortiz Otálvaro, F. Bresolin, R.-P. Kudritzki, B. Lo Faro, A. W. A. Pauldrach, M. Pettini, and S. A. Rix. A Library of Theoretical Ultraviolet Spectra of Massive, Hot Stars for Evolutionary Synthesis. *ApJS*, 189:309–335, August 2010. doi: 10.1088/0067-0049/189/2/309. 35

I. Lewis, M. Balogh, R. De Propris, W. Couch, R. Bower, A. Offer, J. Bland-Hawthorn, I. K. Baldry, C. Baugh, T. Bridges, R. Cannon, S. Cole, M. Colless, C. Collins, N. Cross, G. Dalton, S. P. Driver, G. Efstathiou, R. S. Ellis, C. S. Frenk, K. Glazebrook, E. Hawkins, C. Jackson, O. Lahav, S. Lumsden, S. Maddox, D. Madgwick, P. Norberg, J. A. Peacock, W. Percival, B. A. Peterson, W. Sutherland, and K. Taylor. The 2dF Galaxy Redshift Survey: the environmental dependence of galaxy star formation rates near clusters. *MNRAS*, 334:673–683, August 2002. doi: 10.1046/j.1365-8711.2002.05558.x. 9

H. Lietzen, E. Tempel, P. Heinämäki, P. Nurmi, M. Einasto, and E. Saar. Environments of galaxies in groups within the supercluster-void network. *A&A*, 545:A104, September 2012. doi: 10.1051/0004-6361/201219353. 11

S. Mahajan and S. Raychaudhury. Red star-forming and blue passive galaxies in clusters. *MNRAS*, 400:687–698, December 2009. doi: 10.1111/j.1365-2966.2009.15512.x. 9

F. Mannucci, G. Cresci, R. Maiolino, A. Marconi, and A. Gnerucci. A fundamental

relation between mass, star formation rate and metallicity in local and high-redshift galaxies. *MNRAS*, 408:2115–2127, November 2010. doi: 10.1111/j.1365-2966.2010.17291.x. 88

C. Maraston. Evolutionary population synthesis: models, analysis of the ingredients and application to high-z galaxies. *MNRAS*, 362:799–825, September 2005. doi: 10.1111/j.1365-2966.2005.09270.x. 35

P. Martini, J. S. Mulchaey, and D. D. Kelson. The Distribution of Active Galactic Nuclei in Clusters of Galaxies. *ApJ*, 664:761–776, August 2007. doi: 10.1086/519158. 11

P. Martini, G. R. Sivakoff, and J. S. Mulchaey. The Evolution of Active Galactic Nuclei in Clusters of Galaxies to Redshift 1.3. *ApJ*, 701:66–85, August 2009. doi: 10.1088/0004-637X/701/1/66. 11

MASIL. Galaxy group hickson 44. URL `http://www.masil-astro-imaging.com/home.html`. vi, 6

K. L. Masters, M. Mosleh, A. K. Romer, R. C. Nichol, S. P. Bamford, K. Schawinski, C. J. Lintott, D. Andreescu, H. C. Campbell, B. Crowcroft, I. Doyle, E. M. Edmondson, P. Murray, M. J. Raddick, A. Slosar, A. S. Szalay, and J. Vandenberg. Galaxy Zoo: passive red spirals. *MNRAS*, 405:783–799, June 2010. doi: 10.1111/j.1365-2966.2010.16503.x. 7, 10, 98

I. G. McCarthy, C. S. Frenk, A. S. Font, C. G. Lacey, R. G. Bower, N. L. Mitchell, M. L. Balogh, and T. Theuns. Ram pressure stripping the hot gaseous haloes of galaxies in groups and clusters. *MNRAS*, 383:593–605, January 2008. doi: 10.1111/j.1365-2966.2007.12577.x. 15

S. L. McGee, M. L. Balogh, R. D. E. Henderson, D. J. Wilman, R. G. Bower, J. S. Mulchaey, and A. Oemler, Jr. Evolution in the discs and bulges of group galaxies since

z = 0.4. *MNRAS*, 387:1605–1621, July 2008. doi: 10.1111/j.1365-2966.2008.13340.x. 10, 20

S. L. McGee, M. L. Balogh, R. G. Bower, A. S. Font, and I. G. McCarthy. The accretion of galaxies into groups and clusters. *MNRAS*, 400:937–950, December 2009. doi: 10.1111/j.1365-2966.2009.15507.x. 2, 4, 5, 10, 20

S. L. McGee, M. L. Balogh, D. J. Wilman, R. G. Bower, J. S. Mulchaey, L. C. Parker, and A. Oemler. The Dawn of the Red: star formation histories of group galaxies over the past 5 billion years. *MNRAS*, 413:996–1012, May 2011. doi: 10.1111/j.1365-2966.2010.18189.x. 9

M. Merchán and A. Zandivarez. Galaxy groups in the 2dF Galaxy Redshift Survey: the catalogue. *MNRAS*, 335:216–222, September 2002. doi: 10.1046/j.1365-8711.2002.05623.x. 36, 122

Houjun Mo, Frank van den Bosch, and Simon White. *Galaxy Formation and Evolution*. Cambridge University Press, first edition, 2010. 4

B. Moore, G. Lake, and N. Katz. Morphological Transformation from Galaxy Harassment. *ApJ*, 495:139–151, March 1998. doi: 10.1086/305264. 16, 17

S. Moran, R. S. Ellis, T. Treu, G. P. Smith, and N. Miller. Reflections of Cluster Assembly in the Stellar Populations and Dynamics of Member Galaxies. In *American Astronomical Society Meeting Abstracts*, volume 38 of *Bulletin of the American Astronomical Society*, page 183.03, December 2006. 10, 20

S. M. Moran, R. S. Ellis, T. Treu, G. P. Smith, R. M. Rich, and I. Smail. A Wide-Field Survey of Two z ˜ 0.5 Galaxy Clusters: Identifying the Physical Processes Responsible for the Observed Transformation of Spirals into S0s. *ApJ*, 671:1503–1522, December 2007. doi: 10.1086/522303. 14

A. Muzzin, R. F. J. van der Burg, S. L. McGee, M. Balogh, M. Franx, H. Hoekstra, M. J. Hudson, A. Noble, D. S. Taranu, T. Webb, G. Wilson, and H. K. C. Yee. The Phase Space and Stellar Populations of Cluster Galaxies at z ˜ 1: Simultaneous Constraints on the Location and Timescale of Satellite Quenching. *ApJ*, 796:65, November 2014. doi: 10.1088/0004-637X/796/1/65. 92

A. Nigoche-Netro, J. A. L. Aguerri, P. Lagos, A. Ruelas-Mayorga, L. J. Sánchez, and A. Machado. The Faber-Jackson relation for early-type galaxies: dependence on the magnitude range. *A&A*, 516:A96, June 2010. doi: 10.1051/0004-6361/200912719. 53

NIST. Atomic spectra database lines data. URL `http://physics.nist.gov/cgi-bin/ASD/lines1.pl`. 27, 28

A. G. Noble, T. M. A. Webb, A. Muzzin, G. Wilson, H. K. C. Yee, and R. F. J. van der Burg. A Kinematic Approach to Assessing Environmental Effects: Star-forming Galaxies in a z ˜ 0.9 SpARCS Cluster Using Spitzer 24 μm Observations. *ApJ*, 768: 118, May 2013. doi: 10.1088/0004-637X/768/2/118. 92

A. Oemler, Jr. The Systematic Properties of Clusters of Galaxies. Photometry of 15 Clusters. *ApJ*, 194:1–20, November 1974. doi: 10.1086/153216. 9, 94

L. Old, R. A. Skibba, F. R. Pearce, D. Croton, S. I. Muldrew, J. C. Muñoz-Cuartas, D. Gifford, M. E. Gray, A. v. der Linden, G. A. Mamon, M. R. Merrifield, V. Müller, R. J. Pearson, T. J. Ponman, A. Saro, T. Sepp, C. Sifón, E. Tempel, E. Tundo, Y. O. Wang, and R. Wojtak. Galaxy cluster mass reconstruction project - I. Methods and first results on galaxy-based techniques. *MNRAS*, 441:1513–1536, June 2014. doi: 10.1093/mnras/stu545. 37

J. P. F. Osmond and T. J. Ponman. The GEMS project: X-ray analysis and statistical properties of the group sample. *MNRAS*, 350:1511–1535, June 2004. doi: 10.1111/j.1365-2966.2004.07742.x. 45

S. G. Patel, B. P. Holden, D. D. Kelson, M. Franx, A. van der Wel, and G. D. Illingworth. The UVJ Selection of Quiescent and Star-forming Galaxies: Separating Early- and Late-type Galaxies and Isolating Edge-on Spirals. *ApJL*, 748:L27, April 2012. doi: 10.1088/2041-8205/748/2/L27. 63, 93

Y. Peng, R. Maiolino, and R. Cochrane. Strangulation as the primary mechanism for shutting down star formation in galaxies. *Nature*, 521:192–195, May 2015. doi: 10.1038/nature14439. 15

Y.-j. Peng and R. Maiolino. The dependence of the galaxy mass-metallicity relation on environment and the implied metallicity of the IGM. *MNRAS*, 438:262–270, February 2014. doi: 10.1093/mnras/stt2175. 88

Y.-j. Peng, S. J. Lilly, K. Kovač, M. Bolzonella, L. Pozzetti, A. Renzini, G. Zamorani, O. Ilbert, C. Knobel, A. Iovino, C. Maier, O. Cucciati, L. Tasca, C. M. Carollo, J. Silverman, P. Kampczyk, L. de Ravel, D. Sanders, N. Scoville, T. Contini, V. Mainieri, M. Scodeggio, J.-P. Kneib, O. Le Fèvre, S. Bardelli, A. Bongiorno, K. Caputi, G. Coppa, S. de la Torre, P. Franzetti, B. Garilli, F. Lamareille, J.-F. Le Borgne, V. Le Brun, M. Mignoli, E. Perez Montero, R. Pello, E. Ricciardelli, M. Tanaka, L. Tresse, D. Vergani, N. Welikala, E. Zucca, P. Oesch, U. Abbas, L. Barnes, R. Bordoloi, D. Bottini, A. Cappi, P. Cassata, A. Cimatti, M. Fumana, G. Hasinger, A. Koekemoer, A. Leauthaud, D. Maccagni, C. Marinoni, H. McCracken, P. Memeo, B. Meneux, P. Nair, C. Porciani, V. Presotto, and R. Scaramella. Mass and Environment as Drivers of Galaxy Evolution in SDSS and zCOSMOS and the Origin of the Schechter Function. *ApJ*, 721:193–221, September 2010. doi: 10.1088/0004-637X/721/1/193. 10, 42

J. I. Phillips, C. Wheeler, M. Boylan-Kolchin, J. S. Bullock, M. C. Cooper, and E. J. Tollerud. A dichotomy in satellite quenching around L* galaxies. *MNRAS*, 437: 1930–1941, January 2014. doi: 10.1093/mnras/stt2023. 10

M. Plionis, S. Basilakos, and H. M. Tovmassian. The shape of poor groups of galaxies. *MNRAS*, 352:1323–1328, August 2004. doi: 10.1111/j.1365-2966.2004.08023.x. 5

B. M. Poggianti, I. Smail, A. Dressler, W. J. Couch, A. J. Barger, H. Butcher, R. S. Ellis, and A. Oemler, Jr. The Star Formation Histories of Galaxies in Distant Clusters. *ApJ*, 518:576–593, June 1999. doi: 10.1086/307322. 9

M. Postman and M. J. Geller. The morphology-density relation - The group connection. *ApJ*, 281:95–99, June 1984. doi: 10.1086/162078. 9

M. Prescott, I. K. Baldry, P. A. James, S. P. Bamford, J. Bland-Hawthorn, S. Brough, M. J. I. Brown, E. Cameron, C. J. Conselice, S. M. Croom, S. P. Driver, C. S. Frenk, M. Gunawardhana, D. T. Hill, A. M. Hopkins, D. H. Jones, L. S. Kelvin, K. Kuijken, J. Liske, J. Loveday, R. C. Nichol, P. Norberg, H. R. Parkinson, J. A. Peacock, S. Phillipps, K. A. Pimbblet, C. C. Popescu, A. S. G. Robotham, R. G. Sharp, W. J. Sutherland, E. N. Taylor, R. J. Tuffs, E. van Kampen, and D. Wijesinghe. Galaxy and Mass Assembly (GAMA): the red fraction and radial distribution of satellite galaxies. *MNRAS*, 417:1374–1386, October 2011. doi: 10.1111/j.1365-2966.2011.19353.x. 10

R. N. Proctor and A. E. Sansom. A comparison of stellar populations in galaxy spheroids across a wide range of Hubble types. *MNRAS*, 333:517–543, July 2002. doi: 10.1046/j.1365-8711.2002.05391.x. 56, 57

R. N. Proctor, D. A. Forbes, and M. A. Beasley. A robust method for the analysis of integrated spectra from globular clusters using Lick indices. *MNRAS*, 355:1327–1338, December 2004a. doi: 10.1111/j.1365-2966.2004.08415.x. 56

R. N. Proctor, D. A. Forbes, and M. A. Beasley. A robust method for the analysis of integrated spectra from globular clusters using Lick indices. *MNRAS*, 355:1327–1338, December 2004b. doi: 10.1111/j.1365-2966.2004.08415.x. 56

R. N. Proctor, D. A. Forbes, A. Forestell, and K. Gebhardt. Spatially resolved stellar populations in the isolated elliptical NGC 821. *MNRAS*, 362:857–866, September 2005. doi: 10.1111/j.1365-2966.2005.09312.x. viii, 32

M. Ramella, M. J. Geller, and J. P. Huchra. Groups of galaxies in the Center for Astrophysics redshift survey. *ApJ*, 344:57–74, September 1989. doi: 10.1086/167777. 11

J. Rasmussen, T. J. Ponman, and J. S. Mulchaey. Gas stripping in galaxy groups - the case of the starburst spiral NGC 2276. *MNRAS*, 370:453–467, July 2006a. doi: 10.1111/j.1365-2966.2006.10492.x. 15

J. Rasmussen, T. J. Ponman, J. S. Mulchaey, T. A. Miles, and S. Raychaudhury. First results of the XI Groups Project: studying an unbiased sample of galaxy groups. *MNRAS*, 373:653–665, December 2006b. doi: 10.1111/j.1365-2966.2006.11023.x. 1, 36, 37, 38, 40, 43, 44, 45

J. Rasmussen, J. S. Mulchaey, L. Bai, T. J. Ponman, S. Raychaudhury, and A. Dariush. Witnessing the Formation of a Brightest Cluster Galaxy in a Nearby X-ray Cluster. *ApJ*, 717:958–972, July 2010. doi: 10.1088/0004-637X/717/2/958. 44, 45

J. Rasmussen, J. S. Mulchaey, L. Bai, T. J. Ponman, S. Raychaudhury, and A. Dariush. The Suppression of Star Formation and the Effect of the Galaxy Environment in Low-redshift Galaxy Groups. *ApJ*, 757:122, October 2012. doi: 10.1088/0004-637X/757/2/122. 1, 20, 37, 38, 40, 43, 44, 89

A. L. B. Ribeiro, P. A. A. Lopes, and S. B. Rembold. NoSOCS in SDSS. III. The interplay between galaxy evolution and the dynamical state of galaxy clusters. *A&A*, 556:A74, August 2013. doi: 10.1051/0004-6361/201220801. 7

G. H. Rieke, K. Loken, M. J. Rieke, and P. Tamblyn. Starburst modeling of M82

- Test case for a biased initial mass function. *ApJ*, 412:99–110, July 1993. doi: 10.1086/172904. 43

G. H. Rieke, E. T. Young, C. W. Engelbracht, D. M. Kelly, F. J. Low, E. E. Haller, J. W. Beeman, K. D. Gordon, J. A. Stansberry, K. A. Misselt, J. Cadien, J. E. Morrison, G. Rivlis, W. B. Latter, A. Noriega-Crespo, D. L. Padgett, K. R. Stapelfeldt, D. C. Hines, E. Egami, J. Muzerolle, A. Alonso-Herrero, M. Blaylock, H. Dole, J. L. Hinz, E. Le Floc'h, C. Papovich, P. G. Pérez-González, P. S. Smith, K. Y. L. Su, L. Bennett, D. T. Frayer, D. Henderson, N. Lu, F. Masci, M. Pesenson, L. Rebull, J. Rho, J. Keene, S. Stolovy, S. Wachter, W. Wheaton, M. W. Werner, and P. L. Richards. The Multiband Imaging Photometer for Spitzer (MIPS). *ApJS*, 154:25–29, September 2004. doi: 10.1086/422717. 42

G. H. Rieke, A. Alonso-Herrero, B. J. Weiner, P. G. Pérez-González, M. Blaylock, J. L. Donley, and D. Marcillac. Determining Star Formation Rates for Infrared Galaxies. *ApJ*, 692:556–573, February 2009. doi: 10.1088/0004-637X/692/1/556. 42

A. S. G. Robotham, P. Norberg, S. P. Driver, I. K. Baldry, S. P. Bamford, A. M. Hopkins, J. Liske, J. Loveday, A. Merson, J. A. Peacock, S. Brough, E. Cameron, C. J. Conselice, S. M. Croom, C. S. Frenk, M. Gunawardhana, D. T. Hill, D. H. Jones, L. S. Kelvin, K. Kuijken, R. C. Nichol, H. R. Parkinson, K. A. Pimbblet, S. Phillipps, C. C. Popescu, M. Prescott, R. G. Sharp, W. J. Sutherland, E. N. Taylor, D. Thomas, R. J. Tuffs, E. van Kampen, and D. Wijesinghe. Galaxy and Mass Assembly (GAMA): the GAMA galaxy group catalogue (G^3Cv1). *MNRAS*, 416:2640–2668, October 2011. doi: 10.1111/j.1365-2966.2011.19217.x. 119

E. Roediger and M. Brüggen. Ram pressure stripping of disc galaxies orbiting in clusters - I. Mass and radius of the remaining gas disc. *MNRAS*, 380:1399–1408, October 2007. doi: 10.1111/j.1365-2966.2007.12241.x. 14

Geroge B. Rybicki and Alan P. Lightman. *Radiative Processes in Astrophysics*. Wiley-Interscience, first edition, 1979. 24, 31

S. Salim, R. M. Rich, S. Charlot, J. Brinchmann, B. D. Johnson, D. Schiminovich, M. Seibert, R. Mallery, T. M. Heckman, K. Forster, P. G. Friedman, D. C. Martin, P. Morrissey, S. G. Neff, T. Small, T. K. Wyder, L. Bianchi, J. Donas, Y.-W. Lee, B. F. Madore, B. Milliard, A. S. Szalay, B. Y. Welsh, and S. K. Yi. UV Star Formation Rates in the Local Universe. *ApJS*, 173:267–292, December 2007. doi: 10.1086/519218. 44, 90, 96

E. E. Salpeter. The Luminosity Function and Stellar Evolution. *ApJ*, 121:161, January 1955. doi: 10.1086/145971. 33

D. B. Sanders, B. T. Soifer, J. H. Elias, B. F. Madore, K. Matthews, G. Neugebauer, and N. Z. Scoville. Ultraluminous infrared galaxies and the origin of quasars. *ApJ*, 325:74–91, February 1988. doi: 10.1086/165983. 16

C. L. Sarazin. X-ray emission from clusters of galaxies. *Reviews of Modern Physics*, 58:1–115, January 1986. doi: 10.1103/RevModPhys.58.1. 4

M. Sarzi, J. Falcón-Barroso, R. L. Davies, R. Bacon, M. Bureau, M. Cappellari, P. T. de Zeeuw, E. Emsellem, K. Fathi, D. Krajnović, H. Kuntschner, R. M. McDermid, and R. F. Peletier. The SAURON project - V. Integral-field emission-line kinematics of 48 elliptical and lenticular galaxies. *MNRAS*, 366:1151–1200, March 2006. doi: 10.1111/j.1365-2966.2005.09839.x. 54

R. P. Schiavon. Population Synthesis in the Blue. IV. Accurate Model Predictions for Lick Indices and UBV Colors in Single Stellar Populations. *ApJS*, 171:146–205, July 2007. doi: 10.1086/511753. 35

D. J. Schlegel, D. P. Finkbeiner, and M. Davis. Maps of Dust Infrared Emission

for Use in Estimation of Reddening and Cosmic Microwave Background Radiation Foregrounds. *ApJ*, 500:525–553, June 1998. doi: 10.1086/305772. 37, 43

T. C. Scott, L. Cortese, E. Brinks, H. Bravo-Alfaro, R. Auld, and R. Minchin. Two long H I tails in the outskirts of Abell 1367. *MNRAS*, 419:L19–L23, January 2012. doi: 10.1111/j.1745-3933.2011.01169.x. 14

Michael A. Seeds and Dana E. Backman. *Foundations of Astronomy.* CENGAGE Learning, 13th edition, 2016. xvi, 28

Y. Shen, J. S. Mulchaey, S. Raychaudhury, J. Rasmussen, and T. J. Ponman. Differences in the AGN Populations of Groups and Clusters: Clues to AGN Evolution. *ApJL*, 654:L115–L118, January 2007. doi: 10.1086/511030. 44, 45

I. Strateva, Ž. Ivezić, G. R. Knapp, V. K. Narayanan, M. A. Strauss, J. E. Gunn, R. H. Lupton, D. Schlegel, N. A. Bahcall, J. Brinkmann, R. J. Brunner, T. Budavári, I. Csabai, F. J. Castander, M. Doi, M. Fukugita, Z. Győry, M. Hamabe, G. Hennessy, T. Ichikawa, P. Z. Kunszt, D. Q. Lamb, T. A. McKay, S. Okamura, J. Racusin, M. Sekiguchi, D. P. Schneider, K. Shimasaku, and D. York. Color Separation of Galaxy Types in the Sloan Digital Sky Survey Imaging Data. *AJ*, 122:1861–1874, October 2001. doi: 10.1086/323301. 9

M. Sun, S. S. Murray, M. Markevitch, and A. Vikhlinin. Chandra Observation of A2256: A Cluster at the Early Stage of Merging. *ApJ*, 565:867–876, February 2002. doi: 10.1086/324721. 8

M. Sun, M. Donahue, and G. M. Voit. Hα Tail, Intracluster H II Regions, and Star Formation: ESO 137-001 in Abell 3627. *ApJ*, 671:190–202, December 2007. doi: 10.1086/522690. 14

D. S. Taranu, M. J. Hudson, M. L. Balogh, R. J. Smith, C. Power, K. A. Oman, and

B. Krane. Quenching star formation in cluster galaxies. *MNRAS*, 440:1934–1949, May 2014. doi: 10.1093/mnras/stu389. 20

J. Tennyson. *Astronomical Spectroscopy*. Imperial College Press, first edition, 2005. 23, 24, 28, 29

B. M. Tinsley. Stellar lifetimes and abundance ratios in chemical evolution. *ApJ*, 229: 1046–1056, May 1979. doi: 10.1086/157039. 31

S. Tonnesen, G. L. Bryan, and J. H. van Gorkom. Environmentally Driven Evolution of Simulated Cluster Galaxies. *ApJ*, 671:1434–1445, December 2007. doi: 10.1086/523034. 14

A. Toomre. Mergers and Some Consequences. In B. M. Tinsley and R. B. G. Larson, D. Campbell, editors, *Evolution of Galaxies and Stellar Populations*, page 401, 1977. 16

S. C. Trager, G. Worthey, S. M. Faber, D. Burstein, and J. J. González. Old Stellar Populations. VI. Absorption-Line Spectra of Galaxy Nuclei and Globular Clusters. *ApJS*, 116:1–28, 1998. doi: 10.1086/313099. 47

K.-V. H. Tran, L. Simard, A. I. Zabludoff, and J. S. Mulchaey. The Galaxy Populations of X-Ray-detected, Poor Groups. *ApJ*, 549:172–191, March 2001. doi: 10.1086/319085. 9

C. A. Tremonti, T. M. Heckman, G. Kauffmann, J. Brinchmann, S. Charlot, S. D. M. White, M. Seibert, E. W. Peng, D. J. Schlegel, A. Uomoto, M. Fukugita, and J. Brinkmann. The Origin of the Mass-Metallicity Relation: Insights from 53,000 Star-forming Galaxies in the Sloan Digital Sky Survey. *ApJ*, 613:898–913, October 2004. doi: 10.1086/423264. 87, 88

M. J. Tripicco and R. A. Bell. Modeling the LICK/IDS Spectral Feature Indices Using Synthetic Spectra. *AJ*, 110:3035, December 1995. doi: 10.1086/117744. 48

R. B. Tully. Nearby groups of galaxies. II - an all-sky survey within 3000 kilometers per second. *ApJ*, 321:280–304, October 1987. doi: 10.1086/165629. 5

R. P. van der Marel and M. Franx. A new method for the identification of non-Gaussian line profiles in elliptical galaxies. *ApJ*, 407:525–539, April 1993. doi: 10.1086/172534. 51

A. Vazdekis. Evolutionary Stellar Population Synthesis at 2 Å Spectral Resolution. *ApJ*, 513:224–241, March 1999. doi: 10.1086/306843. 46, 56

A. Vazdekis. Evolutionary Stellar Population Synthesis at 2 Å Spectral Resolution. *Ap&SS*, 276:921–929, March 2001. doi: 10.1023/A:1017536301933. xvi, 61

A. Vazdekis, E. Casuso, R. F. Peletier, and J. E. Beckman. A New Chemo-evolutionary Population Synthesis Model for Early-Type Galaxies. I. Theoretical Basis. *ApJS*, 106: 307, October 1996. doi: 10.1086/192340. 46

A. Vazdekis, P. Sánchez-Blázquez, J. Falcón-Barroso, A. J. Cenarro, M. A. Beasley, N. Cardiel, J. Gorgas, and R. F. Peletier. Evolutionary stellar population synthesis with MILES - I. The base models and a new line index system. *MNRAS*, 404:1639–1671, June 2010. doi: 10.1111/j.1365-2966.2010.16407.x. 35, 52

B. Vollmer, R. Beck, J. D. P. Kenney, and J. H. van Gorkom. Radio Continuum Observations of the Virgo Cluster Spiral NGC 4522: The Signature of Ram Pressure. *AJ*, 127:3375–3381, June 2004. doi: 10.1086/420802. 14

B. Vollmer, J. Braine, C. Pappalardo, and P. Hily-Blant. Ram-pressure stripped molecular gas in the Virgo spiral galaxy NGC 4522. *A&A*, 491:455–464, November 2008. doi: 10.1051/0004-6361:200810432. 14

B. Vollmer, M. Soida, A. Chung, L. Chemin, J. Braine, A. Boselli, and R. Beck. Ram pressure stripping of the multiphase ISM in the Virgo cluster spiral galaxy NGC 4438. *A&A*, 496:669–675, March 2009. doi: 10.1051/0004-6361/200811140. 14

B. Vollmer, M. Soida, J. Braine, A. Abramson, R. Beck, A. Chung, H. H. Crowl, J. D. P. Kenney, and J. H. van Gorkom. Ram pressure stripping of the multiphase ISM and star formation in the Virgo spiral galaxy NGC 4330. *A&A*, 537:A143, January 2012. doi: 10.1051/0004-6361/201117680. 14

A. von der Linden, V. Wild, G. Kauffmann, S. D. M. White, and S. Weinmann. Star formation and AGN activity in SDSS cluster galaxies. *MNRAS*, 404:1231–1246, May 2010. doi: 10.1111/j.1365-2966.2010.16375.x. 20

J. M. Vrtilek, E. O'Sullivan, L. P. David, K. Kolokythas, S. Giacintucci, S. Raychaudhury, and T. J. Ponman. CLoGS - The Complete Local-Volume Groups Survey. In *AAS/High Energy Astrophysics Division*, volume 13 of *AAS/High Energy Astrophysics Division*, page 116.06, April 2013. 119

B. Vulcani, B. M. Poggianti, R. A. Finn, G. Rudnick, V. Desai, and S. Bamford. Comparing the Relation Between Star Formation and Galaxy Mass in Different Environments. *ApJL*, 710:L1–L6, February 2010. doi: 10.1088/2041-8205/710/1/L1. 20

W. Wang and S. D. M. White. Satellite abundances around bright isolated galaxies. *MNRAS*, 424:2574–2598, August 2012. doi: 10.1111/j.1365-2966.2012.21256.x. 10

S. M. Weinmann, F. C. van den Bosch, X. Yang, and H. J. Mo. Properties of galaxy groups in the Sloan Digital Sky Survey - I. The dependence of colour, star formation and morphology on halo mass. *MNRAS*, 366:2–28, February 2006. doi: 10.1111/j.1365-2966.2005.09865.x. 10

A. R. Wetzel, J. L. Tinker, and C. Conroy. Galaxy evolution in groups and clusters: star formation rates, red sequence fractions and the persistent bimodality. *MNRAS*, 424:232–243, July 2012. doi: 10.1111/j.1365-2966.2012.21188.x. 10, 19

A. R. Wetzel, J. L. Tinker, C. Conroy, and F. C. van den Bosch. Galaxy evolution in groups and clusters: satellite star formation histories and quenching time-scales in a hierarchical Universe. *MNRAS*, 432:336–358, June 2013. doi: 10.1093/mnras/stt469. 19

B. C. Whitmore, D. M. Gilmore, and C. Jones. What determines the morphological fractions in clusters of galaxies? *ApJ*, 407:489–509, April 1993. doi: 10.1086/172531. 9

B. Willman, F. Governato, J. Wadsley, and T. Quinn. The origin and properties of intracluster stars in a rich cluster. *MNRAS*, 355:159–168, November 2004. doi: 10.1111/j.1365-2966.2004.08312.x. 17, 19

C. Wolf, A. Aragón-Salamanca, M. Balogh, M. Barden, E. F. Bell, M. E. Gray, C. Y. Peng, D. Bacon, F. D. Barazza, A. Böhm, J. A. R. Caldwell, A. Gallazzi, B. Häusler, C. Heymans, K. Jahnke, S. Jogee, E. van Kampen, K. Lane, D. H. McIntosh, K. Meisenheimer, C. Papovich, S. F. Sánchez, A. Taylor, L. Wisotzki, and X. Zheng. Optically-Passive Spirals: the Missing Link in Gradual Star Formation Suppression upon Cluster Infall. In W. Wang, Z. Yang, Z. Luo, and Z. Chen, editors, *The Starburst-AGN Connection*, volume 408 of *Astronomical Society of the Pacific Conference Series*, page 248, October 2009. 7, 10, 98

G. Worthey and D. L. Ottaviani. Hγ and Hδ Absorption Features in Stars and Stellar Populations. *ApJS*, 111:377–386, August 1997. doi: 10.1086/313021. xvi, 46, 56, 61

G. Worthey, S. M. Faber, J. J. Gonzalez, and D. Burstein. Old stellar populations. 5:

Absorption feature indices for the complete LICK/IDS sample of stars. *ApJS*, 94: 687–722, October 1994. doi: 10.1086/192087. xvi, 31, 35, 48, 61

M. Yagi, M. Yoshida, Y. Komiyama, N. Kashikawa, H. Furusawa, S. Okamura, A. W. Graham, N. A. Miller, D. Carter, B. Mobasher, and S. Jogee. A Dozen New Galaxies Caught in the Act: Gas Stripping and Extended Emission Line Regions in the Coma Cluster. *AJ*, 140:1814–1829, December 2010. doi: 10.1088/0004-6256/140/6/1814. 14

A. I. Zabludoff and J. S. Mulchaey. The Properties of Poor Groups of Galaxies. I. Spectroscopic Survey and Results. *ApJ*, 496:39–72, March 1998. doi: 10.1086/305355. 9, 21, 40

F. Zwicky. Multiple Galaxies. *Ergebnisse der exakten Naturwissenschaften*, 29:344–385, 1956. 17

F. Zwicky. Multiple Galaxies. *Handbuch der Physik*, 53:373, 1959. 17